TAILORING THE LIGAND SHELL OF QUANTUM DOTS TOWARDS IMPROVED PHOTOCATALYTIC CHARGE TRANSFER

Jonathan Ronald Lee

Stephenson Institute for Renewable Energy

Department of Physics

Thesis submitted in accordance with the requirements of the

University of Liverpool for the degree of Doctor in Philosophy

January 2018

ABSTRACT

This work describes research that investigated the incorporation of colloidal semiconductor quantum dots (QDs) as light absorbers in photocatalytic systems. Initial work was conducted to assemble hybrid photocatalysts consisting of CdS QDs and cobaloxime molecular catalysts for hydrogen generation as a means to store solar energy. A strategy was developed for the covalent attachment of cobaloximes to the QDs to enhance the rate of electron transfer to the catalyst. Under illumination, these materials evolved hydrogen from an aqueous solution containing the hole scavenger sodium sulfite. Further study of these materials suggested that the cobaloxime complexes actually serve as pre-catalysts for an active species that is deposited on the surface of QDs during illumination. It was also found that the stabilising ligands that coat the surface of QDs to maintain colloidal stability are highly influential, in some cases dictating the catalytic activity of the overall system. For hydrogen evolution to proceed, these molecules must be partially removed from the QD surface to facilitate access by hole scavengers. This process occurs through photo-oxidation of the ligands, which ultimately compromises the stability of the particles in solution. It is therefore necessary to reconcile the need for long-term stability with catalytic activity in QD-based photocatalysts.

To address the dilemma presented in trying to optimise both stability and activity in QD-based photocatalysts, ligands were sought which could actively transfer holes from the QD core to scavengers in solution. Such a material could remain bound to the surface of QDs, imparting colloidal stability without restricting charge transfer. Transient absorption spectroscopy was used to study the electronic effects of candidate ligands on the charge carrier dynamics of CdSe QDs to assess their potential for promoting hole transfer. An investigation of hydrophilic aminothiol molecules was conducted, comparing alkyl and aromatic analogues. Stabilisation of QDs by 4-aminothiophenol in acidic aqueous conditions was shown to extend the lifetime of conduction band electrons, attributed to an interruption of the Auger relaxation process due to hole delocalisation from the QD core onto the ligand. In the presence of hole scavengers, however, no evidence was observed for facilitated hole transfer from QDs.

A similar study of hydrophilic dithiocarbamates was then undertaken comparing alkyl and aromatic analogues. A size-dependence study was first performed, which showed that the molecules induced larger red shifts in the optical spectra of strongly

confined CdSe QDs upon adsorption than in larger QDs as a result of enhanced hole delocalisation onto the dithiocarbamate (DTC) ligand anchoring group. Transient absorption measurements demonstrated an acceleration of the relaxation of conduction band electrons in QDs functionalised with DTCs relative to thiols, which was similarly correlated with QD size. In the presence of sodium sulfite, the lifetime of conduction band electrons was dramatically extended in QDs stabilised by an aromatic DTC derived from 4-aminobenzoic acid, while the alkyl analogue exhibited no such effect. This result provided evidence that a DTC ligand could promote hole transfer from QDs to scavengers in solution while colloidally stabilising the particles. These findings should enable the development of QD-based photocatalysts that are both catalytically active and colloidally stable.

LIST OF PUBLICATIONS

The following papers were published in peer-reviewed journals during my PhD studies:

- Jonathan R. Lee, Wei Li, Alexander J. Cowan, and Frank Jäckel. "Hydrophilic, Hole-Delocalizing Ligand Shell to Promote Charge Transfer from Colloidal CdSe Quantum Dots in Water" *J. Phys. Chem. C*, (2017) **121**, 15160-15168.

- Wei Li, Jonathan R. Lee, and Frank Jäckel. "Simultaneous Optimization of Colloidal Stability and Interfacial Charge Transfer Efficiency in Photocatalytic Pt/CdS Nanocrystals" *ACS Appl. Mater. Interfaces*, (2016) **8**, 29434-29441.

- Emily R. Draper, Jonathan R. Lee, Matthew Wallace, Frank Jäckel, Alexander J. Cowan and Dave J. Adams. "Self-Sorted Photoconductive Xerogels" *Chem. Sci.* (2016) **7**, 6499-6505.

- James J. Walsh, Jonathan R. Lee, Emily R. Draper, Stephen M. King, Frank Jäckel, Martijn A. Zwijnenburg, Dave J. Adams, and Alexander J. Cowan. "Controlling Visible Light Driven Photoconductivity in Self-Assembled Perylene Bisimide Structures" *J. Phys. Chem. C* (2016) **120**, 18479-18486.

ACKNOWLEDGEMENTS

To Dr Frank Jäckel and to Dr Alex Cowan,

Thank you for giving me the opportunity to pursue this research, to work in your labs, and for all of your guidance, suggestions, proofreading, and the innumerable other ways you supported me during this project.

To Dr Wei Li,

Thank you for everything you taught me in the first years of my PhD, from nanoparticle synthesis to ultrafast spectroscopy, and for all of your patience and generosity along the way.

To Dr James Walsh

For everything in the lab, the odd pint, and for being a bit of Dublin in Liverpool, cheers buddy.

To Dr Gaia Neri,

Thank you for all your help in the early days and beyond, for your synthetic wizardry and advice, and the ligand hand-me-downs.

To everyone else in the Stephenson Institute,

Thank you for all the different ways you may have helped me in this project, whether you knew it or not.

To my family - Annemarie, Clive, and Suzanne,

Thank you for your unwavering love and support throughout, and in everything.

To A.-C.

This would have been a lot harder without you.

CONTENTS

List of Tables

List of Figures

1. INTRODUCTION

1.1 Overview

This chapter establishes the context in which the research presented in this thesis was conducted. The concept of photocatalytic generation of fuels to store solar energy is introduced, with a focus on water splitting, along with a brief overview of particulate semiconductor photocatalysts. Next, some practical aspects of semiconductor nanocrystals are described to support the discussion of these materials throughout the text. Finally, one of the primary characterisation techniques used for this work, transient absorption spectroscopy, is described. The information in this chapter is general, and provides a basis from which to approach the rest of the thesis. More specific introductions are given at the beginning of each experimental results chapter, including reviews of relevant literature and theory relevant to the material presented in that chapter.

1.2 Background

For two years consecutively, renewable energy technologies have accounted for the majority of new power generation capacity installed globally, with twice as much investment committed to renewables as to fossil fuel projects.[1] Grid parity between renewable and fossil fuel power generation is thought to have been achieved in more than thirty countries, and increasingly, it is more economical to install solar capacity than coal capacity.[2] Despite the healthy market conditions for photovoltaics, storing this energy for later use remains a fundamental technical challenge. In their 2006 review article discussing strategies to address this issue, Lewis and Nocera stated the situation bluntly: "*In the absence of cost-effective storage, solar electricity can never be a primary energy source for society, because of the diurnal variation in local insolation*."[3]

The possibility of storing solar energy directly as a fuel by mimicking natural photosynthetic processes has intrigued scientists for more than a century.[4] Such a scheme, often referred to as "artificial photosynthesis", would use sunlight to drive chemical reactions to produce "solar fuels." In natural photosynthesis, carbon dioxide and water are decomposed enzymatically and reassembled as carbohydrates, with molecular oxygen generated as a waste product.[5] Within this complex process, the decomposition of water to hydrogen and oxygen itself represents an attractive energy storage pathway, one which the eminent electrochemist Allen Bard has

described – if driven by sunlight – as "*a 'Holy Grail' renewable energy source... that produces a clean and storable fuel*."[6]

The overall water splitting reaction is described by two half-reactions, consisting of an oxidative oxygen evolution reaction (OER) and a reductive hydrogen evolution reaction (HER):

$$2H_2O \rightarrow 4H^+ + O_2 + 4e^- \qquad \text{(OER)}$$

$$4H^+ + 4e^- \rightarrow 2H_2 \qquad \text{(HER)}$$

$$\mathbf{2H_2O \rightarrow 2H_2 + O_2} \qquad (\Delta G = 4.92 \text{ eV})$$

As shown, the process requires that four electrons be rearranged between the reactants and products. The free energy change, $\Delta G = 4.92$ eV, represents the amount of energy stored by splitting two water molecules. An electrochemical system for water splitting must therefore impart a minimum energy of 1.23 V to each electron for the reaction to proceed. The grand challenge of artificial photosynthesis is to harvest this energy from solar photons and to efficiently store it in the chemical bonds of a fuel.

In 1972, Fujishima and Honda published what may be regarded as the foundational paper in the field of photo-driven water splitting, in which an electrochemical cell consisting of a TiO_2 photoelectrode and a platinum electrode was shown to produce hydrogen and oxygen without an external bias when irradiated with ultraviolet light.[7] This report might have remained of purely academic interest, however the following year an oil embargo imposed by Arab OPEC countries following conflict in the Middle East precipitated the 1973 energy crisis in the West, in which oil prices spike dramatically.[8] The crisis highlighted the need to explore alternative energy sources, motivating a surge of research into photovoltaic and photocatalytic technology.

By the early 1980s, significant progress had been made in the conceptualisation of practical systems to convert solar energy and store it as chemical fuel.[9,10] In addition to photoelectrochemical systems in the style of the Fujishima-Honda cell, which use one or more photoactive electrodes to harvest

photons, homogenous and heterogeneous photocatalytic systems were also devised to couple light absorption and fuel generation. Homogeneous systems are comprised of molecular sensitisers and catalysts in solution, both of which are typically coordination complexes, although organic sensitisers can also be used.[11–13] Heterogeneous systems involve components that are of a different phase than the reactants, such as colloidal semiconductor or metallic nanoparticles.[14–16] In recent years, homogeneous and heterogeneous catalytic components have increasingly been combined to produce so-called "hybrid" photocatalysts in order to benefit from the specific advantages of the individual components, for example by interfacing molecular catalysts with semiconductor absorbers.[17–19]

This thesis explores the incorporation of colloidal semiconductor nanocrystals as the light absorbing component in hybrid photocatalytic systems, using cadmium chalcogenides as model absorbers. Before presenting the experimental results of this research, some aspects of semiconductor nanocrystals in the context of photocatalysis are discussed. The development of contemporary methods used to synthesise semiconductor nanoparticles is then briefly described, along with some practical issues in handling these materials as a consequence of the synthetic method. Physical properties of these semiconductors arising at the nanoscale which are relevant to the thesis generally are also highlighted. Finally, an overview of the primary method that was used herein to investigate the behaviour of the semiconductor nanocrystals, ultrafast transient absorption spectroscopy, is provided.

1.3 Particulate Photocatalysts

Photocatalysts based on colloidal semiconductor particles were among the earliest systems for light-driven water splitting to be investigated.[9,10,20] Particulate photocatalysts have also been shown to be the most economical option for implenting photocatalytic energy storage.[16,21] An ideal semiconductor material for photocatalysis would be capable of absorbing photons in the visible region of the solar spectrum and of using photogenerated electrons and holes directly to drive both the reductive and oxidative half-reactions of water splitting in Figure 1-1 (left). Unfortunately, while many semiconductors exist with band gaps in the visible region, very few possess the required band alignments to catalyse both proton reduction and

water oxidation.[22] A further complication in creating a photocatalyst from a single material arises due to the different kinetics of the two water splitting half reactions, where the slower water oxidation process means that photogenerated holes tend to accumulate and oxidise the semiconductor.[23,24]

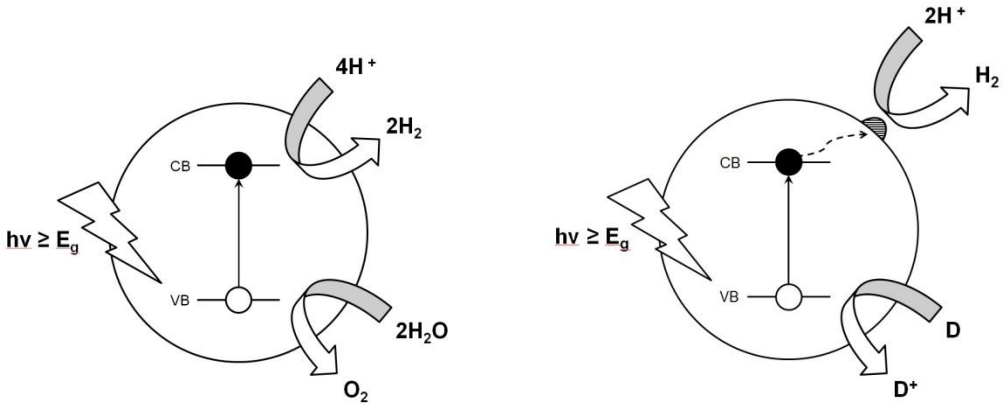

Figure 1-1. Schematic representations of particulate photocatalysts. (Left) An ideal material capable of catalysing both water splitting half-reactions. (Right) A system that uses a co-catalyst to catalyse the proton reduction half reaction in the presence of a hole scavenger, D/D^+.

Due to the difficulties in producing a photocatalyst capable of full water splitting, particulate photocatalysts are often prepared that drive one half reaction in isolation. Rather than attempting to also optimise the other half reaction concurrently, the associated charge carriers can be removed from the particle by adding an electron or hole scavenger to the photocatalyst solution. Another issue is encountered when a semiconductor has a band energy sufficient for catalysis, but the kinetics of the reaction on the surface of the material are sluggish. In these cases a co-catalyst can be introduced onto the particle surface to accelerate product formation.[25,26] These strategies for augmenting particulate photocatalysts are illustrated in Figure 1-1 (right), where a scavenger is used to remove holes from the semiconductor valence band, and electrons are transferred from the conduction band to a co-catalyst that reduces protons to hydrogen.

Materials such as CdS, CdSe, WO_3, TiO_2, ZnO, and $SrTiO_3$ featured prominently in early studies of particulate photocatalysts, with Pt and RuO_2 often

employed as co-catalysts for the hydrogen and oxygen evolution reactions, respectively.[10,27] Today, cadmium chalcogenides remain a popular choice for the absorber material in photocatalyst studies due to the fact that their absorption spans the entire visible spectrum.[28,29] Noble metals such as platinum are still widely used as co-catalysts, however attention has increasingly been directed to the development of catalytic systems that instead use earth-abundant elements.[30,31] Pairing semiconductor nanocrystals with co-catalysts such as Co or Ni appears to be a promising avenue for the creation of scaleable particulate photocatalysts.[32–34]

1.3.1 Semiconductor Nanocrystal/Molecular Catalyst Hybrids

A notable area of contemporary research into particulate photocatalysts is the development of hybrid materials that integrate semiconductor nanocrystal absorbers with coordination complex catalysts. Coordination complexes provide well-defined active sites for catalysis that can be synthetically tuned to optimise activity, while their ligand spheres can be modified with functional groups to anchor the catalyst to the surface of semiconductors.[35–37] Some molecular catalysts are also highly efficient, operating with low overpotentials.[23,38] In a hybrid photocatalytic system, this would minimise energetic losses between photon absorption and product formation, resulting in a greater proportion of solar energy being stored. Additionally, many of the most efficient molecular catalysts for water splitting half-reactions are based on earth-abundant elements such as Co, Ni, or Fe, which enhances the attraction of incorporating these materials in hybrid photocatalysts.[23,39]

1.4 Semiconductor Nanocrystals

1.4.1 Evolution of Synthetic Methods

Early work with colloidal semiconductors in the 1980s was hampered by poor reproducibility, wide size distributions, and the natural tendency of particles towards aggregating.[40] Simple precipitation reactions were used which yielded particles of the desired material but produced bare crystallites that quickly degraded in solution.[41–43] By the early 1990s, inverse micelle syntheses had become the standard method for nanocrystal preparation.[44] In a typical synthesis, a metal salt dissolved in a polar solvent was dispersed in a non-polar solvent with the aid of a surfactant to form the inverse micelles. A dispersion of the second precursor was similarly prepared. Upon

combining the two dispersions, the micelles exchanged contents, forming the desired material within individual micelles. This encapsulation offered some protection against aggregation, provided the micelle remained intact.

Modern state-of-the-art routes for semiconductor nanocrystal synthesis evolved directly from inverse micelle syntheses.[45] Rather than forming micelles, surfactant molecules are used to form coordination complexes of precursors, enabling dissolution in organic solvents. These complexes are relatively stable and so require elevated temperatures react to form the desired semiconductor, which in turn requires high-boiling point solvents. Long-chain aliphatics are typically used for this purpose. To synthesise a cadmium chalcogenide semiconductor, the metal and chalcogen precursors prepared and heated separately. The reaction is initiated by injection of one solution into the other at elevated temperatures, hence these routes are referred to as "hot-injection" syntheses. After injection, small clusters nucleate as the precursors interact, forming bonds between precursors and displacing the coordinating surfactant ligands from the component atoms.[46] This growth process means that partially reacted precursors at the surface retain one or more ligands, which stabilise the growing cluster.[47] The surfactants introduced to the nanocrystal surface during synthesis are referred to as "native" ligands.[48,49] In contrast to particles synthesised by precipitation methods, nanocrystals prepared via hot-injection routes possess excellent long-term colloidal stability, on the order of months or years.[50] Hot-injection methods also produce nanocrystals with narrow size distributions, which facilitates rigourous study of size-dependent properties.[51]

1.4.2 The Ligand Shell

A critical step in the incorporation of hot-injection semiconductor nanocrystals into photocatalytic systems is the replacement of the aliphatic native ligands with hydrophilic molecules to permit dispersion of the particles in water. The most reliable method to perform a "ligand exchange" with cadmium chalcogenide semiconductors is to expose the nanocrystals to thiol molecules.[52–54] The thiol functional group binds strongly to cadmium atoms, displacing native ligands from the nanocrystal surface.[48] If there is a polar or ionic functional group on the thiol ligand molecule, e.g. a carboxylate, this will impart hydrophilicity to the nanocrystal, stabilising it in water or other polar solvents. In context of assembling hybrid

photocatalysts, ligand exchange provides the opportunity to introduce additional functionality to nanocrystals, such as anchoring a molecular catalyst to the surface.

Surface ligands have the potential to affect nanocrystals in ways beyond colloidal stability. Ligand molecules can induce or passivate surface defects, altering characteristics of nanocrystals such as photoluminescence or charge carrier lifetimes.[55,56] Some ligands are also capable of extensive electronic interaction with nanocrystals, resulting in significant changes in the optical absorption of particles or photoprotective effects.[57–59] In nanocrystal-based photocatalytic systems, the presence or absence of ligands can dictate the distribution of products generated under illumination.[60] Clearly, manipulation of the ligand shell is a powerful strategy to modulate the properties of semiconductor nanocrystals.

1.4.3 Quantum Dots

The work presented in this thesis was conducted using a specific class of semiconductor nanocrystals called "quantum dots" (QDs). These particles are roughly spherical in shape and have a physical radius comparable to the exciton Bohr radius of the constituent material. The exciton Bohr radius is a quantity that describes the spatial extent of an exciton, i.e. a quasi-particle that describes a hydrogen-like bound state of an electron and hole in a semiconductor. The exciton Bohr radius defines the scale at which quantum confinement effects begin to affect the overall properties of a semiconductor nanocrystal; in particular, when optical and electronic properties start to exhibit size-dependence. In CdS and CdSe, the semiconductors used throughout this work, the exciton Bohr radii are 2 nm and 4 nm, respectively.[61]

Quantum confinement arises from the spatial restriction imposed on charge carriers by the limited volume of a QD, wherein wavefunctions must drop to zero at the interface. As the dimensions of a QD become smaller relative to the excitonic Bohr radius, quantum confinement becomes more pronounced as a result of the increasing spatial restriction of the wavefunctions. This boundary condition also results in quantization of the energy levels that an electron or hole can occupy while residing in the QD. In practice, this means that features in the extinction spectra of QDs can be assigned to transitions between specific states in the semiconductor valence band and conduction band, illustrated in Figure 1-2.[62]

Carrier confinement in QDs has several practical implications in the context of photocatalysts that incorporate them as light absorbers. The first consideration is that the absorption of QDs can be tuned by synthesising particles of different sizes.[63] As the dimensions of particles decrease, the spacing between energy levels increases. In a photocatalytic system where electrons are transferred from QDs to a catalyst, an increase in the energetic offset between the donor and acceptor states can result in an acceleration of charge transfer and possibly of product formation.[64,65]

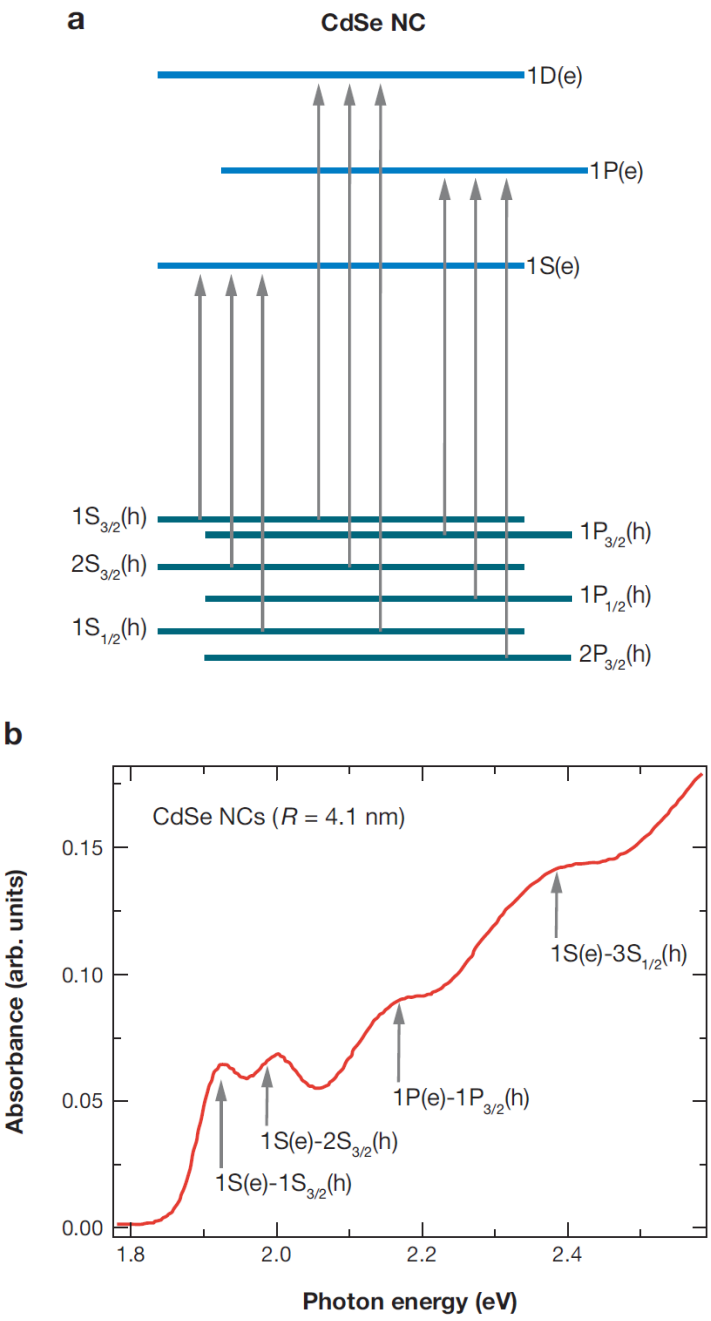

Figure 1-2. (a) Schematic representation of quantised energy levels in the valence and conduction bands of CdSe QDs; (b) Correlation of features in the extinction spectrum of CdSe QDs with transitions between specific states in the valence and conduction bands. Reproduced from Ref [62].

1.5 Transient Absorption Spectroscopy

Transient absorption spectroscopy (TAS) is a broad term encompassing any time-resolved pump-probe technique that monitors spectral evolution over time following excitation of a sample. In a typical experiment, two laser beams are directed onto the same region of a sample, with one serving to excite or "pump" the sample. The other beam is used to probe the excited state of the sample created by the pump pulse. A time zero is defined as the point when pump and probe pulses are both spatially and temporally overlapped, arriving at the same location on the sample at the same moment in time. In this case, the probe pulse interacts with the sample in its ground state, before excitation by the pump pulse induces any electronic changes. A transient spectrum is then accumulated by varying the time delay between the arrival of pump and probe pulses at the sample.

Pump pulses excite the sample, populating the upper states of electronic transitions accessible in the material. This process is referred to as "bleaching" because the pumped transition is no longer capable of light absorption, given the occupation of the upper state. Probe pulses with sufficient energy to excite the same transition are therefore not absorbed, and are transmitted through the sample to the spectrometer. Comparing the extinction of the ground states and excited states, the latter now absorbs less light. This represents a negative change in the absorbance, ΔA. In a transient absorption spectrum, a negative ΔA signal therefore signifies bleaching. Positive ΔA signals also arise in transient spectra, representing new transitions accessible from the electronically excited state or energetically shifted ground state transitions.

1.6 References

(1) McCrone, A.; Moslener, U.; d'Estais, F.; Grüning, C. *Global Trends in Renewable Energy Investment 2017*. Frankfurt School-UNEP Centre/BNEF. **2017**.

(2) Bleich, K.; Guimaraes, R. D. Renewable Infrastructure Investment Handbook: A Guide for Institutional Investors. World Economic Forum. **2016**.

(3) Lewis, N. S.; Nocera, D. G. Powering the Planet: Chemical Challenges in Solar Energy Utilization. *Proc. Natl. Acad. Sci. U. S. A.* **2006**, *103*, 15729–15735.

(4) Ciamician, G. The Photochemistry of the Future. *Science.* **1912**, *36*, 385–394.

(5) Nelson, N.; Ben-Shem, A. The Complex Architecture of Oxygenic Photosynthesis. *Nat. Rev. Mol. Cell Biol.* **2004**, *5*, 971–982.

(6) Bard, A. J.; Fox, M. A. Artificial Photosynthesis: Solar Splitting of Water to Hydrogen and Oxygen. *Acc. Chem. Res.* **1995**, *28*, 141–145.

(7) Fujishima, A.; Honda, K. Electrochemical Photolysis of Water at a Semiconductor Electrode. *Nature* **1972**, *238*, 37–38.

(8) Barsky, R. B.; Kilian, L. Oil and the Macroeconomy Since the 1970s. **2004**, *J. Econ. Perspect.* 18, 115–134.

(9) Bard, A. J. Photoelectrochemistry. *Science.* **1980**, *207*, 139–144.

(10) Grätzel, M. Artificial Photosynthesis: Water Cleavage into Hydrogen and Oxygen by Visible Light. *Acc. Chem. Res.* **1981**, *14*, 376–384.

(11) Gray, H. B.; Maverick, A. W. Solar Chemistry of Metal Complexes. *Science.* **1981**, *214*, 1201–1205.

(12) Hawecker, J.; Lehn, J. M.; Ziessel, R. Efficient Homogeneous Photochemical Hydrogen Generation and Water Reduction Mediated by Cobaloxime or Macrocyclic Cobalt Complexes. *Nouv. J. Chim.* **1983**, *7*, 271–277.

(13) Lazarides, T.; McCormick, T.; Du, P.; Luo, G.; Lindley, B.; Eisenberg, R. Making Hydrogen from Water Using a Homogeneous System without Noble Metals. *J. Am. Chem. Soc.* **2009**, *131*, 9192–9194.

(14) Karkas, M. D.; Verho, O.; Johnston, E. V.; Åkermark, B. Artificial Photosynthesis: Molecular Systems for Catalytic Water Oxidation. *Chem. Rev.* **2014**, *114*, 11863–12001.

(15) Hisatomi, T.; Takanabe, K.; Domen, K. Photocatalytic Water-Splitting Reaction from Catalytic and Kinetic Perspectives. *Catal. Letters* **2014**, *145*, 95–108.

(16) Fabian, D. M.; Hu, S.; Singh, N.; Houle, F. A; Hisatomi, T.; Domen, K.; Osterloh, F. E.; Ardo, S. Particle Suspension Reactors and Materials for Solar-Driven Water Splitting. *Energy Environ. Sci.* **2015**, *8*, 2825–2850.

(17) Cao, S.-W.; Liu, X.-F.; Yuan, Y.-P.; Zhang, Z.-Y.; Fang, J.; Loo, S. C. J.; Barber, J.; Sum, T. C.; Xue, C. Artificial Photosynthetic Hydrogen Evolution over g-C_3N_4 Nanosheets Coupled with Cobaloxime. *Phys. Chem. Chem. Phys.* **2013**, *15*, 18363–18366.

(18) Gimbert-Suriñach, C.; Albero, J.; Stoll, T.; Fortage, J.; Collomb, M.-N.; Deronzier, A.; Palomares, E.; Llobet, A. Efficient and Limiting Reactions in Aqueous Light-Induced Hydrogen Evolution System Using Molecular Catalysts and Quantum Dots Efficient and Limiting Reactions in Aqueous Light-Induced Hydrogen Evolution System Using Molecular Catalysts and Quantum Dots. *J. Am. Chem. Soc.* **2014**, *136*, 7655–7661.

(19) Huang, J.; Mulfort, K. L.; Du, P.; Chen, L. X. Photodriven Charge Separation Dynamics in CdSe/ZnS Core/Shell Quantum Dot/Cobaloxime Hybrid for Efficient Hydrogen Production. *J. Am. Chem. Soc.* **2012**, *134*, 16472–16475.

(20) Kalyanasundaram, K.; Borgarello, E.; Duonghong, D.; Gratzel, M. Cleavage of Water by Visible-Light Irradiation of Colloidal CdS Solutions; Inhibition of Photocorrosion by RuO_2. *Angew. Chem. Int. Ed. Engl.* **1981**, *20*, 987–988.

(21) Pinaud, B. A.; Benck, J. D.; Seitz, L. C.; Forman, A. J.; Chen, Z.; Deutsch, T. G.; James, B. D.; Baum, K. N.; Baum, G. N.; Ardo, S.; *et al.* Technical and Economic Feasibility of Centralized Facilities for Solar Hydrogen Production

via Photocatalysis and Photoelectrochemistry. *Energy Environ. Sci.* **2013**, *6*, 1983–2002.

(22) Smith, W. A.; Sharp, I. D.; Strandwitz, N. C.; Bisquert, J. Interfacial Band-Edge Energetics for Solar Fuels Production. *Energy Environ. Sci.* **2015**, *8*, 2851–2862.

(23) Blakemore, J. D.; Crabtree, R. H.; Brudvig, G. W. Molecular Catalysts for Water Oxidation. *Chem. Rev.* **2015**, *115*, 12974–13005.

(24) Berr, M. J.; Wagner, P.; Fischbach, S.; Vaneski, A.; Schneider, J.; Susha, A. S.; Rogach, A. L.; Jäckel, F.; Feldmann, J. Hole Scavenger Redox Potentials Determine Quantum Efficiency and Stability of Pt-Decorated CdS Nanorods for Photocatalytic Hydrogen Generation. *Appl. Phys. Lett.* **2012**, *100*, 223903.

(25) Yang, J.; Wang, D.; Han, H.; Li, C. Roles of Cocatalysts in Photocatalysis and Photoelectrocatalysis. *Acc. Chem. Res.* **2013**, *46*, 1900–1909.

(26) Wen, F.; Li, C. Hybrid Artificial Photosynthetic Systems Comprising Semiconductors as Light Harvesters and Biomimetic Complexes as Molecular Cocatalysts. *Acc. Chem. Res.* **2013**, *46*, 2355–2364.

(27) Hagfeldt, A.; Gratzel, M. Light-Induced Redox Reactions in Nanocrystalline Systems. *Chem. Rev.* **1995**, *95*, 49–68.

(28) Pietryga, J. M.; Park, Y. S.; Lim, J.; Fidler, A. F.; Bae, W. K.; Brovelli, S.; Klimov, V. I. Spectroscopic and Device Aspects of Nanocrystal Quantum Dots. *Chem. Rev.* **2016**, *116*, 10513–10622.

(29) Yu, W. W.; Peng, X. Formation of High-Quality CdS and Other II-VI Semiconductor Nanocrystals in Noncoordinating Solvents: Tunable Reactivity of Monomers. *Angew. Chem. Int. Ed. Engl.* **2002**, *41*, 2368–2371.

(30) Ran, J.; Zhang, J.; Yu, J.; Jaroniec, M.; Qiao, S. Z. Earth-Abundant Cocatalysts for Semiconductor-Based Photocatalytic Water Splitting. *Chem. Soc. Rev.* **2014**, *43*, 7787–7812.

(31) Reece, S. Y.; Hamel, J. A.; Sung, K.; Jarvi, T. D.; Esswein, A. J.; Pijpers, J. J. H.; Nocera, D. G. Wireless Solar Water Splitting Using Silicon-Based Semiconductors and Earth-Abundant Catalysts. *Science* **2011**, *334*, 645–648.

(32) Han, Z.; Qiu, F.; Eisenberg, R.; Holland, P. L.; Krauss, T. D. Robust Photogeneration of H_2 in Water Using Semiconductor Nanocrystals and a Nickel Catalyst. *Science* **2012**, *338*, 1321–1324.

(33) Simon, T.; Bouchonville, N.; Berr, M. J.; Vaneski, A.; Adrović, A.; Volbers, D.; Wyrwich, R.; Döblinger, M.; Susha, A. S.; Rogach, A. L.; *et al.* Redox Shuttle Mechanism Enhances Photocatalytic H_2 Generation on Ni-Decorated CdS Nanorods. *Nat. Mater.* **2014**, *13*, 1013–1018.

(34) Manzi, A.; Simon, T.; Sonnleitner, C.; Döblinger, M.; Wyrwich, R.; Stern, O.; Stolarczyk, J. K.; Feldmann, J. Light-Induced Cation Exchange for Copper Sulfide Based CO_2 Reduction. *J. Am. Chem. Soc.* **2015**, *137*, 14007–14010.

(35) Andreiadis, E. S.; Jacques, P.-A.; Tran, P. D.; Leyris, A.; Chavarot-Kerlidou, M.; Jousselme, B.; Matheron, M.; Pécaut, J.; Palacin, S.; Fontecave, M.; *et al.* Molecular Engineering of a Cobalt-Based Electrocatalytic Nanomaterial for H_2 Evolution under Fully Aqueous Conditions. *Nat. Chem.* **2012**, *5*, 48–53.

(36) Willkomm, J.; Muresan, N. M.; Reisner, E. Enhancing H_2 Evolution Performance of an Immobilised Cobalt Catalyst by Rational Ligand Design. *Chem. Sci.* **2015**, *6*, 2727–2736.

(37) Neri, G.; Walsh, J. J.; Wilson, C.; Reynal, A.; Lim, J. Y. C.; Li, X.; White, A. J. P.; Long, N. J.; Durrant, J. R.; Cowan, A. J. A Functionalised Nickel Cyclam Catalyst for CO_2 Reduction: Electrocatalysis, Semiconductor Surface Immobilisation and Light-Driven Electron Transfer. *Phys. Chem. Chem. Phys.* **2015**, *17*, 1562–1566.

(38) Razavet, M.; Artero, V.; Fontecave, M. Proton Electroreduction Catalyzed by Cobaloximes: Functional Models for Hydrogenases. *Inorg. Chem.* **2005**, *44*, 4786–4795.

(39) Coutard, N.; Kaeffer, N.; Artero, V.; Armaroli, N.; Balzani, V.; Gordon, R. B.; Bertram, M.; Graedel, T. E.; Vesborg, P. C. K.; Jaramillo, T. F.; *et al.* Molecular Engineered Nanomaterials for Catalytic Hydrogen Evolution and Oxidation. *Chem. Commun.* **2016**, *52*, 13728–13748.

(40) Alivisatos, A. P. Birth of a Nanoscience Building Block. *ACS Nano* **2008**, *2*, 1514–1516.

(41) Bawendi, M. G.; Steigerwald, M. L.; Brus, L. E. The Quantum Mechanics of Larger Semiconductor Clusters ("Quantum Dots"). *Annu. Rev. Phys. Chem.* **1990**, *41*, 477–496.

(42) Hotchandani, S.; Kamat, P. V. Charge-Transfer Processes in Coupled Semiconductor Systems. Photochemistry and Photoelectrochemistry of the Colloidal CdS-ZnO System. *J. Phys. Chem.* **1992**, *96*, 6834–6839.

(43) Kamat, P. V.; Dimitrijevic, N. M. Photoelectrochemistry in Semiconductor Particulate Systems. 13. Surface Modification of Cadmium Sulfide Semiconductor Colloids with Diethyldithiocarbamate. *J. Phys. Chem.* **1989**, *93*, 4259–4263.

(44) Pileni, M. P.; Motte, L.; Petitt, C. Synthesis of Cadmium Sulfide in Situ in Reverse Micelles: Influence of the Preparation Modes on Size, Polydispersity, and Photochemical Reactions. *Chem. Mater.* **1992**, *4*, 338–345.

(45) De Mello Donegá, C.; Liljeroth, P.; Vanmaekelbergh, D. Physicochemical Evaluation of the Hot-Injection Method, a Synthesis Route for Monodisperse Nanocrystals. *Small* **2005**, *1*, 1152–1162.

(46) Bullen, C. R.; Mulvaney, P. Nucleation and Growth Kinetics of CdSe Nanocrystals in Octadecene. *Nano Lett.* **2004**, *4*, 2303–2307.

(47) Yin, Y.; Alivisatos, A. P. Colloidal Nanocrystal Synthesis and the Organic-Inorganic Interface. *Nature* **2005**, *437*, 664–670.

(48) Anderson, N. C.; Hendricks, M. P.; Choi, J. J.; Owen, J. S. Ligand Exchange and the Stoichiometry of Metal Chalcogenide Nanocrystals: Spectroscopic Observation of Facile Metal-Carboxylate Displacement and Binding. *J. Am. Chem. Soc.* **2013**, *135*, 18536–18548.

(49) Knauf, R. R.; Lennox, J. C.; Dempsey, J. L. Quantifying Ligand Exchange Reactions at CdSe Nanocrystal Surfaces. *Chem. Mater.* **2016**, *28*, 4762–4770.

(50) Wang, W.; Banerjee, S.; Jia, S.; Steigerwald, M. L.; Herman, I. P. Ligand Control of Growth, Morphology, and Capping Structure of Colloidal CdSe Nanorods. *Chem. Mater.* **2007**, *19*, 2573–2580.

(51) Klimov, V. I.; McBranch, D. W.; Leatherdale, C. A.; Bawendi, M. G. Electron and Hole Relaxation Pathways in Semiconductor Quantum Dots. *Phys. Rev. B* **1999**, *60*, 13740–13749.

(52) Hines, D. A.; Kamat, P. V. Recent Advances in Quantum Dot Surface Chemistry. *ACS Appl. Mater. Interfaces* **2014**, *6*, 3041–3057.

(53) Murphy, C. J. CdS Nanoclusters Stabilized by Thiolate Ligands: A Mini-Review. *J. Clust. Sci.* **1996**, *7*, 341–350.

(54) Ben-Shahar, Y.; Scotognella, F.; Waiskopf, N.; Kriegel, I.; Dal Conte, S.; Cerullo, G.; Banin, U. Effect of Surface Coating on the Photocatalytic Function of Hybrid CdS-Au Nanorods. *Small* **2015**, *11*, 462–471.

(55) Baker, D. R.; Kamat, P. V. Tuning the Emission of CdSe Quantum Dots by Controlled Trap Enhancement. *Langmuir* **2010**, *26*, 11272–11276.

(56) Wuister, S. F.; Donega, C. D. M.; Meijerink, A. Influence of Thiol Capping on the Exciton Luminescence and Decay Kinetics of CdTe and CdSe Quantum Dots. *J. Phys. Chem. B* **2004**, *108*, 17393–17397.

(57) Frederick, M. T.; Weiss, E. A. Relaxation of Exciton Confinement in CdSe Quantum Dots by Modification with a Conjugated Dithiocarbamate Ligand. *ACS Nano* **2010**, *4*, 3195–3200.

(58) Tan, Y.; Jin, S.; Hamers, R. J. Influence of Hole-Sequestering Ligands on the Photostability of CdSe Quantum Dots. *J. Phys. Chem. C* **2013**, *117*, 313–320.

(59) Tan, Y.; Jin, S.; Hamers, R. J. Photostability of CdSe Quantum Dots Functionalized with Aromatic Dithiocarbamate Ligands. *ACS Appl. Mater. Interfaces* **2013**, *5*, 12975–12983.

(60) Kuehnel, M. F.; Wakerley, D. W.; Orchard, K. L.; Reisner, E. Photocatalytic Formic Acid Conversion on CdS Nanocrystals with Controllable Selectivity for H_2 or CO. *Angew. Chemie - Int. Ed.* **2015**, *54*, 9627–9631.

(61) Madelung, O. *Semiconductors: Data Handbook*; Springer-Verlag: Berlin, 2004.

(62) Klimov, V. I. Spectral and Dynamical Properties of Multiexcitons in Semiconductor Nanocrystals. *Annu. Rev. Phys. Chem.* **2007**, *58*, 635–673.

(63) Kovalenko, M. V; Manna, L.; Cabot, A.; Hens, Z.; Talapin, D. V; Kagan, C. R.; Klimov, X. V. I.; Rogach, A. L.; Reiss, P.; Milliron, D. J.; *et al.* Prospects of Nanoscience with Nanocrystals. *ACS Nano* **2015**, *9*, 1012–1057.

(64) Robel, I.; Kuno, M.; Kamat, P. V. Size-Dependent Electron Injection from Excited CdSe Quantum Dots into TiO_2 Nanoparticles. *J. Am. Chem. Soc.* **2007**, *129*, 4136–4137.

(65) Zhao, J.; Holmes, M. A.; Osterloh, F. E. Quantum Confinement Controls Photocatalysis: A Free Energy Analysis for Photocatalytic Proton Reduction at CdSe Nanocrystals. *ACS Nano* **2013**, *7*, 4316–4325.

2. EXPERIMENTAL

2.1 Overview

This chapter provides details of the materials and methods used in the experiments discussed in the chapters that follow. Synthetic and preparative protocols are grouped by chapter, and generally appear in the order in which they are mentioned in the text. A general methods section is also presented, which includes a detailed description of the ultrafast laser and transient absorption system used in Chapter 4 and Chapter 5. All reagents were purchased from Sigma-Aldrich or Fisher Scientific, unless otherwise noted, and used without further purification.

2.2 CdS QD/Cobaloxime Hybrid Photocatalysts (Chapter 3)

Cobaloxime complexes were prepared using the method of Trogler et al.[1] The ligand 4-pyridyl-phosphonic acid was gratefully received from another member of the group, Dr Gaia Neri.

2.2.1 Synthesis of $Co(dmgH)_2Cl_2$

1.35 g $CoCl_2 \cdot 6H_2O$ was dissolved in 150 mL acetone in a conical flask. 1.38 g dimethylglyoxime (2.1 molar equivalents) were then added to the flask, turning the solution from deep blue to a very dark purple. The flask was covered with aluminium foil and left to sit for 24 hours, after which dark green crystals had formed on the bottom of the flask. The remaining solution was decanted, and the crystals were collected by filtration, washed with acetone, and dried. 1.873 g were recovered at 91% yield. **^{1}H NMR** (400 MHz, DMSO-d_6) δ ppm 2.34 (s, 12H, -CH_3). **CHN microanalysis**: Calculated for $C_8H_{14}N_4O_4Cl_2Co$: C, 26.7; H, 3.9; N, 15.6 %. Found: C, 26.8; H, 4.1; N 15.5 %. **ESI-MS**: 289 [M^+-2Cl]. **ATR-FTIR** (ν, cm^{-1}): 1608 (w.), 1480 (br.), 1438, 1380, 1348, 1218 (br.), 1108, 1070.

2.2.2 Synthesis of $Co(dmgH)_2PyCl$, "CoPy"

127 mg $Co(dmgH)_2Cl_2$ was dispersed in 5 mL methanol by sonication for 10 minutes in a 10 mL round-bottomed flask. 50 µL triethylamine was added slowly with stirring. After 5 minutes, 30 µL pyridine was added. The solution was then heated to 40 °C. The solution was left to stir for 1 hour, then cooled to room temperature. 5 mL milliQ water was added and the flask was covered with foil and left unstirred to crystallise overnight. 65 mg of brown, needle-like crystals were recovered by filtration, with a 42% yield. **^{1}H NMR** (400 MHz, DMSO-d_6) δ ppm

8.04 (2H, d, py), 7.90 (1H, t, py), 7.47 (2H, t, py), 2.32 (12H, s, -C*H*$_3$). **CHN microanalysis**: Calculated for $C_{13}H_{19}N_5O_4ClCo$: C, 38.7; H, 4.7; N, 17.4 %. Found: C, 38.6; H, 4.7; N 17.4 %.

2.2.3 Synthesis of (Et_3NH)-[$CoCl(dmgH)_2$(pyridyl-4-hydrophosphonate)], "CoPyP"

54 mg $Co(dmgH)_2Cl_2$ was dispersed in 5 mL methanol with sonication. 21 µL triethylamine was then added. After stirring for 5 minutes, 24 mg pyridyl-4-phosphonic acid was added. The solution was then heated for one hour at 40 °C. After cooling, 10 mL ethyl acetate was added. The precipitate was collected by filtration, washed with ethyl acetate, and dried. 40 mg were recovered for a 55% yield. **^{1}H NMR** (400 MHz, D_2O) δ ppm 8.1 (2H, m, py), 7.55 (2H, m, py), 3.21 (6H, q, CH_3CH_2N), 2.43 (12H, s, -C*H*$_3$), 1.29 (9H, t, CH_3CH_2N); **^{31}P NMR** (162 MHz) 5.76 (1P, s, -*P*O(OH)$_2$); **CHN microanalysis**: Calculated for $C_{19}H_{35}N_6O_7ClCoP$: C, 39.0; H, 6.0; N, 14.4 %. Found: C, 35.6; H, 5.2; N 14.2 %.

2.2.4 Synthesis of $Co(dmgH)_2$(4-mercaptopyridine)Cl, "CoPyS"

75 mg $Co(dmgH)_2Cl_2$ was dispersed in 5 mL methanol with sonication. 30 µL triethylamine was added with stirring. 24 mg 4-mercaptopyridine was then added to the solution, resulting in the formation of a dark brown precipitate. The solid was collected by filtration and washed with methanol, followed by ethyl acetate. 65 mg product was collected (72% yield). **^{1}H NMR** (400 MHz, DMF-d_7) δ ppm 8.57 (2H, m, py), 7.88 (2H, m, py), 2.52 (12H, s, -C*H*$_3$). **CHNS microanalysis**: Calculated for $C_{13}H_{19}N_5SO_4ClCo$: C, 35.8; H, 4.4; N, 16.1; S, 7.4 %. Found: C, 35.0; H, 4.2; N 15.4; S, 7.4 %.

2.2.5 Synthesis of $Co(dmgH)_2$(4-methyl isonicotinate)Cl, "CoPyMe"

50 mg $Co(dmgH_2)Cl_2$ was dispersed in 5 mL methanol in a 10 mL round-bottomed flask. 18.2 µL triethylamine was added with stirring. After five minutes, 17.5 µL methyl isonicotinate was added. The temperature was then raised to 40 °C and maintained for one hour. Upon cooling the product began to crystallise. The solid was collected by filtration and washed with ethyl acetate. 25 mg were recovered for a 39% yield. **^{1}H NMR** (400 MHz, $CDCl_3$) δ ppm 8.46 (2H, m, py), 7.75 (2H, m, py), 3.93 (3H, s, -OC*H*$_3$), 2.40 (12H, s, -C*H*$_3$). **CHN microanalysis**:

Calculated for $C_{15}H_{21}N_5O_6ClCo$: C, 39.0; H, 4.6; N, 15.2 %. Found: C, 40.5; H, 6.1; N 13.6 %.

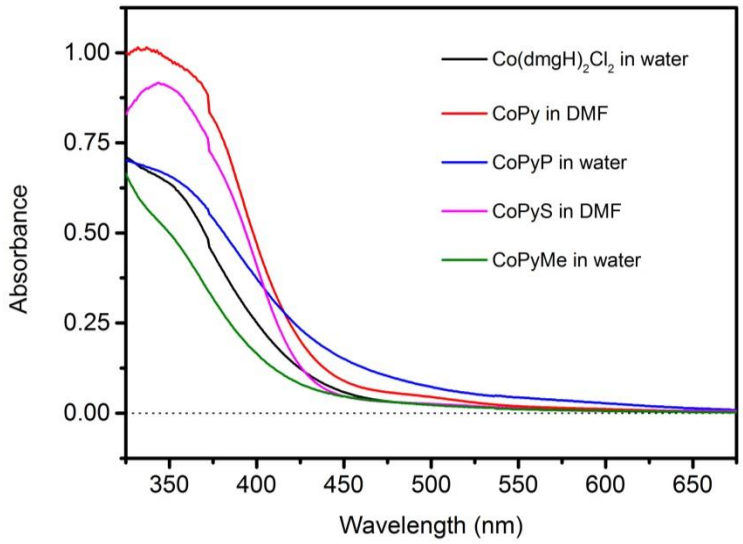

Figure 2-1 Extinction spectra of cobaloximes. 0.3 mM $Co(dmgH)_2Cl_2$; 0.5 mM CoPy; 0.7 mM CoPyP; 0.06 mM CoPyS; 0.5 mM CoPyMe.

2.2.6 Electrochemistry

Electrochemical characterisation of cobaloximes was performed with a PalmSens3 potentiostat (Alvatek). Measurements were conducted in a three-necked, pear-shaped flask using a glassy carbon working electrode, a platinum mesh counter electrode, and a silver wire quasi-reference electrode. Potentials were referenced against the ferrocene/ferrocenium (Fc/Fc^+) couple. Solutions with a volume of 10 mL were prepared in DMF with 0.1 M tetrabutylammonium hexafluorophosphate ($TBAPF_6$) as the supporting electrolyte and a cobaloxime concentration of 1 mM. Solutions were purged with argon for 30 minutes before measurement. The potential was varied at a scan rate of 100 mV/s. Blank scans were performed with the electrolyte before each experiment to confirm that no catalytically active material was present on the working electrode. Scans of the solutions containing each cobaloxime were then recorded. Next, a solution containing 1 molar equivalent (with respect to the concentration of cobaloxime) of the organic acid triethylammonium chloride (Et_3N-HCl) was injected into the flask before recording another scan to

assess the catalytic activity of the cobaloxime for proton reduction. Lastly, 0.5 mL ferrocene stock solution (3 mM) was injected into the flask and a final scan was performed.

2.2.7 Synthesis of CdS QDs

Prepared according to the method of Yu and Peng.[4]

57 mg cadmium oxide, 1.91 mL oleic acid, and 20.25 mL 1-octadecene were combined in a 50 mL three-necked flask fitted with a thermocouple and a septum and connected to a Schlenk line. These quantities, in combination with the growth time used here, yielded ~4 nm diameter QDs. The solution was vacuum degassed for 20 minutes at room temperature. In a separate two-necked flask fitted with a septum and connected to a Schlenk line, 6 mL 1-octadecene and 6 mL sulfur stock solution (77 mg sulfur dissolved in 60 mL 1-octadecene) were vacuum degassed for 20 minutes at room temperature. The flask containing the cadmium solution was then heated to 300 °C under nitrogen. After cooling to 250 °C and allowing the temperature to stabilise, 11.4 mL of the sulfur solution was steadily injected into the cadmium mixture with rapid stirring. The combined solution was re-heated and maintained in the range 245-255 °C for 6 minutes for particle growth. The heating jacket was then removed and the solution allowed to cool to room temperature.

To purify the QDs, the crude reaction mixture was split evenly between three centrifuge tubes (~11 mL each), to which 10 mL hexane was added, followed by 20 ml ethanol. The tubes were cooled at 4 °C for 1 hour, then centrifuged at 10800 rpm for 10 minutes. After discarding the clear supernatant, the yellow QD pellet was dissolved in 10 mL hexane, to which 20 mL ethanol was then added. The tube was refrigerated for 1 hour, then centrifuged at 10800 for 10 minutes. This step was repeated three times, with a stock solution of the QDs collected in 5 mL chloroform after the third cycle.

To validate the synthesis, transmission electron microscopy was used to image the resulting QDs. A representative micrograph is shown in Figure 2-2, acquired using a Jeol JEM-3010 microscope.

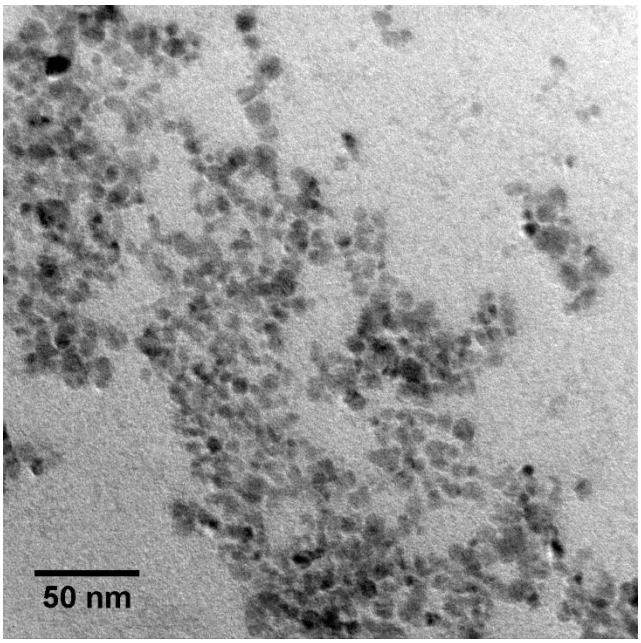

Figure 2-2. Transmission electron micrograph of CdS QDs.

After confirming by TEM that QDs had indeed been synthesised using this procedure, subsequent batches of QDs were characterised by UV-Vis spectroscopy. Formulae determined by Yu et al.[5] provide for the calculation of the average particle diameter (*D*, in nm) of CdS QDs using the wavelength of the maximum of excitonic absorption (λ, in nm) in the exctinction spectrum, and for the calculation of the QD extinction coefficient (ε) using the calculated diameter and the energy of the excitonic absorption (Δ*E*, in eV):

$$D = (-6.6521 \times 10^{-8})\lambda^3 + (1.9557 \times 10^{-4})\lambda^2 - (9.2352 \times 10^{-2})\lambda + (13.29)$$

$$\varepsilon = 5500\ \Delta E\ (D)^{2.5}$$

2.2.8 Phase Transfer of QDs to Water

QDs were transferred from organic solvent to water by performing a ligand exchange with hydrophilic thiols. In a typical procedure, 0.5 mL CdS QD stock solution in chloroform was diluted to 10 mL in the same solvent. An aqueous solution was then prepared consisting of 30 mg D,L-cysteine (or 28 µL 3-mercaptopropionic acid) in 10 mL milliQ water, and adjusted to pH 9 with tetramethylammonium hydroxide. The two solutions were then shaken together in a separatory funnel for 30 minutes, then allowed to equilibrate overnight. The aqueous

layer containing the QDs was collected and purified by successive concentration and dilution cycles in a Vivaspin 20 centrifugal filtration tube (MWCO 5,000). Samples were centrifuged at 8000 rpm for 60 minutes.

2.2.9 "Co-adsorption" Assembly of CdS QD/Cobaloxime Hybrid Photocatalysts

30 mg D,L-cysteine hydrochloride was dissolved in 10 mL milliQ water and adjusted to pH 9 with tetramethylammonium hydroxide. 10 mg cobaloxime (CoPyP or CoPyS) was dispersed in 10 mL milliQ water by sonication, and added to the cysteine solution. 0.5 mL CdS QD stock solution in chloroform was diluted to 10 ml, and shaken with the aqueous ligand solution for 30 min. The solution was left overnight to equilibrate. The aqueous phase was centrifuged at 8000 rpm for 10 minutes to remove undissolved cobaloxime. The yellow supernatant containing the hybrid photocatalysts was then centrifuged at 8000 rpm for 1 hour in a Vivaspin 20 centrifugal filtration tube. The eluent was discarded, and the concentrentrated filtrate was redispersed in milliQ water. The centrifugation process was repeated twice more, with the concentrate collected as a stock solution after the final cycle. The hybrid photocatalyst stock solution was stored under argon at 4 °C. The material was characterised by UV-Vis spectrscopy to determine the final concentration of QDs[5], and by ICP-OES to determine the cobaloxime concentration, the results of which are discussed in Chapter 3.

2.2.10 "In-situ" Assembly of CdS QD/Cobaloxime Hybrid Photocatalysts

1 mL CdS QD stock solution was diluted to 20 mL in chloroform. 60 mg D,L-cysteine hydrochloride was dissolved in 20 mL milliQ water and adjusted to pH 9 with tetramethylammonium hydroxide. The two solutions were shaken together in a separatory funnel for 30 minutes and left to equilibrate overnight. The QDs were purified by three successive cycles of concentration and dilution in Vivaspin 20 filtration tubes. Samples were centrifuged at 8000 rpm for 60 minutes. The final concentrate was collected in 10 mL milliQ water and used as a stock solution. The QD stock solution was stored under argon at 4 °C. Stock solutions of cobaloximes were prepared by dissolution of 15 mg in milliQ water. To dissolve CoPyS, the

solution was adjusted to pH 9 with tetramethylammonium hydroxide. The solutions were then analysed by ICP-OES to determine the precise cobalt concentration.

The photocatalyst solutions were prepared in the reactor vessel by combining stock solutions of QDs, cobaloximes, and sodium sulfite with milliQ water . The volume of cobaloxime stock solution added to the reactor was varied to achieve the desired catalyst concentration, with the volume of water adjusted accordingly to maintain a constant solution volume in all experiments.

2.2.11 DMATP-functionalised CdS QDs

A stock solution of 4-dimethylaminothiophenol (DMATP) was prepared by dissolving 0.8 mg in 1.7 mL chloroform (~3.3 mM). 0.5 mL CdS QD stock solution in chloroform was diluted to 5 mL, followed by addition of 250 µL DMATP stock solution, such that the ratio of DMATP:QDs was approximately 25:1. The solution was then left stirring overnight. After equilibrating, the QDs were flocculated by addition of methanol and centrifuged for 10 minutes at 8000 rpm. The supernatant containing excess DMATP and displaced ligands was discared, and the QD pellet was redispersed in 0.5 mL chloroform and used for assembly of hybrid photocatalysts as described above using the "co-adsorption" method.

2.2.12 Hydrogen Evolution Measurements

The reactor vessel (Starna Cells) for photocatalytic hydrogen evolution is pictured below in Figure 2-3. Two septum caps permitted sampling of the internal headspace by syringe. Both ends of the vessel were quartz glass. The vessel was 5 cm in length, with a diameter of 2.5 cm. The total internal volume was 18.2 mL.

Figure 2-3. Vessel for photocatalytic hydrogen evolution experiments.

All photocatalyst solutions were prepared to a volume of 7 mL and OD 1.5 (as measured at the wavelength of the band-edge absorption maximum) over the 5cm pathlength of the reactor vessel, as measured at the excitonic absorption of the QDs. Samples were illuminated with a 450 W FL-1039 Xe source (Horiba Scientific), fitted with a cooled IR filter to minimise heating of the sample. The lamp light was further attenuated using a band-pass filter (430 ± 70 nm). The spectrum of the filtered lamp output reaching the sample, as measured by a USB2000+XR1 spectrometer (Ocean Optics), is shown in Figure 2-4, overlaid with the extinction spectrum of a typical CdS QD sample for comparison. A PM100A power meter with a S302C thermal sensor (Thorlabs) was used to ensure equal incident power (30 mW/cm^2) on the reactor vessel in each experiment.

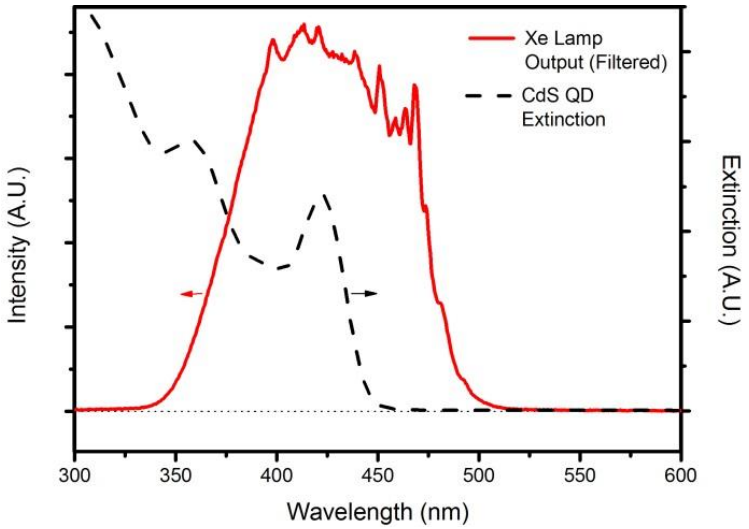

Figure 2-4. Spectrum of filtered lamp light used to illuminate photocatalyst samples. CdS QD extinction spectrum included for comparison.

In a typical hydrogen evolution experiment, the Xe lamp was switched on and allowed to stabilise for 30 minutes, during which time the vessel containing the photocatalyst solution was thoroughly purged with argon. The output of the lamp was then shielded while the vessel was positioned. A baseline was then established by extracting an aliquot of the vessel headspace for analysis to confirm the absence of air and hydrogen. The shielding was then removed from the lamp, and the sample was illuminated for 8 hours with constant stirring by a small magnetic stirrer inside the vessel. The headspace was then sampled periodically, typically at hourly intervals.

The composition of the reactor headspace was analysed by gas chromatography (GC) using a 436-GC (Scion Instruments) fitted with a BRP 81025 column (Bruker) packed with 5 Å molecular sieves. The carrier gas was argon. Hydrogen, oxygen, and nitrogen were quantified by a thermal conductivity detector. The detector response was calibrated using a commercial gas mixture (Scientific and Technical Gases Ltd) which contained 1 ± 0.02 % each of hydrogen, oxygen, and nitrogen in argon.

2.3 Hydrophilic Aminothiols as Ligands for CdSe QDs (Chapter 4)

2.3.1 Synthesis of CdSe QDs

Prepared according to the method of Yu and Peng.[4]

57 mg CdO, 4.27 mL oleic acid, and 17.88 mL 1-octadecene were combined in a three-necked, round-bottomed flask fitted with a thermocouple, a septum, connected to a Schlenk line and vacuum degassed for 20 min at room temperature, then for 20 min at 100 °C. The flask was then heated to 300 °C under N_2, and cooled to 250 °C. In a separate two-necked round-bottomed flask fitted with a septum and connected to a Schlenk line, 6 mL 1-octadecene and 6 mL selenium stock solution (190 mg Se powder and 1.2 mL tri-n-octylphosphine dissolved in 60 mL 1-octadecene) were degassed for 30 min at room temperature. 11.4 mL Se solution was then steadily injected into the hot Cd precursor solution. The temperature was maintained in the range 245-255 °C for 5 minutes for particle growth. The heating jacket was then removed and the solution allowed to cool to room temperature. The QDs were purified using the method previously described for CdS QDs in the Chapter 3 section above, i.e. successive flocculation with ethanol, centrifugation, and redispersion in hexane. A stock solution of CdSe QDs was collected in 5 mL chloroform.

As for the CdS QDs above, the QDs were characterised by UV-Vis spectroscopy to determine the size and concentration of QDs using the formulae determined by Yu et al.[5] for CdSe QDs (where D and λ have units of nm):

$$D = (1.6122 \times 10^{-9})\lambda^4 - (2.6575 \times 10^{-6})\lambda^3 + (1.6242 \times 10^{-3})\lambda^2 - (0.4277)\lambda + (41.57)$$

$$\varepsilon = 1600\ \Delta E\ (D)^3$$

2.3.2 DMATP-Functionalisation of CdSe QDs in Chloroform

To prepare samples with various QD:DMATP ratios, a concentrated solution of DMATP was prepared in chloroform. CdSe QD stock solution was then diluted, and divided equally among separate vials. Based on the OD of the solution (i.e. the QD concentration), an appropriate volume of ligand solution was then added to each vial of CdSe QDs. Chloroform was then added as needed to achieve a consistent

concentration of QDs in each sample. The solutions were left to equilibrate overnight. The samples were prepared with QD:DMATP ratios of 1:0 (control), 1:1, and 1:5.

2.3.3 Phase Transfer of CdSe QDs with Aminothiol Ligands

To prepare the hydrochloride salt of a given aminothiol ligand, 2-aminoethanethiol or 4-aminothiophenol was dissolved in a minimum volume of ethanol. To this solution, 1.1 molar equivalents of concentrated hydrochloric acid were added. The ethanol was then evaporated slowly, yielding the crystalline HCl salt. In a typical ligand exchange, 1 mmol of ligand salt was dissolved in 3 mL of water and shaken with 150 µL CdSe QD stock solution diluted to 3 mL in chloroform. The aqueous phase was separated and purified by centrifugation in a Vivaspin 20 filtration tube. The QD concentrate was then redispersed in milliQ water and adjusted to pH 3 with HCl or tetramethylammonium hydroxide as needed to create a stock solution.

2.3.4 Sample Preparation for Transient Absorption Spectroscopy

Stock solutions of AET QDs or ATP QDs were diluted to OD 0.5 with milliQ water. A total volume of 360 µL was transferred to a cuvette fitted with a septum and degassed with argon. To collect spectra of the QDs in the presence of the electron scavenger methyl viologen, concentrated stock solutions of the scavenger were prepared and added to the QD solution to minimise sample dilution. Similarly, a stock solution of ascorbic acid was prepared with a concentration of 1 M, such that addition of 40 µL to the cuvette would achieve a concentration of 0.1 M. When methanol was used, 40 µL was added to achieve 10% v/v concentration.

2.4 Hydrophilic Dithiocarbamates as Ligands for CdSe QDs (Chapter 5)

2.4.1 Synthesis of CdSe QDs

The same general procedure was used as previously described for the CdSe QD synthesis in the Chapter 4 section. To achieve the different sizes of QDs used in the experiments discussed in Chapter 5, the concentration of oleic acid in the cadmium precursor flask, and the particle growth time, were varied as follows:

2.5 nm QDs: 57 mg CdO, 0.427 mL oleic acid, 21.9 mL 1-ODE
2 minutes growth time at 250 °C

3.5 nm QDs: 57 mg CdO, 0.427 mL oleic acid, 21.9 mL 1-ODE
6 minutes growth time at 250 °C

4.5 nm QDs: 57 mg CdO, 4.27 mL oleic acid, and 17.88 mL 1-ODE
5 minutes growth time at 250 °C

2.4.2 Ligand Exchange Procedure

To prepare dithiocarbamate ligand solutions, 360 mg tetramethylammonium hydroxide was dissolved in 1.5 mL methanol, followed by 1 mmol of either β-alanine or 4-aminobenzoic acid. 80 µL carbon disulfide was then added dropwise to the amine solution with rapid stirring. MPA ligand solutions were prepared by adding 1 mmol of the thiol to a solution of 180 mg TMAH in 1.5 mL MeOH. Ligand exchanges were performed by dropwise addition of 300 µL CdSe QD stock in chloroform to the desired ligand solution with rapid stirring at ~0 °C. After equilibration for 3-4 hours, the QD solution was diluted with milliQ water to 4 mL total volume and shaken with 2 mL chloroform to extract displaced hydrophobic ligands. The aqueous phase was then purified by concentration in Vivaspin 20 filtration tubes by centrifugation at 8000 rpm for 60 minutes to remove excess ligand and amine precursor impurities from the dithiocarbamate synthesis. The QD concentrate was then diluted to 2 mL volume with milliQ water. Stock solutions of QDs were adjusted to pH 9 using tetramethylammonium hydroxide or HCl as necessary.

2.4.3 Sample Preparation for Transient Absorption Spectroscopy

Stock solutions of Ala-DTC QDs, AmBz-DTC QDs, and MPA QDs were diluted to OD 0.6 with milliQ water A total volume of 360 µL was transferred to a cuvette fitted with a septum and degassed with argon. To collect spectra of the QDs in the presence of a hole scavenger, 40 µL of a concentrated stock solution (e.g. 1 M sodium sulfite) was added to 0.1 M.

2.5 General Methods

2.5.1 Steady-State Optical Measurements

Extinction spectra were collected on a Shimadzu UV-2600 spectrophotometer in 10 mm path length quartz cuvettes. FT-IR measurements were performed on a Bruker Vertex spectrometer in attenuated total reflectance (ATR) mode. Photoluminescence measurements were carried out on a Perkin Elmer LS 55 fluorescence spectrometer. For comparison of emission yields, samples were prepared to the same optical density, as measured at the wavelength of the band edge absorption feature maximum.

2.5.2 Compositional Measurements

ICP-OES (Ciros Vision by SPECTRO Analytical Instruments, Inc.), ESI-MS (Micromass LCT by Waters Corp.), and CHNS elemental microanalysis (vario MICRO cube by Elementar Analysensysteme GmbH) were conducted by Analytical Services based in the Department of Chemistry at the University of Liverpool.

2.5.3 Transient Absorption Spectroscopy

Femtosecond laser pulses were produced by a PHAROS laser head (Light Conversion, Ltd) using Yb:KGW as the active medium, operated at a repetition rate of 10 kHz. Pulses had a wavelength of 1030 ± 3 nm and a duration of 280 fs at FWHM. An ORPHEUS optical parametric amplifier (Light Conversion, Ltd) in tandem with a LYRA harmonic generator (Light Conversion, Ltd) produced the desired wavelength for sample excitation. Pump beam intensity was adjusted with a continuosly variable neutral density (N.D.) filter to achieve pulse energies of ~10 nJ/pulse, as measured with a Vega laser power and energy meter in conjunction with a 3A-P thermal power/energy sensor (Ophir Photonics). A portion of the PHAROS

output was also used to pump a Ti:sapphire crystal to generate a white light continuum for the probe beam, which provided for spectral observation in the region 475-900 nm. The probe beam was focused on the sample to a spot size of ~100 μm diameter and was overlapped completely by the pump beam, which had a spot size of ~500 μm diameter. Spectra were acquired with a HELIOS transient absorption system (Ultrafast Systems, LLC) with a response time of ~400 fs (~1.5x the laser pulse length). The layout of the optical components of the HELIOS is shown in Figure 2-5. Datasets were collected by randomly stepping the variable optical delay line and averaging the signal for 1 s at each delay time. Samples were measured in a 2 mm path length quartz cuvette fitted with a rubber septum and magnetically stirred. Transient spectra were chirp-corrected using the commercial Surface Xplorer (Ultrafast Systems, LLC) software package.

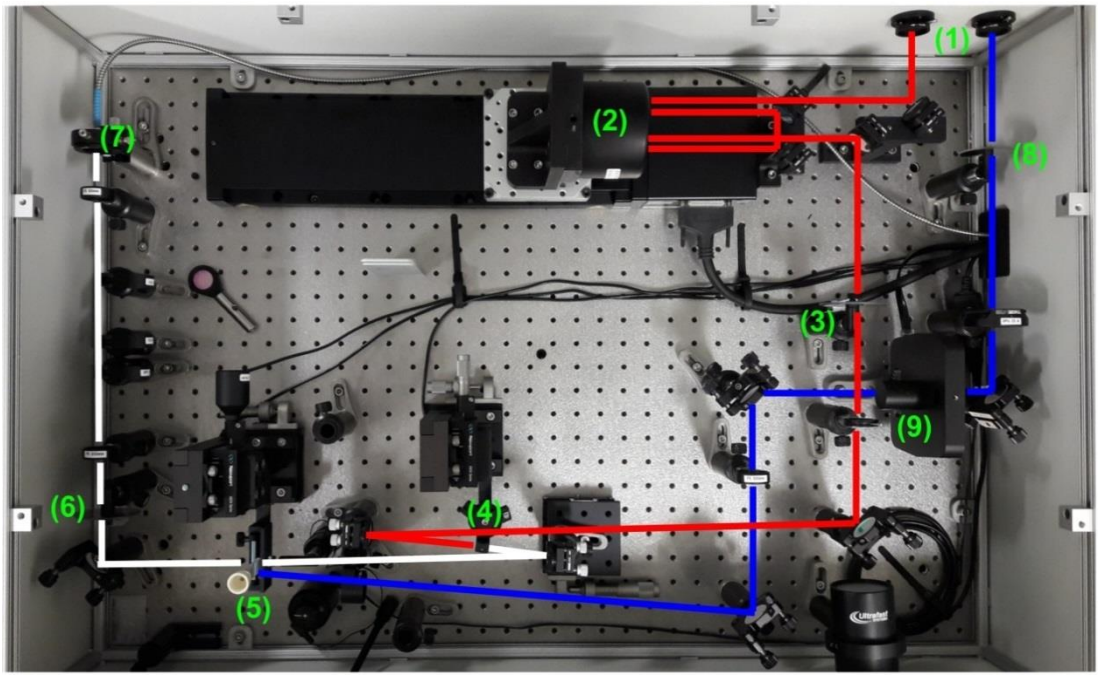

Figure 2-5. Photograph of the Helios transient absorption bench, with beam paths indicated and significant components numbered.

(Blue) Pump beam

(Red) PHAROS output beam

(White) Probe beam

(1) Inlet apertures from laser system

(2) Variable optical delay line

(3) Continuously variable N.D. filter

(4) Ti:sapphire crystal

(5) Sample stage

(6) Continuously variable N.D. filter

(7) Fiber optic to spectrometer

(8) Continuously variable N.D. filter

(9) Beam chopper

2.6 References

(1) Trogler, W. C.; Stewart, R. C.; Epps, L. A.; Marzilli, L. G. Cis and Trans Effects on the Proton Magnetic Resonance Spectra of Cobaloximes. *Inorg. Chem.* **1974**, *13*, 1564–1570.

(2) Lakadamyali, F.; Reisner, E. Photocatalytic H_2 Evolution from Neutral Water with a Molecular Cobalt Catalyst on a Dye-Sensitised TiO_2 Nanoparticle. *Chem. Commun.* **2011**, *47*, 1695–1697.

(3) Du, P.; Schneider, J.; Luo, G.; Brennessel, W. W.; Eisenberg, R. Visible Light-Driven Hydrogen Production from Aqueous Protons Catalyzed by Molecular Cobaloxime Catalysts. *Inorg. Chem.* **2009**, *48*, 4952–4962.

(4) Yu, W. W.; Peng, X. Formation of High-Quality CdS and Other II-VI Semiconductor Nanocrystals in Noncoordinating Solvents: Tunable Reactivity of Monomers. *Angew. Chem. Int. Ed. Engl.* **2002**, *41*, 2368–2371.

(5) Yu, W. W.; Qu, L.; Guo, W.; Peng, X. Experimental Determination of the Extinction Coefficient of CdTe, CdSe, and CdS Nanocrystals. *Chem. Mater.* **2003**, *15*, 2854–2860.

3. CdS QD/Cobaloxime Hybrid Photocatalysts for Hydrogen Generation

3.1 Overview

This chapter reviews attempts to create hybrid photocatalysts for hydrogen production by interfacing cobaloxime molecular catalysts with CdS quantum dots. Anchoring group effects have been reported in dye-sensitised solar cells, where the functional group binding a dye to the porous oxide electrode influences the overall device behaviour.[1–3] Cobaloximes were therefore synthesised which possessed either thiol or phosphonate functional groups for binding to the QDs. It was thought that the strong linkage formed between thiols and CdS might result in accelerated electron transfer from the QDs to the molecular catalysts, and that this could manifest as a more active photocatalytic system.

Electrochemical measurements were conducted to determine the reduction potentials of the complexes and to confirm their catalytic activity for proton reduction. Upon combining the cobaloximes with CdS QDs and a hole scavenger in water, hydrogen evolution was observed under illumination. The hydrogen evolution behaviour varied significantly between batches, so numerous experiments were conducted to explore the origin of this inconsistency which are discussed throughout this chapter. These studies conclude that the cobaloximes likely act as pre-catalysts which decompose on the QD surface under illumination to form an uncharacterised active species. Additionally, the cysteine ligands which colloidally stabilise the QDs are removed under illumination, leading to particle aggregation. While investigating methods to prevent QD aggregation, partial removal of the ligands was found to be essential to hydrogen evolution. Some of the strategies explored to control ligand oxidation are then discussed, the results of which motivated the work presented in subsequent chapters.

3.2 Introduction

3.2.1 Cobaloximes as Proton Reduction Catalysts

Cobaloximes were popularised in the 1960s as model compounds for studying the organometallic chemistry of the cobalt centre in vitamin B_{12}.[4–6] The name is a portmanteau of the two general defining characteristics of this family of complexes, namely a cobalt centre with ligands coordinated via oxime functional groups. By the

late 1970s, it was known that cobaloximes could be protonated by strong acids to form hydrides, which would subsequently evolve hydrogen.[7] In 1983, Hawecker et al. reported homogeneous photochemical hydrogen evolution from nonaqueous solvent using $[Ru(bipy)_3]^{2+}$ as a sensitiser.[8] Shortly thereafter, a 1986 study by Connolly and Espenson demonstrated that a cobaloxime catalysed the oxidation of Cr(II), Eu(II), and V(II) resulting in significant hydrogen evolution.[9]

Following the structural characterisation of the active sites of Fe-Fe and Ni-Fe hydrogenase enzymes and subsequent attempts to recreate some of their activity with model complexes, interest in cobaloximes as hydrogen evolution catalysts intensified. In 2005, Razavet et al. were first to report an electrochemical study of several cobaloximes as functional models for hydrogenases, employing the prototypical cobaloxime, $Co(dmgH)_2(Py)Cl$ and two analogues bearing *para*-functionalised pyridine ligands.[10] Later that year, workers in the groups of Peters and Lewis published a similar study investigating electrocatalytic hydrogen evolution by BF_2-bridged cobaloximes.[11] Both studies were conducted in organic solvents and used strong acids as proton sources.

Given the electrochemical activity of cobaloximes for hydrogen evolution, they were obvious candidates for photochemical systems. In 2008, a paper from the Artero group reported a system incorporating cobaloximes and Ru(bipy) chromophores into heterobinuclear complexes for hydrogen production.[12] The catalysts were active under non-aqueous conditions, but interestingly the performance of the system diminished when water was used as a proton source. It is therefore interesting that a contemporaneous report from Du et al. demonstrated efficient photochemical hydrogen evolution using two different cobaloximes and a Pt sensitiser in 3:2 $MeCN:H_2O$ (v/v) with TEOA as a sacrificial electron donor, achieving twice the turnover of the Artero system.[13] Evidently, the catalytic activity of cobaloximes is highly sensitive to the conditions under which they are studied. Homogeneous photocatalytic hydrogen production by a cobaloxime was also shown using the organic dye Eosin Y as the sensitiser in 1:1 $MeCN:H_2O$ (v/v), which removed expensive noble metals from the system altogether.[14]

In 2011, Lakadamyali and Reisner reported hydrogen evolution from neutral water by immobilising cobaloximes and ruthenium dyes on TiO_2 nanoparticles via phosphonate anchoring groups.[15] Under visible light and in the presence of a hole scavenger, TEOA, the photoexcited sensitiser injected electrons into the TiO_2, which were subsequently transferred to the cobaloxime to drive proton reduction. The activity of this system under visible light is noteworthy, however the efficiency of the system doubled upon direct excitation of the TiO_2 with UV light in the absence of the dye. Eliminating electron injection from a sensitiser to a scaffold, along with the associated loss pathways, might therefore improve the performance of a hybrid catalytic system. Immobilised cobaloximes have since been extensively studied by the Reisner group in both particulate and electrode systems.[16–20]

Narrow band gap semiconductors that absorb visible light have also been used as sensitisers for cobaloximes in photocatalytic systems. A 2011 study by Wen et al. investigated cobaloximes with either pyridine, 4-dimethylaminopyridine, or 2-mercaptopyridine as axial ligands in combination with bulk CdS nanoparticles for hydrogen evolution from DMF and MeCN using TEOA as a hole scavenger.[21] The thiol-substituted cobaloxime was found to be the most active, which the authors speculated was a result of improved binding to the CdS particles. Given that the substituent is at the 2-position of the pyridine ligand, however, it seems unlikely that it could interact with the CdS surface.

The following year, Huang et al. published a transient absorption study demonstrating electron transfer from CdSe/ZnS core/shell QDs to a phosphonate-functionalised cobaloxime in toluene.[22] In the same study, hydrogen evolution was also reported from the QD/cobaloxime assembly when triethylamine hydrochloride and TEOA were added as a proton source and hole scavenger, respectively. The activity of the system was likely aided by the insolubility of the cobaloxime in toluene, ensuring that the catalyst remained confined at the QD surface. This study also highlights an issue commonly encountered in the literature, where studies of photocatalytic materials are performed under conditions very different from those used for hydrogen generation, limiting their applicability. In this case, transferring the CdSe/ZnS core/shell QDs to water, a more appropriate solvent for proton reduction, would fundamentally change the behaviour of the system. Gimbert-Suriñach et al. used CdTe QDs as sensitisers for the

same phosphonate-functionalised cobaloxime and another macrocyclic cobalt catalyst in water with ascorbate as a hole scavenger, but found the cobaloxime to be minimally active under their conditions.[23] CdSe QDs have also been used as sensitisers for cobaloximes, with both materials grafted to a p-type NiO photoelectrode for hydrogen production from water.[24]

3.2.2 Interfacing Molecular Catalysts with QDs

To assemble a semiconductor nanocrystal-molecular catalyst hybrid photocatalyst, integration of the light absorption and scaffold functions would be achieved by using semiconductor QDs with energy gaps in the visible region. For cadmium and zinc chalcogenide materials, post-synthetic ligand exchanges are typically performed using thiol molecules, especially to achieve phase transfer to polar solvents after hot-injection syntheses. The thiol group binds tightly to these materials, serving as an anchoring group, while judicious selection of the functionality elsewhere on the ligand molecule imparts the desired property (e.g. solubility). Exploiting the thiol linkage to achieve a ligand shell with both stabilising and catalytic components was therefore an attractive option. These thiol-immobilised catalysts could then be compared to species bearing phosphonate groups, which would be more labile in binding to nanocrystals.

Cobaloximes for catalytic hydrogen evolution have typically been prepared with an axial pyridine ligand, which improves catalytic activity but also provides a straightforward means of introducing a functional group to the catalyst.[10,25] To introduce a given functional group to the cobaloxime, a pyridine bearing the desired substituent is simply combined with the $Co(dmgH)_2Cl_2$ precursor during synthesis, displacing one of the chloride ligands. The nitrogen atom in the pyridine ring coordinates to the cobalt centre, leaving functional groups in the *meta* and *para* positions facing outwards.

A cobaloxime with a phosphonate anchoring group, $[CoCl(dmgH)_2$(pyridyl-4-hydrophosphonate)$][Et_3NH]$, "CoPyP", was synthesised according to the method of Lakadamyali et al.[15] The thiol analogue, $CoCl(dmgH)_2$(4-mercaptopyridine), "CoPyS", was prepared by the same method. The structures of these cobaloximes are shown in

Figure 3-1. The complexes were characterised by NMR and elemental (CHNS) microanalysis, the results of which are described in Chapter 2.

3.3 Electrochemical Measurements of Cobaloximes

To confirm the catalytic activity of the prepared cobaloximes, cyclic voltammograms (CVs) of the complexes were recorded in DMF. Ferrocene (Fc) was used as an internal reference standard, such that all potentials are measured against that of the ferrocene (II/III) redox couple, which appears at E = 0.450 V vs SCE in DMF).[26] To provide a point of comparison, the classic cobaloxime $Co(dmgH)_2(Py)Cl$ was also included in the electrochemical experiments, which was prepared according to the method of Schrauzer.[27]

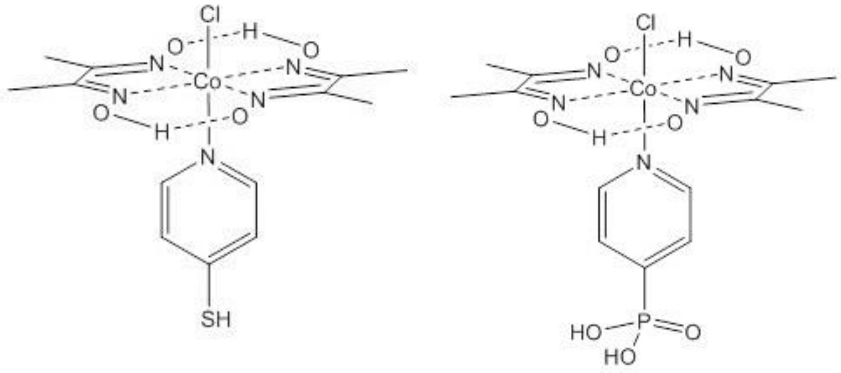

Figure 3-1. Structures of cobaloxime complexes with thiol (CoPyS) or phosphonate (CoPyP) anchoring groups for adsorption to CdS QDs.

Figure 3-2 illustrates the redox behaviour of the cobaloximes (black traces). As the potential is swept cathodically, peaks appear at -0.9 V and -1.5 V vs Fc/Fc^+. The cobalt centre of cobaloximes has a starting oxidation state of +3, so these features correspond to Co(III/II) and Co(II/I) reduction processes, respectively. The measured reduction potentials are in good agreement with published values for CoPy[10], CoPyP[17], and CoPyS[25]. The peak associated with the oxidative process for the Co(III/II) couple is shifted by ~700 mV relative to the reductive process for the complexes, as observed by other researchers, who ascribed this to irreversible loss of the axial halide ligand.[10] The

reversibility of the Co(II/I) process varies between the complexes. For CoPy, a clear oxidative peak appears when the scan direction reverses, however the equivalent current responses are much weaker in the voltammograms of CoPyP and CoPyS. This observation implies that the initial electrochemical state of these cobaloximes is not fully regenerated after the anodic sweep, which may indicate some degradation of the complexes.

It is worth noting that, despite bearing axial pyridine ligands with substituents of varying electron donating or withdrawing ability, there is little variation in the reduction potentials of the three cobaloximes, consistent with previous studies.[10,28] Rather than shifting the potentials of the cobaloxime redox couples, the pyridine ligands affect the kinetics of hydrogen evolution. Electron donating axial ligands increase the pK_a of the protonated hydride intermediate, which leads to faster catalytic turnover.[25] Modification of the equatorial ligand structure (e.g. replacement of methyl groups with phenyl groups, introduction of difluoroborate bridges) is required to significantly shift cobaloxime redox potentials.[11]

Rigorous drying of the solvent was not undertaken before electrochemical measurements. DMF is hygroscopic, so small amounts of water were likely to be present, however significant currents from proton reduction are not observed in these CVs. To observe proton reduction, and therefore to confirm the suitability of these materials for hydrogen evolution in hybrid photocatalysts, a source of protons is required. For this purpose, one molar equivalent of the organic acid triethylamine hydrochloride (Et_3N-HCl, also triethylammonium chloride) was introduced to the solution after the initial scans of each cobaloxime. As shown by the red traces in the CVs, clear current enhancements are visible at potentials corresponding to the Co(II/I) couple for all three cobaloximes, a strong indication of catalytic proton reduction. Current enhancement at the potential of the Co(II/I) couple is consistent with the proposed mechanism for hydrogen evolution by cobaloximes in which the Co(I) species is protonated to form a Co(III) hydride which subsequently evolves hydrogen.[29,30]

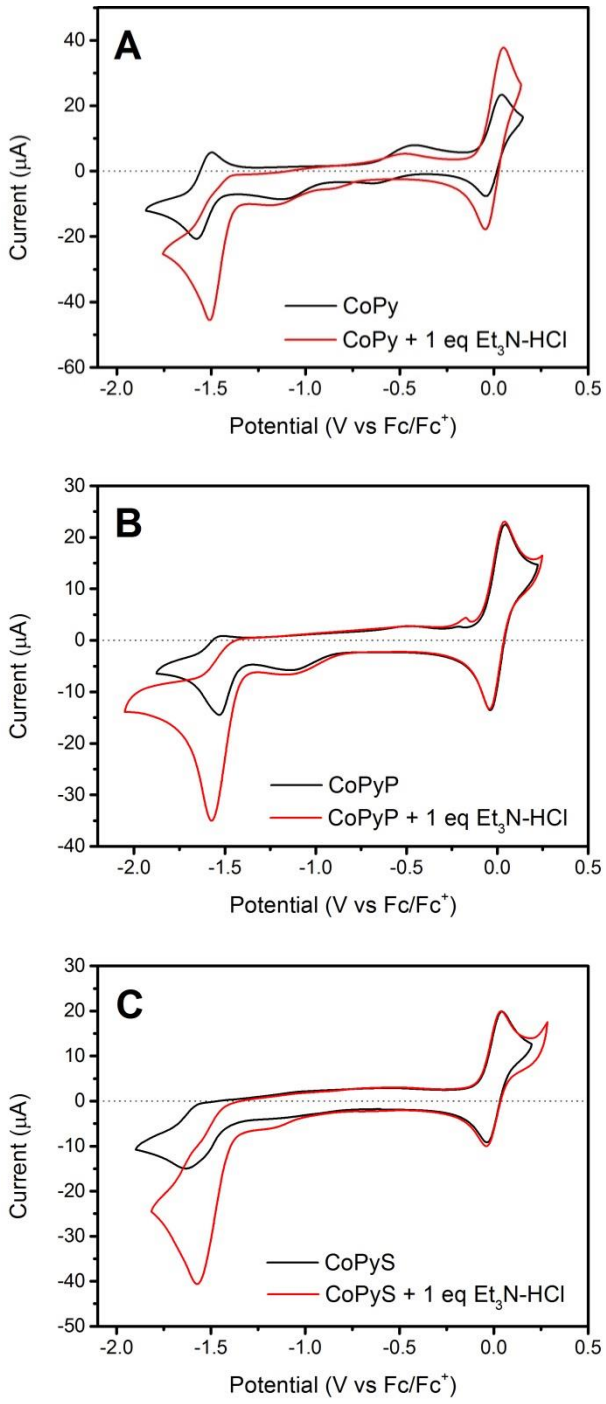

Figure 3-2. Cyclic voltammograms of cobaloximes recorded in DMF with 0.1 M $TBAPF_6$, electrolyte, scan rate 100 mV/s, glassy carbon WE, Pt mesh CE. 1 mM catalyst. Potentials referenced against the ferrocene/ferrocenium (Fc/Fc^+) couple which appears in these voltammograms as the reversible peak centred at 0 V. Triethylammonium chloride was used as a proton source.

3.4 Preparation of QD/Cobaloxime Hybrid Photocatalysts

After confirming the electrochemical activity of the synthesised cobaloximes, we set about preparing semiconductor nanocrystal-molecular catalyst hybrid photocatalysts. Within our research group CdS QDs were routinely synthesised, and their absorption properties and band alignment with the cobaloxime molecular catalyst made them an attractive option as a sensitiser component in a hybrid photocatalyst. The proposed hybrid scheme is illustrated in Figure 3-3, along with an energy diagram of the states expected to govern hydrogen evolution by the system. The band alignments of the CdS are based on the absorption onset in the extinction spectrum of the QDs and previous experimental work published by our group.[31] The cobaloxime reduction potentials were converted to NHE from the measured values versus the ferrocene/ferrocenium couple by adding 0.7 V to the values as measured in DMF.[26,32] The sulfite potential was inferred for pH 9 from published values.[33] It should be noted that although the sulfite potential is more negative than the conduction band edge of the CdS QDs and both reduction potentials of the cobaloximes, control experiments in the dark show no hydrogen evolution from the system.

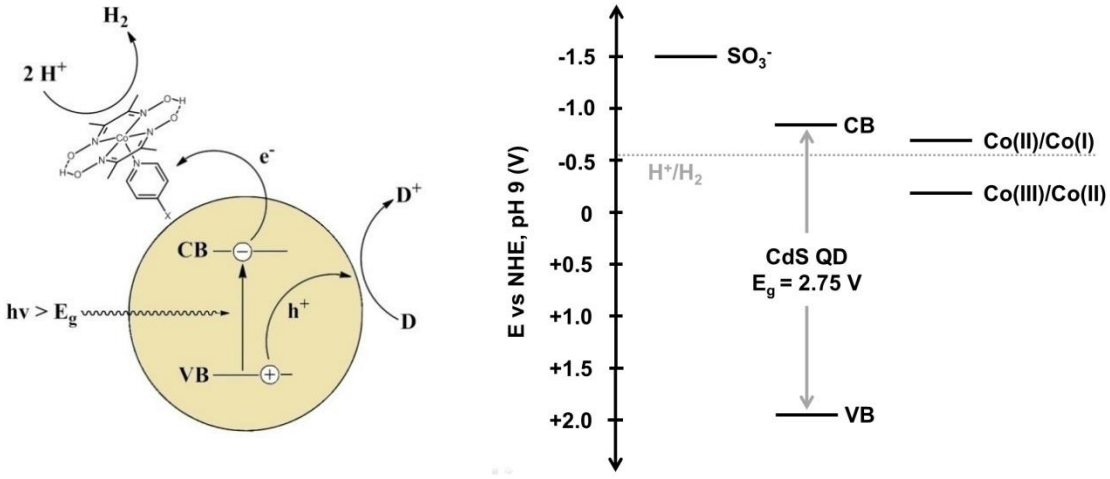

Figure 3-3. (Left) Representative scheme depicting the operation of the hybrid photocatalyst. (Right) Energy level diagram showing the alignment of states involved in the generation of hydrogen by the hybrid photocatalyst.

Our initial approach to assembling the hybrid system was to combine the components during the phase transfer process in which the as-synthesised nanocrystals are functionalised with hydrophilic ligands and transferred to aqueous solution. We reasoned that introducing the catalyst at this stage, at the same time as the stabilising ligands, would result in a mixed ligand shell composed of both stabilising ligands and molecular catalysts adsorbed to the nanocrystal surface. In this co-adsorption approach, we supposed that, provided an excess of catalyst, the nanocrystals would be maximally loaded but ultimately limited by the colloidal stability of the hybrid material. Excessively functionalised nanocrystals would be expected to precipitate from solution, leaving only colloidally stable particles.

To prepare the hybrid materials, stock solution of the as-synthesised QDs was diluted in chloroform and shaken together with an aqueous solution of stabilising ligand and catalyst at alkaline pH. D,L-cysteine, a short chain amino acid with a terminal thiol group, was used as the ligand.[34–36] Successful phase transfer was evident from the colour inversion of the organic and aqueous layers in the separatory funnel. The solution was then allowed to equilibrate overnight. The crude aqueous product solution contained excess catalyst and ligand, which were removed by successive concentration and dilution cycles in centrifugal membrane tubes. These disposable devices contain a polyethersulfone (PES) membrane which allows liquids to pass but traps particles with even single-nanometre dimensions. Three purification cycles were used as standard, each resulting in dilution of the unwanted materials in solution by a factor of ~100, while the QD concentration remains relatively constant. The first wash was typically brown in colour as a result of the excess cobaloxime. Subsequent washes appeared colourless. Stock solutions of the hybrid photocatalysts were collected and stored for later use. An extinction spectrum was collected of each material, shown in Figure 3-4. Based on the position of the excitonic absorption, the QDs have an average diameter of 4 nm.[37]

A redshift of 2-3 nm is observed after ligand exchange. The width of the excitonic peak does not change appreciably, indicating that the size distribution of the particles has not been affected (e.g. through etching). At longer wavelengths (>450 nm) the extinction is near zero, as expected for energies below the band gap of the nanocrystals. Gradually increasing extinction, beginning in the red region, is indicative

of particle agglomeration, where aggregates of particles have achieved dimensions sufficient to scatter visible light. The spectra in Figure 3-4 therefore indicate that the stock solutions are composed of well-dispersed colloidal particles. The enhanced absorption in the UV region is due to the cobaloximes (see Fig. 2-1 for spectra of the complexes).

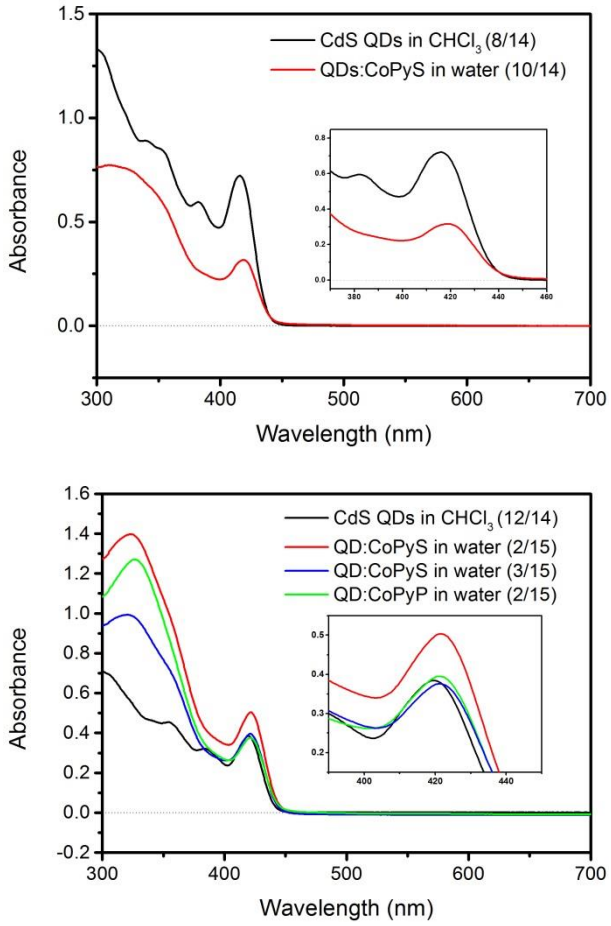

Figure 3-4. Extinction spectra of as-synthesised QDs in $CHCl_3$ compared to those of the hybrid photocatalysts. Preparation dates shown for reference. Note that the QDs within each plot are from the same synthetic batch, but were ligand-exchanged separately.

3.4.1 Surface Assembly of Cobaloximes

While working with these materials, attempts were made at surface assembly of thiol-bound cobaloximes. Before phase transfer, 4-mercaptopyridine was added to the as-synthesised QDs in chloroform. After phase transfer, these pyridines would remain on the QD surface. Subsequently exposing them to the cobaloxime precursor, $Co(dmgH)_2Cl_2$, as in the standard synthetic procedure, might achieve complexation with the adsorbed ligands. This approach would potentially provide for tuning the number of cobaloximes per nanocrystal, and eliminate competition between cobaloximes and stabilising ligands. In practice, this approach was challenging, often leading to precipitation of the particles and so was abandoned.

3.5 Hydrogen Evolution by Hybrid Photocatalysts

To evaluate the prepared materials as hydrogen evolution catalysts, the hybrids were combined with sodium sulfite as a hole scavenger in aqueous solutions. For experimental consistency, and to maximise the absorption by material in our reactor, the absorbance of photocatalyst solutions was adjusted to 0.3 at the wavelength corresponding to the maximum of the first excitonic absorption feature. Using a consistent absorbance for experiments (and using QDs from the same ligand exchange batch) ensures a similar concentration of nanocrystals is used for each experiment. The reactor had a sample path length of 5 cm, giving total absorbance of 1.5 for the photocatalyst solution. Given the Beer-Lambert relationship $A = log_{10}(I_0/I) = -log_{10}T$, this implies that ~97% of incident light at that wavelength is absorbed by the sample. The reactor was illuminated with a Xenon lamp providing incident power of 30 mW at the reactor face. The sample was purged with argon prior to experiments and then stirred during the experiment with a magnetic stirrer. Aliquots of the headspace gas (Ar) were extracted and analysed by gas chromatography.

Several batches of the photocatalyst were produced and measured, implementing the same protocol for each preparation. The results are presented in Figure 3-5. The hybrid photocatalysts composed of QDs and cobaloximes indeed evolved hydrogen under illumination, and at higher rates than the QDs alone. Hydrogen production by the CdS QDs in the absence of cobaloximes occurred at a comparable rate to published values under similar conditions in water on a per-QD basis.[38] In some instances, an

induction period was observed, usually lasting around 1 hour, in which hydrogen is either evolved slowly or not at all, despite the system being illuminated. This induction period was extended in some samples, for which the rate of hydrogen generation continued to increase over the first 3-4 hours before becoming constant during the final hours of the experiment.

Prior to illumination, the solutions of hybrid catalysts and sodium sulfite were optically clear, with a uniform yellow colour from the well-dispersed colloidal CdS QDs. Within the first hour, however, the solutions became cloudy as the QDs began to aggregate and scatter lamp light. Although the aggregation process continued for the duration of the experiment, it did not appear to diminish the rate of hydrogen production, even when visible aggregates had formed. Towards the end of the experiments, the QDs had lost their colloidal stability such that the aggregates would settle at the bottom of the reactor if not for the constant agitation of the stirring bar. This aggregation process is due to oxidation of the thiol anchoring group of cysteine by photo-generated holes in the QDs, resulting in ligand removal and particle destabilisation.[39–41] While hydrogen continues to be evolved on the time scale of these experiments, the loss of colloidal stability and subsequent aggregation undermines the efficacy of a QD-based system, primarily in terms of interfacial surface area and light absorption. Attempts to address this issue are discussed later in the chapter.

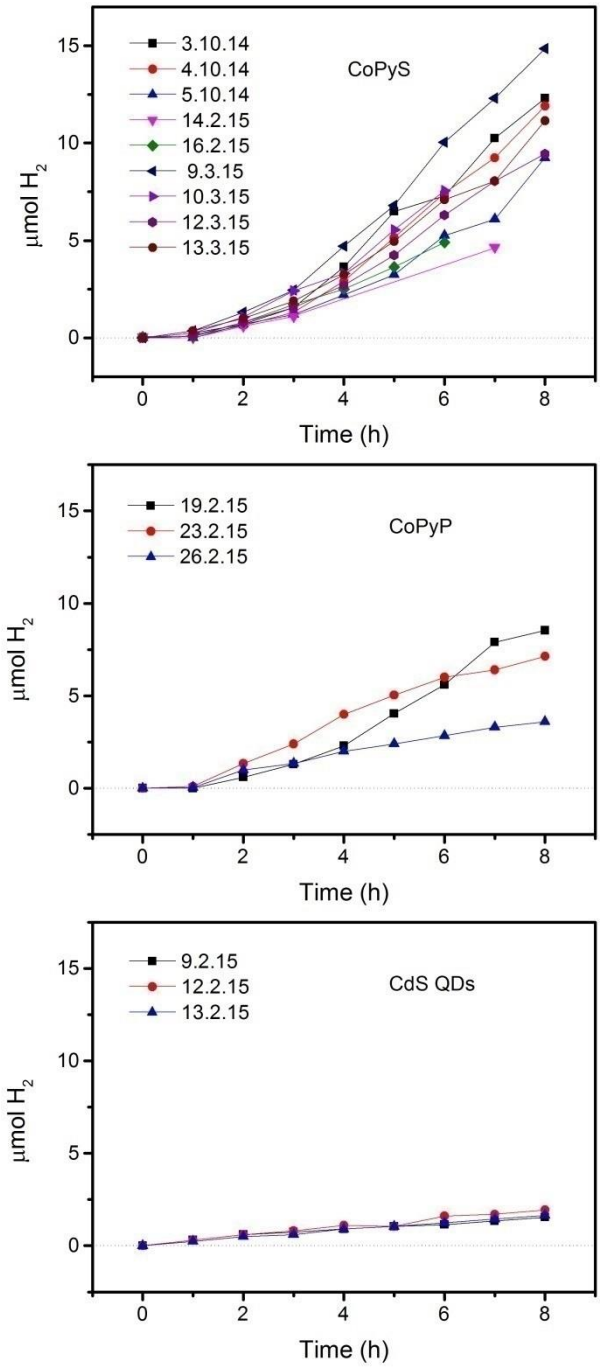

Figure 3-5. Hydrogen evolution for hybrid systems comprised of CdS QDs and either CoPyS (top) or CoPyP (middle). Control experiments with only CdS QDs are included (bottom). Experiments were conducted in water at pH 9 with 0.1 M Na_2SO_3 as hole scavenger. [QD] = 0.5 µM.

As the experiments with the hybrid photocatalysts were repeated, the hydrogen evolved by the QD-cobaloxime hybrids was seen to vary considerably experiment-to-experiment, as well as batch-to-batch, for both phosphonate and thiol anchoring groups. In contrast, hydrogen evolution by the semiconductor nanocrystals themselves, while more modest, was very reproducible. Given the variability in the performance of the materials, we sought to correlate the amount of hydrogen evolved with the cobalt content of the materials. We used ICP-OES to precisely quantify the amount of cobalt in each material, which would reflect the quantity of cobaloxime present. Upon comparing the amounts of cobalt in each batch of hybrid catalyst solution, it appeared that even single parts per million differences in the amount of catalyst present could lead to differences in hydrogen evolution activity. Cadmium and sulfur content was also analysed. The ICP-OES results are presented in Table 3-1. No obvious trend appeared relating hydrogen yield to cobalt content.

	QD:CoPyS (3,4,5/10/14)	**QD:CoPyS (14,16/2/15)**	**QD:CoPyS (9,10,12,13/3/15)**	**QD:CoPyP (19,23,26/2/15)**	**QD (9,12,13/2/15)**
Total H_2 in 8 hr (μmol)	12.3, 11.9, 9.3	4.7 (7 h), 4.9 (6 h)	14.9, 7.6 (6h), 9.5, 11.2	8.6, 7.2, 3.6	1.6, 2.0, 1.7
Stock [Co] (ppm)	5.88	3.76	2.63	5.22	--
[Co] in reactor (μM)	18.0	15.9	11.3	23.6	--
Cobaloximes per QD	36	31.8	22.6	47.2	0

Table 3-1. Tabulated hydrogen evolution data from multiple batches of hybrid photocatalysts.

3.6 Filtration Experiments

The results of the ICP-OES analysis motivated closer examination of the protocol used for preparing the hybrid materials. To gain some insight into the relative amounts of adsorbed cobaloxime and free cobaloxime in the product solution, the

persistence of cadmium, sulfur, and cobalt in the samples during material preparation and purification was investigated. PES membrane tubes were again used as a means to separate the functionalised nanocrystals from the ligand/catalyst solution. A batch of each hybrid material was prepared, then purified using the same concentration-dilution process as previously, concentrating the QDs by centrifugation then re-dispersing them to their original volume. Note that while three filtration cycles were used in the original protocol for preparation of the hybrid photocatalysts, five cycles were performed here, with the eluent from each cycle reserved for analysis. The cadmium, sulphur, and cobalt content was then measured by ICP-OES. The results are plotted in Figure 3-6, with the quantities normalised to the content of each element present in the eluent of the first filtration cycle. The actual measured values are presented in Table 3-2.

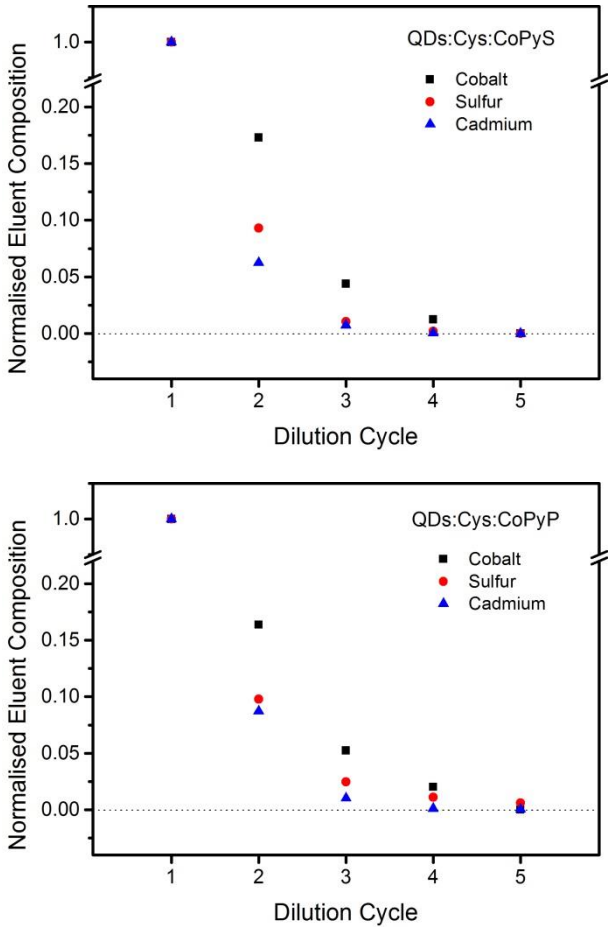

Figure 3-6. Quantification of cobalt, sulfur, and cadmium content in the eluent solutions after each filtration cycle, normalised to the initial content of each element as measured by ICP-OES.

	CoPyS				CoPyP		
	[Cd] ppm	[S] ppm	[Co] ppm		[Cd] ppm	[S] ppm	[Co] ppm
Eluent 1	12.197	468.737	22.518		10.816	444.666	34.071
Eluent 2	0.763	44.785	4.185		0.943	43.55	6.758
Eluent 3	0.091	6.236	1.326		0.111	11.040	3.121
Eluent 4	0.005	2.235	0.63		0.013	4.962	2.069
Eluent 5	-0.000	1.307	0.354		0.004	2.739	1.410
Product	95.034	364.45	0.36		109.068	481.77	1.488
Error	±0.011	±0.035	±0.071		±0.011	±0.035	±0.071

Table 3-2. Elemental content of eluents and hybrid photocatalyst product solutions during purification, measured by ICP-OES.

The plots show that while Cd and S are washed from the material in roughly the same proportions, relatively more cobalt appears in the eluent after each cycle. Given the materials present are diluted equally between filtration cycles, this result is somewhat unexpected. After the first cycle, the hybrids are retained above the PES membrane along with some of the surrounding solution containing free species. Any cobaloxime that was adsorbed to the QDs persists into the next cycle, along with the Cd, S, and Co residues in solution. Upon re-dispersing the filtrate in MilliQ water, the relative amounts of residual Cd, S, and Co would not be expected to change. It appears that upon dilution some adsorbed cobaloxime is leeched from the surface of the QDs into solution as a new equilibrium is established. Over the course of five cycles, there is a consistently higher proportion of cobalt eluted with respect to the content of the previous cycle, more than for the residual cadmium or sulfur.

The cadmium detected in Eluent 1 for both samples was most likely displaced from the cadmium-rich QD surface during the ligand exchange procedure and solubilised by binding to cysteine.[42] This population of soluble cadmium is diluted to near the detection limit of the spectrometer over the five filtration cycles. A significant

amount of cadmium persists in the product (i.e. within the QDs retained above the PES membrane), as expected. The measured value of cadmium in the product was validated by approximating the QDs as 4.2 nm diameter spheres, taking the number of QDs present in 10 mL solution (1.9×10^{-8} mol), and the density of CdS (4.8 g/cm^3) to predict ~160 ppm Cd in the product. This figure is within a factor of 2 of the measured ICP-OES values for the samples, which is reasonable close considering the spherical simplification and size polydispersity of the QDs.

Sulfur is present in relatively large amounts in the eluent of the first filtration cycle due to the large excess of cysteine used in the ligand exchange protocol (30 mg in 10 mL water, ~20 mM). Although the sulfur content of successive eluents decreases, the quantity detected in the final product appears unreasonably high. Based on the above estimate for the amount of cadmium in the product, roughly 50 ppm of sulfur would be expected to be present for stoichiometric CdS (~30 ppm when adjusted for the measured Cd values). Additional sulfur is contributed to the total present in the materials by the cysteine surface ligands, but still does not account for the quantity measured in the product. It therefore seems that the product samples had been contaminated somehow during preparation or handling.

Lastly, the cobalt quantities measured in both Eluent 1 samples are sensible, given that 5 mg of cobaloxime were added initially to the ligand exchange solutions for these experiments. These values provide for a relatively accurate determination of the number of cobaloximes present in each sample due to the fact that each molecular catalyst contains just one cobalt atom. After five filtration cycles, the concentrations of 6.1 μM CoPyS and 25.2 μM CoPyP in the product solutions of hybrid photocatalysts correspond to Co:QD ratios of 3:1 and 12:1, respectively. These concentrations are in good agreement with the materials detailed in Table 3-1 considering the additional filtration cycles used here. Again approximating the QDs as spherical, their surface areas (~55 nm^2) would be sufficient to accommodate this number of cobaloximes, given a footprint of ~1 nm^2 for the catalysts.[15,28]

This experiment showed that although some of the complexes may exist in solution in the samples, the cobaloximes can effectively adsorb to the QDs. The apparent desorption of cobaloximes from the hybrid photocatalysts upon dilution in

water provides evidence for the complexes being initially bound. Additionally, the relative amounts of cobalt in the CoPyS sample eluents are consistently lower than those in the CoPyP eluents beyond the first filtration cycle, which suggests that the thiol linkage may indeed help to reduce desorption of CoPyS.

3.7 In-Situ Assembly of Hybrid Photocatalysts

The hydrogen evolution activity of the materials appeared to be very sensitive to the cobalt content. Given that the protocol for photocatalyst preparation did not reproducibly incorporate the same amount of catalyst into the hybrids, the method appeared to be inadequate for evaluating potentially subtle differences in activity that might arise from functional group effects. To more precisely evaluate hydrogen evolution as a function of catalyst concentration, hybrid photocatalysts were assembled in-situ using stock solutions of both QDs and cobaloximes.

A large batch of QDs was ligand-exchanged so that the same batch could be used for all experiments to minimise experimental differences arising from the degree of functionalisation. The QD stock solution was stored in a glass vial purged with argon at 4 °C. The extinction spectrum of the QDs is shown in Figure 3-7. The maximum at 423 nm implies an average particle diameter of 4.2 nm.[37]

Stock solutions of the cobaloximes were also prepared and analysed by ICP-OES to precisely quantify the amount of cobalt present. For the hydrogen evolution experiments, cobaloxime concentrations equivalent to those present in the best performing batch of co-adsorbed photocatalysts were initially used. The catalyst concentration was then varied systematically around this value while keeping the QD concentration constant at ~ 0.5 µM, based on the absorbance.[37] In Figure 3-8, the results are presented as the time course of each individual hydrogen evolution experiment, plotted alongside comparisons of the total yield of hydrogen produced during each experiment.

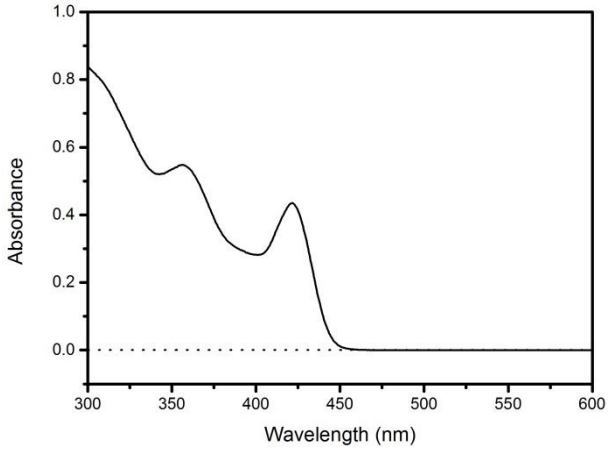

Figure 3-7. Extinction spectrum of the CdS QDs stock solution in water, used for cobaloxime concentration dependence experiments.

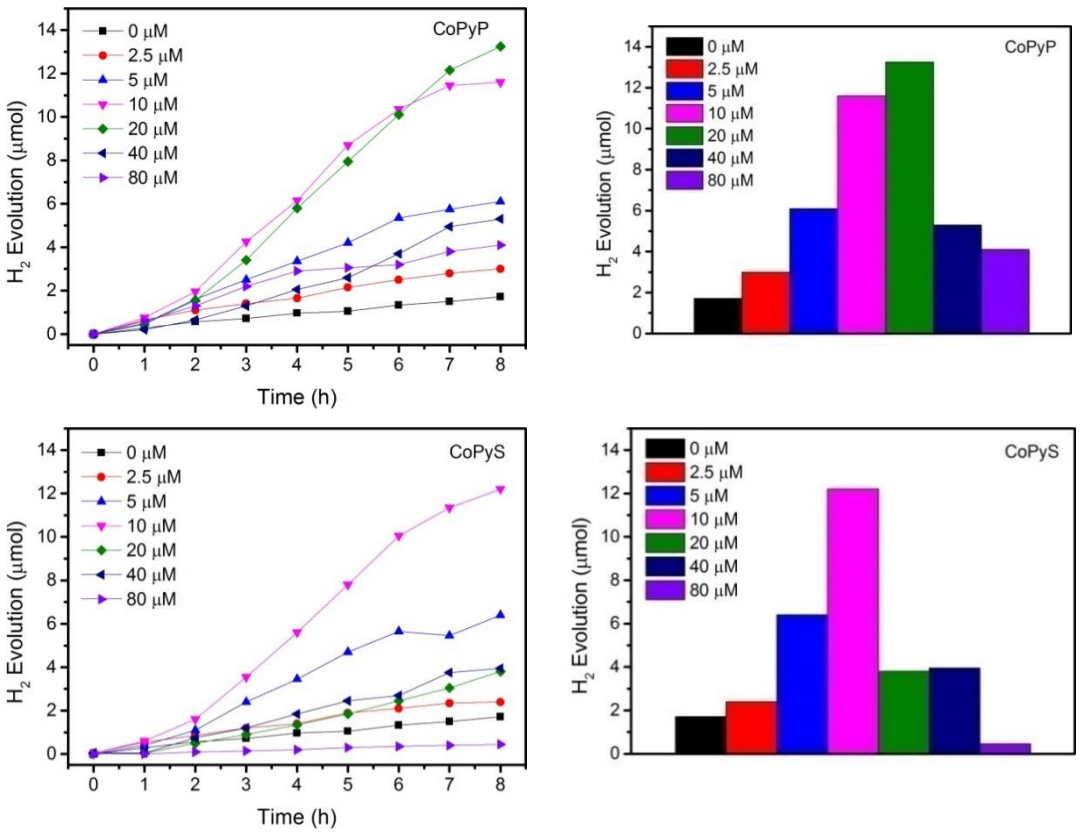

Figure 3-8. Cobaloxime concentration dependence of H_2 evolution by the hybrid materials.

The behaviour of CoPyS and CoPyP is almost identical in terms of hydrogen production within the range studied, with roughly the same optimum cobaloxime concentration, in the region of 10-20 μM. The performance of CoPyS drops sharply as the concentration is increased beyond 10 μM, becoming essentially inactive by 80 μM and producing less hydrogen than even the CdS QD control group. A similar decrease in activity is observed beyond 20 μM for CoPyP. At the higher catalyst concentrations, light absorption by the cobaloximes becomes non-negligible in the 400-450 nm region (see Fig 2-1). The observed decrease in hydrogen yields is therefore likely to be due to competitive light absorption by the catalysts at the expense of the QDs, resulting in fewer photo-generated electrons to drive proton reduction. CoPyS absorbs ~6 times more strongly than CoPyP at 423 nm, the wavelength of the CdS QD band edge absorption maximum, so the effect of competitive light absorption on hydrogen production is more pronounced in the CdS QD/CoPyS system. At the highest concentration measured, light absorption from CoPyS is comparable to that of the QDs, with absorbances equivalent to 0.30 and 0.37, respectively, over a 1 cm pathlength. While the reason for the discrepancy in light absorption between the two cobaloximes is not clear, the impact on the hydrogen evolution activity is apparent in Figure 3-8 (right-hand panels). At a concentration of 80 μM, the CoPyP system produced 4.1 μmol H_2 while the CoPyS system evolved just 0.45 μmol H_2. Competitive light absorption by CoPyS also likely accounts for some of the batch-to-batch variation in hydrogen production discussed in section 3.5. The amounts of CoPyS present in those materials would contribute 10-20% of the total sample absorbance (implying an equivalent overestimation of the concentration of QDs from the stated 0.5 μM), however this does not explain the variable hydrogen production between experiments that used material from the same batch of photocatalyst.

The turnover number (TON) is a useful metric to quantify catalytic activity, defined as the number of moles of product generated per mole of catalyst. For molecular catalysts, the turnover number can be a rather precise quantity, with each individual coordination complex regarded as an “active site”. If the catalytic species or active site is not well characterised, perhaps consisting of multiple atoms (e.g. a cluster or particle), the turnover number becomes less meaningful. From a practical perspective, the turnover number can still be useful for evaluating the economy of a given system by

relating the amount of product generated to the amount of material used, whatever the nature of the active species.

In Figure 3-9, the hydrogen evolution activity for each cobaloxime concentration dependence experiment is evaluated in terms of the turnover number (solid markers). Earlier experiments are included on the same plot in which functionalisation of QDs with cobaloximes was attempted using the co-adsorption method (hollow markers). The result is a concentration curve that highlights the optimum concentration of cobaloxime for the concentration of quantum dots used in the experimental protocol (0.5 µM).

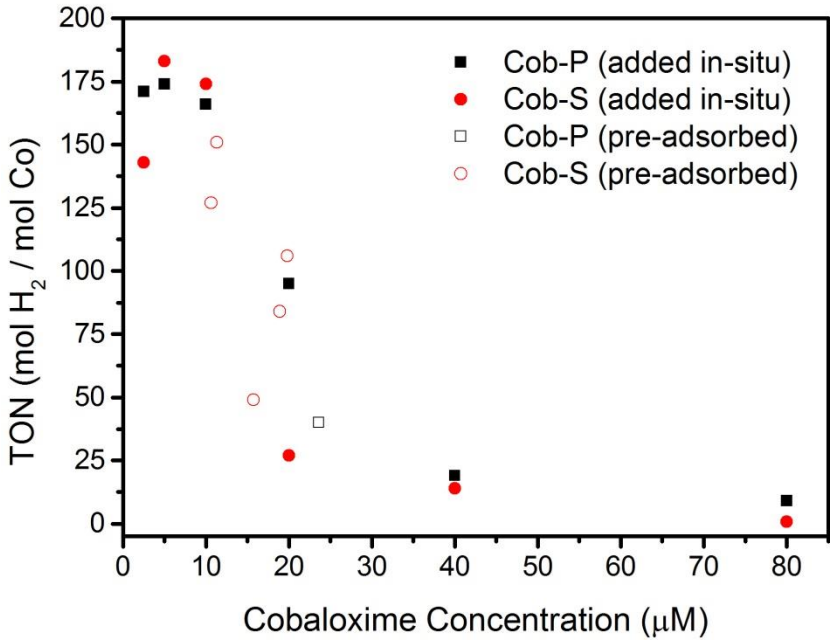

Figure 3-9. Turnover number (TON) as a function of cobaloxime concentration, as determined by ICP-OES. [QD] = 0.5 µM.

When plotted in terms of the turnover number, it is clear that lower concentrations of 10-20 cobaloximes per QD are more active, while at 40 and 80 µM the per atom performance is more than an order of magnitude lower. Interestingly, the point on the plot where the activity curve changes fastest is precisely the concentration regime where the previously prepared "pre-adsorbed" hybrid photocatalyst samples lie; in retrospect, it is perhaps not surprising that hydrogen evolution by the hybrid materials

was so inconsistent, especially considering the competitive light absorption by cobaloximes, particularly CoPyS, at higher concentrations.

3.8 In-Situ Adsorption of Cobalt Species to QDs

Following the study of the cobaloxime concentration dependence of hydrogen evolution by the hybrid materials, the adsorption behaviour of cobaloximes over the course of a typical hydrogen evolution experiment became of interest. Combining the QDs and cobaloximes shortly before use by the in-situ assembly approach had achieved comparable activity to that of "pre-adsorbed" batches. This indicated that the interaction between the catalyst and absorber that led to the observed activity was established during illumination through some photo-initiated process.

As an initial data point, the concentration of cobaloxime in solution before and after 8 hours of illumination was measured. Twice the usual amount of photocatalyst solution was prepared by combining QDs, CoPyS, and sodium sulfite stock solutions in the normal proportions. This solution was then divided evenly between the reactor, from which hydrogen evolution was measured, and a purged sample vial fitted with a septum, which was wrapped in foil to exclude light and positioned alongside the reactor during the experiment. After eight hours, 6.15 μmol H_2 had been evolved by the illuminated sample. Both solutions were then centrifuged in PES membrane tubes to separate the nanocrystals from the rest of the solution, and the eluent was submitted for elemental analysis. The results are shown in Table 3-3.

	Dark	**Illuminated**
[Co] (ppm)	0.690 ± 0.018	0.023 ± 0.018

Table 3-3. Cobalt content of hydrogen evolution solutions following removal of CdS QDs, measured by ICP-OES, with and without illumination.

Based on the ICP-OES result, and the uncertainty in the measurement, virtually no cobalt remained in the illuminated solution. This implies that most of the cobalt had somehow been incorporated with the QDs, which do not pass through the PES

membrane. It is possible that under illumination stabilising ligands are removed, which creates space on the QD surface for the cobaloximes to adsorb, however based on the results of the filtration experiments (i.e. the weak interaction with the QDs) it was suspected that a photodeposition process might be occurring.

This result motivated a similar experiment, this time with the intention of tracking the solution concentration of cobalt at intervals during hydrogen evolution. A large volume of photocatalyst solution was prepared in the reactor so as to permit aliquots of sufficient volume (~1 mL) to be removed periodically over 8 hours. Fixed volumes of solution were removed each time, diluted to the same volume, then centrifuged in PES membrane tubes to separate the QDs. The cobalt content in the eluents was then quantified by ICP-OES. Hydrogen evolution was monitored in parallel by GC. The results are plotted in Figure 3-11.

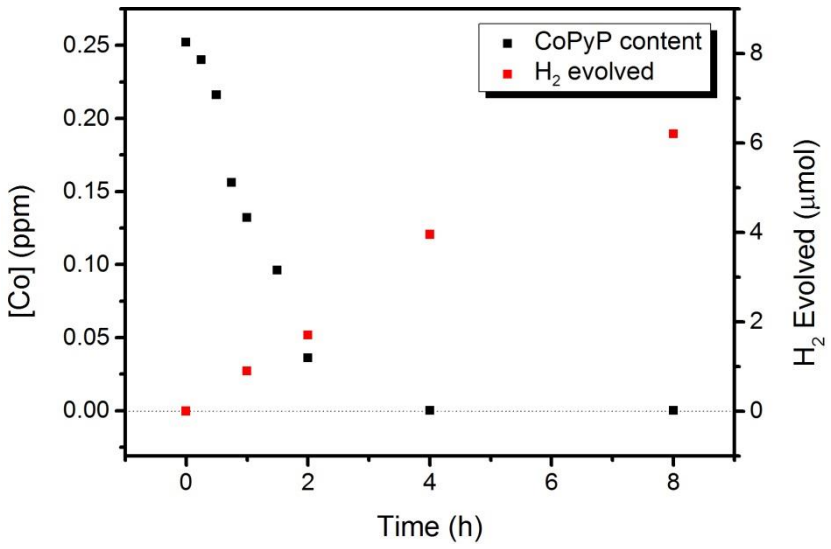

Figure 3-10. Concentration of free cobalt in solution over the course of a typical H_2 evolution experiment.

Evidently, the solution concentration of cobalt begins decreasing from the time the lamp is turned on, while hydrogen was observed to evolve steadily. After 4 hours, cobalt in solution is totally depleted, however based on the rate of the decrease the process is likely complete after just 3 hours. Interestingly, hydrogen evolution proceeds

at a constant rate from the time illumination begins and does not change significantly while cobalt in solution is depleted. This experiment supported the hypothesis that a photodeposition process was taking place, corroborating the result of the previously discussed experiment with CoPyS. Both cobaloximes seemed to be susceptible to this process.

3.9 Comparison of "Binding" vs "Non-Binding" Cobaloximes

The filtration experiments had shown that the interaction of CoPyS and CoPyP with the QDs was rather weak, despite the presence of functional groups that could in theory anchor the complexes to CdS. To investigate whether the anchoring groups played any role in promoting hydrogen evolution by the hybrid system, cobaloximes were synthesised that did not possess such functional groups. Further, given the suspicion that a photodeposition or decomposition process might be occurring, it was conceivable that binding of the complexes to the QDs would actually promote this process.

"Non-binding" cobaloximes are shown in Figure 3-12. The first was prepared with a methyl isonicotinate ligand, a pyridine which bears a methyl ester group at the 4-position of the ring, referred to as "CoPyMe". This functional group would not be expected to bind strongly to the surface of the QDs due to the hindered ester. The second non-binding cobaloxime was simply the dichloride complex, $Co(dmgH)_2Cl_2$, which is normally used as a precursor for preparing pyridine-ligated cobaloximes.[43,28] Synthetic and characterisation details are included in Chapter 2.

H_2 evolution experiments were conducted comparing the activity of hybrid systems incorporating either binding or non-binding cobaloximes and CdS QDs. Stock solutions of the cobaloximes were prepared and measured by ICP-OES to precisely determine the cobalt content, so that the concentration of cobaloxime could be adjusted to ensure consistent ratios of cobaloximes and QDs in each experiment.

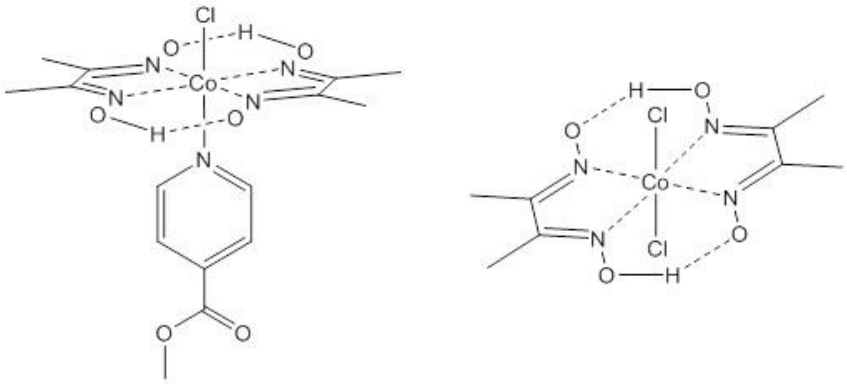

Figure 3-11. Structures of "non-binding" cobaloximes CoPyMe (left) and $Co(dmgH)_2Cl_2$ (right).

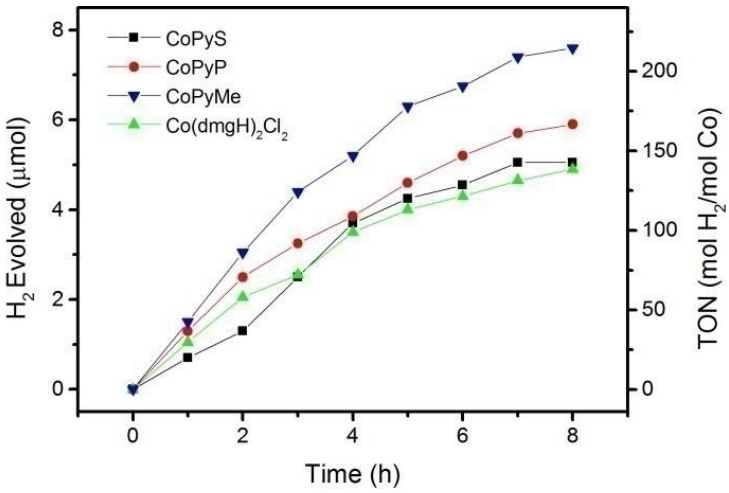

Figure 3-12. Hydrogen evolution from hybrid systems of CdS QDs and cobaloximes that have anchoring groups (CoPyS, CoPyP) and cobaloximes that do not (CoPyMe, $Co(dmgH)_2Cl_2$).

The results of hydrogen evolution experiments with these four complexes are illustrated in Figure 3-13. The findings were somewhat surprising, in that $Co(dmgH)_2Cl_2$, without an axial pyridine, was similarly active to CoPyS and CoPyP, while the non-binding CoPyMe was even more active than the "binding" versions. Cobaloxime activity is known to improve upon introduction of an axial pyridine ligand, which shifts the catalyst reduction potentials more positive, so the fact that the

dichloride complex provided comparable activity to CoPyS and CoPyP was unexpected.[10] As discussed in the context of the electrochemical measurements in section 3.5, the electron donating or withdrawing nature of the pyridine ligands affects the turnover rate of cobaloximes, which should manifest as different hydrogen yields over time. The pyridine ligand in CoPyMe is electron withdrawing, which would be expected to reduce the pK_a of the cobaloxime hydride intermediate and therefore to slow hydrogen turnover relative to a more donating pyridine ligand, as in CoPyS.[25] Clearly, the CoPyMe system produced the most hydrogen, and the anticipated trend is reversed, so another factor, such as the QD-cobaloxime interaction via the pyridine ligand *para* substituent, might be more influential overall to the hydrogen yield. Interestingly, no induction period is evident in Figure 3-13 before the onset of hydrogen production, which would be expected if a photodeposition process formed the active species; rather, this observation lends support to the hypothesis that the intact cobaloximes operate as catalysts for proton reduction.

Having identified the sensitivity of hydrogen evolution by the hybrids to cobaloxime concentration, and with concerns as to the nature of the catalytically active species, the control experiments performed early in the project using cobalt chloride were revisited. The standard hydrogen evolution experiment was performed using the optimised concentration determined in previous experiments, and the hydrogen evolution was found to be comparable to that achieved with the prepared cobalt complexes. Unfortunately, it appeared the initial control experiments had used a cobalt chloride concentration that was significantly above the optimum concentration and therefore suppressed significant hydrogen evolution.

3.10 Light Intensity Dependence

The performance of cobalt chloride as a co-catalyst did not preclude cobaloxime from behaving as a molecular catalyst. It was hypothesised that at lower light intensities, any catalytic advantage that cobaloximes could have over cobalt chloride might be magnified. If a photodeposition process was in fact occurring and causing cobaloximes to decompose on the QD surface, reducing the light intensity might impede this process and allow cobaloximes to operate intact.

Neutral density filters were used to reduce the intensity of light incident on the reactor, while retaining the spectral distribution of the lamp used in previous experiments. CoPyS and cobalt chloride were compared as catalysts using stock solutions of each to control the concentration. The results are shown in Figure 3-14. Cobalt chloride consistently outperformed the cobaloxime, offering further evidence that the complexes were simply acting as pre-catalysts. Introducing cobalt chloride to the system likely meant that Co^{2+} species were more readily available for photodeposition of the active species, whereas the cobalt atom of a cobaloxime would be relatively unavailable before its ligands are removed. Hydrogen evolution by the cobalt chloride co-catalyst scaled precisely with light intensity, while the yield in the presence of the cobaloxime was significantly lower. If decomposition of the cobaloximes to form the active species was photo-driven, the presence of fewer photo-generated carriers to induce the process would result in slower formation of the catalyst.

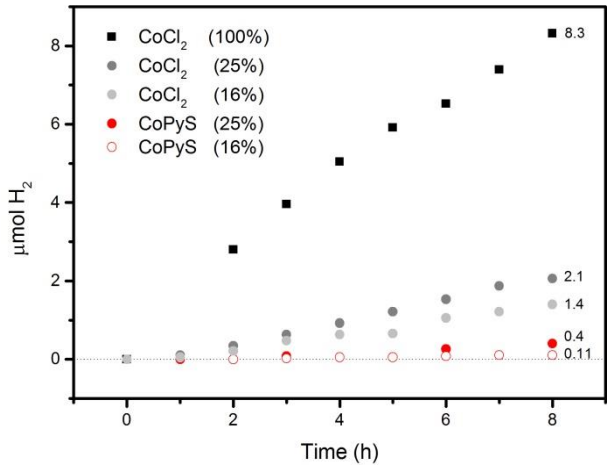

Figure 3-13. Light intensity dependent H_2 evolution by CdS QDs with either CoPyS or $CoCl_2$ as a co-catalyst.

3.11 Literature Context of Results

By the time the experiments described in this chapter were concluding, stability issues with cobaloximes had come to be more widely acknowledged in the literature. Lakadamyali et al. had demonstrated that when hydrogen evolution by a cobaloxime-based dye-sensitised system eventually ceased, it could be restarted by adding fresh dimethylglyoxime ligand to the solution.[44] Including excess ligand in the solution from the start of photocatalysis prolonged hydrogen evolution. Addition of fresh pyridine ligand had no such effect. Covalently linking equatorial, bidentate glyoxime ligands to form tetradentate macrocycles via methylene or difluoroborate bridges had been used to improve cobaloxime stability in early homogeneous studies[11,45,46], and the approach had now been adopted for immobilised systems, as illustrated by the examples in Figure 3-15. Muresan and co-workers sought to address stability by appending an anchoring functionality directly onto a tetradentate glyoxime ligand.[16] Willkomm et al. used a similar approach, but also tethered a pyridine to the framework in such a way that it could coordinate to the cobalt centre, improving activity.[20] Should the pyridine dissociate, it is held in close proximity to the metal centre to promote coordination again. In a notable example, Andreiadis et al. grafted cobaloximes to a carbon nanotube electrode, resulting in exceptional aqueous stability and activity.[47]

Reproduced from [16]

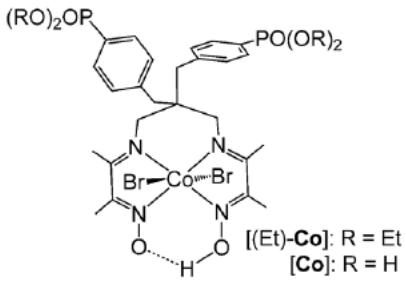

Reproduced from [20]

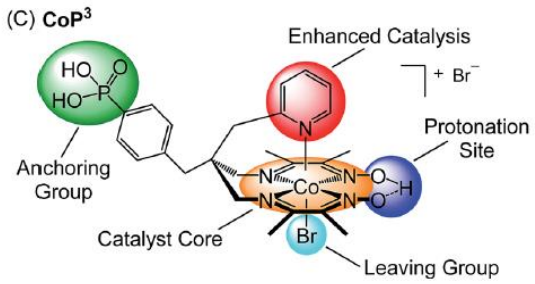

Reproduced from [47]

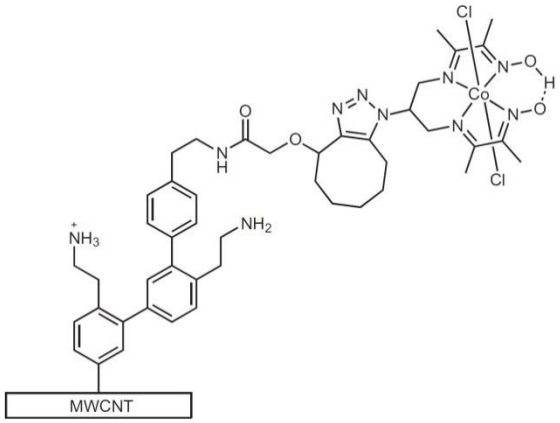

CoPyP

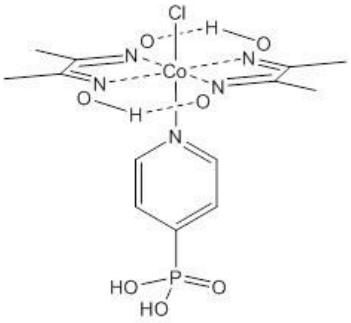

Figure 3-14. Examples of cobaloximes from the literature illustrating strategies to stabilise the complex against decomposition. The structure of one of the cobaloximes investigated in this project (CoPyP) is included for comparison.

Comparing these more elaborate ligand frameworks to the simple cobaloxime structure used in this project, the latter is clearly at greater risk of decomposition. An electrochemical study using a nickel analogue of these simple cobaloximes demonstrated that the complex decomposed on the electrodes upon redox cycling to form metallic deposits.[48] A more recent study by Kaeffer et al. demonstrated that a cobaloxime degrades electrochemically under the acidic aqueous conditions previously used to benchmark cobaloximes, resulting in deposition of cobalt-based nanoparticles.[49] Such studies unfortunately lend support to our suspicion that the cobaloximes did not

remain intact as molecular catalysts, but rather likely served as precatalysts that for an uncharacterised active species.

Contemporaneously to our experimentation, a paper was published by Chang et al. reporting results that caused us to seriously reconsider the behaviour of cobaloximes in hybrid system.[38] The authors used CdS QDs as light absorbers and evaluated photocatalytic hydrogen evolution from water by either a cobaloxime (CoPyP), $CoCl_2$ or $Co(NO_3)_2$. Significantly, the photocatalytic activity was found to be the same whether the cobaloxime or the cobalt salts were used as co-catalyst. Control experiments indicated that the catalytic species was actually formed in situ under illumination and was independent of the cobalt source. Given that almost identical materials were used in their study and ours, these results carried additional significance and appeared to confirm that cobaloximes were simply pre-catalysts in the "hybrid" photocatalytic materials that have been discussed in this chapter. Another important aspect of the study by Chang et al. was the use of "stripped" QDs, and an assessment of their activity in the photocatalytic system as compared to QDs coated with 3-mercaptopropionic acid (MPA). The native oleate ligands were removed from the CdS QDs by exposure to Me_3OBF_4 in DMF, which resulted in "bare" QDs which remained colloidal due to charge-stabilisation by the tetrafluoroborate anions. Although these particles aggregated upon dilution in water, their hydrogen evolution activity was shown to be vastly superior (~two orders of magnitude) to the MPA-coated QDs. This strategy of intentionally stripping ligands from the QDs to promote photocatalysis serves as an important counterpoint for the rest of the work discussed in this thesis.

3.12 Impact of Surface Ligands on Hydrogen Evolution Activity.

Earlier in this chapter, it was noted that extensive particle aggregation occurred during hydrogen evolution by the QD-cobaloxime materials. The process was attributed to oxidation of the thiol group of the stabilising ligand, cysteine, by photo-generated holes in the QDs resulting in ligand desorption and particle agglomeration.[39–41] Besides contributing to inconsistency in the hydrogen evolution behaviour, ligand photo-oxidation compromises the utility of QDs in a particulate photocatalytic system and hinders fundamental studies. Parallel to the investigation of the cobaloxime complexes

described previously in this chapter, strategies were explored for preventing ligand oxidation and extending the lifetime of QD-based photocatalysts.

At the beginning of this project, the surface ligands were regarded as a relatively insignificant component of the hybrid system. Cysteine was used as the stabilising ligand for CdS QDs for historical reasons within our lab, through inherited protocols, however 3-mercaptopropionic acid (MPA) was used for the same purpose in many reports in the literature.[50–52] Upon inspection of their structures (Figure 3-16), the molecules were thought to perform equivalently as stabilising ligands; both possess a thiol anchoring group and a carboxylic acid tail group for interaction with polar solvents. The length of the molecules is the same, meaning the ligand shells should be of similar thickness.

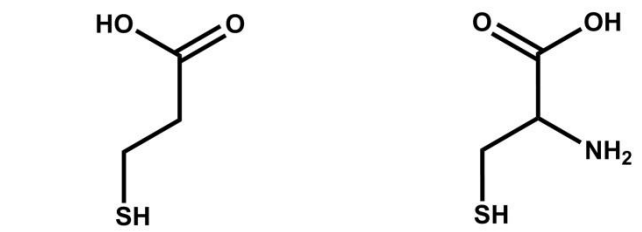

Figure 3-15. Structures of MPA and cysteine stabilising ligands for CdS QDs.

The amine group of cysteine, however, plays a subtle role, contributing additional electron richness to the molecule relative to MPA. This property has been observed to play a role in charge transfer. In a QD-sensitised solar cell, a six-fold enhancement in the incident photon-to-current efficiency was measured when cysteine was used as a linker, compared to MPA.[53] The authors speculated that the increased electron density across the molecule, as well as the donor-acceptor abilities of the amine group, might promote charge transfer. Hines and Kamat cited the same study in their review of quantum dot surface chemistry, adding that cysteine was likely to extract holes from the QD sensitisers.[54] In a colloidal system, a consequence of extracting holes would be ligand oxidation, and therefore removal from the QDs. This ligand removal

should aid hydrogen evolution by improving surface access by hole scavengers, but would also undermine the stability of QDs.

Cysteine was replaced with MPA to assess if the two ligands behaved analogously as the stabilising ligand for hybrid photocatalysts. The first indication that this might not be the case came while performing the QD ligand exchange. In the ligand exchange protocol, diluted QD stock solution in chloroform was shaken with an aqueous solution of the ligand at alkaline pH. When using cysteine, a typical ligand exchange required 25-30 minutes of continuous shaking before the QDs transferred to the aqueous phase, implying sufficient functionalisation with the ligand. QDs were completely transferred to the aqueous phase within 1 minute of shaking with a solution of MPA, suggesting that the molecule had an even greater affinity for the CdS surface. This qualitative observation speaks to the relative strength of MPA binding compared to cysteine, arising from the greater basicity of the former molecule.[55,56]

After collecting the stock solutions of cysteine- and MPA-functionalised QDs, hydrogen evolution experiments were performed using QDs without a co-catalyst, as well as in the presence of either CoPyS or $CoCl_2$. The results are shown in Figure 3-17. Evidently, QDs functionalised with cysteine can generate small amounts of hydrogen on their own under illumination, but addition of either the cobaloxime or cobalt chloride increases the activity significantly. In the case of MPA-coated QDs, no hydrogen evolution is observed for QDs or QDs with cobalt chloride. Hydrogen is generated in the presence of CoPyS, but with only ~20% the yield achieved using cysteine as a stabilising ligand. QD aggregation was noticeable reduced in the MPA-functionalised samples.

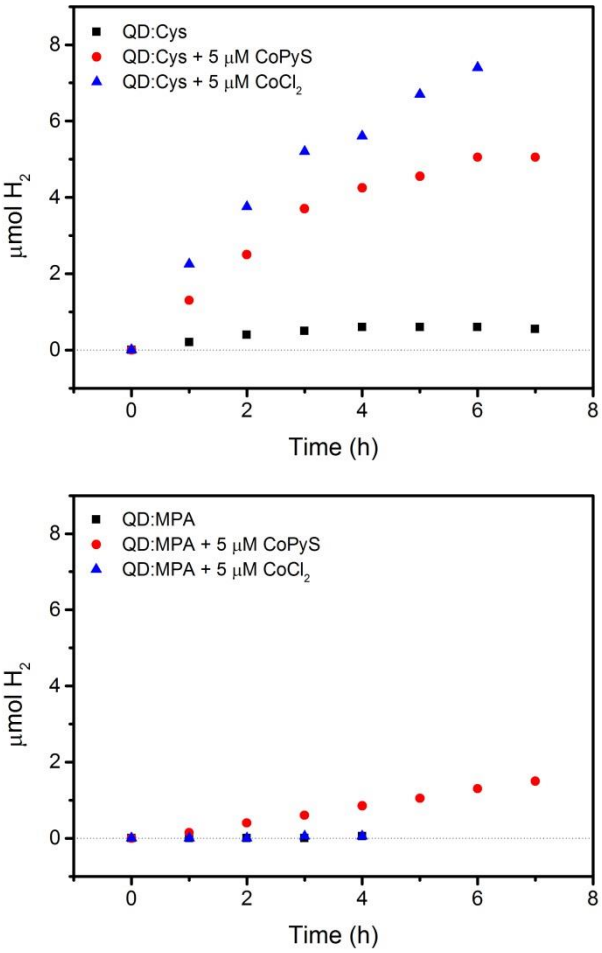

Figure 3-16. Hydrogen evolution by CdS QDs bearing either cysteine (top) or MPA (bottom) stabilising ligands, in the absence and presence of the co-catalysts CoPyS or $CoCl_2$.

To check whether photo-oxidation of MPA was simply slower than that of cysteine, an extended experiment was conducted in which solutions of MPA-functionalised QDs with either CoPyS or $CoCl_2$ were illuminated continuously for 24 hours. The results are plotted in Figure 3-18. Interestingly, hydrogen evolution did eventually begin at a moderate rate when $CoCl_2$ was used as the co-catalyst, whereas CoPyS was minimally active. Note that this result using the cobaloxime contradicts the findings presented in Figure 3-17, where ~1 μmol H_2 was evolved by nominally the same system over 7 hours of illumination. While there are likely to be variations in the degree of QD ligand functionalisation that contribute to the variation in hydrogen yields between experiments, this result may also indicate that CoPyS operated as a molecular catalyst under circumstances that prevented formation of an active species by $CoCl_2$ on the QD surface.

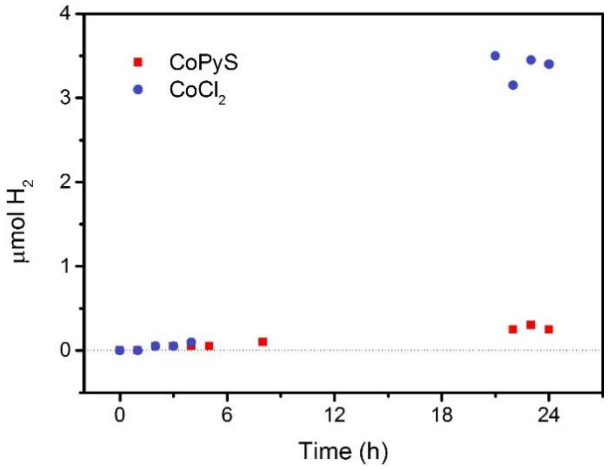

Figure 3-17. Long-term hydrogen evolution experiment using MPA-coated CdS QDs in the presence of 50 μM CoPyS or $CoCl_2$ co-catalyst.

Under extended illumination, it was speculated that Co^{2+} species from cobalt chloride could penetrate the MPA ligand shell, due to their relatively smaller size, to establish the catalytically active sites at the QD surface, while the cations contained within the bulkier cobaloximes could not. Once an active site is formed, it could act as a sink for electrons; charge separation could then occur, leaving holes within the QD core that eventually oxidise ligands.[36] Once the ligand shell is partially compromised and hole scavengers can reach the QD surface, hydrogen evolution proceeds. This

experiment also implies that the induction period observed prior to hydrogen evolution for some materials relates to ligand removal.

The apparently slower photo-oxidation of MPA compared to cysteine is thought to be due to the difference in the oxidation potentials of these ligands. In Figure 3-19, these potentials are shown relative to the valence band edge of CdS QDs, which corresponds to the energy of the photo-generated holes responsible for ligand oxidation. The oxidation potential of cysteine is more than 700 mV more negative than that of MPA, meaning that the driving force for hole transfer from the QD valence band is significantly greater. As a result, the rate of hole transfer will also be faster, leading to more rapid oxidation of cysteine ligands.

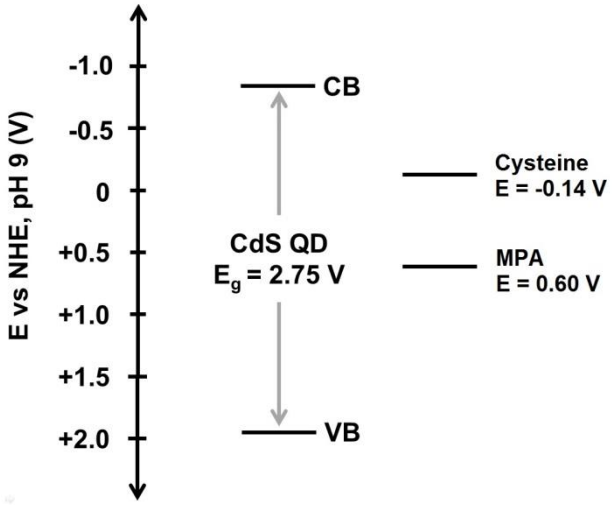

Figure 3-18. Energy level diagram illustrating the alignment of the oxidation potentials of the QD ligands cysteine and MPA relative to the band edges of CdS QDs. Cysteine[57,58] and MPA[56] oxidation potentials, as well as the QD band energies[32], were adjusted for pH 9 from published values.

The contrasting hydrogen evolution behaviour of cysteine- and MPA-functionalised QDs highlights the stabilising ligands as important components of colloidal QD-based photocatalytic systems. While both ligands provide the same colloidal stabilisation for the QDs after phase transfer, their individual susceptibilities to oxidation leads to very different catalytic activities under illumination. The less negative oxidation potential of MPA translates to slower removal from the QDs, inhibiting

hydrogen evolution. Cysteine, on the other hand, is more readily oxidised, exposing the QD surface to hole scavengers and facilitating photocatalysis, but also compromising colloidal stability. The presence or absence of just one amine group on the molecules that coat the QDs comes to dictate the overall activity of the system.

These experiments underline a dilemma in designing a QD-based photocatalyst in which colloidal stability and catalytic activity appear to be in opposition to each other. A robust ligand shell promotes particle dispersion and longevity but restricts charge transfer to and from the QDs. In considering ways to address this problem, the study by Chang et al.[38] exemplifies one method, namely, intentional post-synthetic stripping of ligands from QDs before assembly of photocatalysts. Another strategy was explored in a publication from our group, in which CdS QDs with Pt co-catalysts were stabilised in-situ by additional ligands (TEOA) in the surrounding solution that loosely coordinate to the QDs once the original cysteine ligand shell is partially removed.[57] In the presence of TEOA, hydrogen evolution by the CdS/Pt photocatalysts was prolonged by a factor of ten, demonstrating that aggregation of QDs undermines catalytic activity in such systems. The regimes of ligand coverage that were identified in this study, and how they relate to the observed activity, are summarised in Figure 3-20.

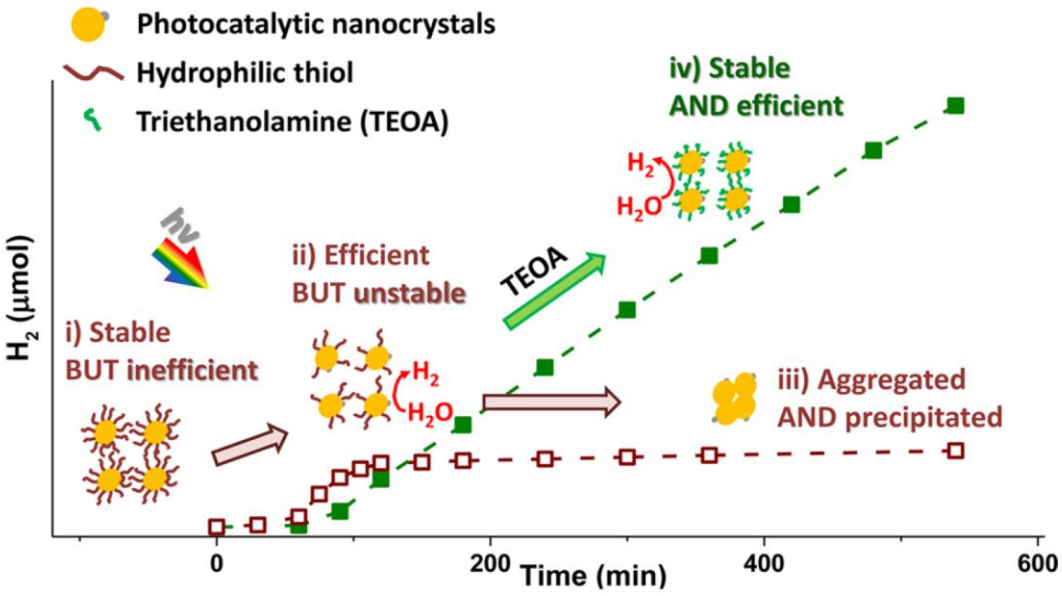

Figure 3-19. Scheme depicting the evolution of the cysteine ligand shell of CdS/Pt photocatalysts during hydrogen evolution, and the effect of in-situ stabilisation by TEOA. Reproduced from [59].

Besides ligand stripping and in-situ stabilisation, a third approach existed for balancing colloidal stability and catalytic activity of QDs in which ligands that actively promote hole scavenging are introduce to the ligand shell. If an adsorbed molecule could accept holes from the QD core and relay them to scavengers in solution, oxidation of other ligands might be avoided, thereby preventing particle aggregation. Two embodiments were envisaged. In the first, a hole transfer ligand could be integrated into the ligand shell among molecules that only provide colloidal stabilisation; in the second, a single molecule would be capable of promoting hole transfer while also imparting colloidal stability to QDs. Exploration of these strategies constitutes the remainder of this thesis.

3.13 Hole-Delocalising Molecule to Mitigate Ligand Oxidative

In searching for molecules that might behave as a hole transfer ligands, a paper by Tan et al. provided inspiration.[58] The authors had demonstrated that treating CdSe QDs with an aromatic ligand, 4-dimethylaminothiophenol (DMATP), offered significant protection to QDs against photo-oxidation while adsorbed to TiO2

electrodes. Their analysis, supported by DFT calculations, suggested that electron donation by the *para*-amino substituent promoted hole delocalisation away from the thiol anchoring group and onto the ligand itself. It was thought that this behaviour, in the context of colloidal QDs, might prevent or slow oxidation of cysteine, as depicted in Figure 3-21. Although DMATP would not provide any aqueous colloidal stability itself, its thiol group meant that it could be easily adsorbed to CdS alongside hydrophilic thiols.

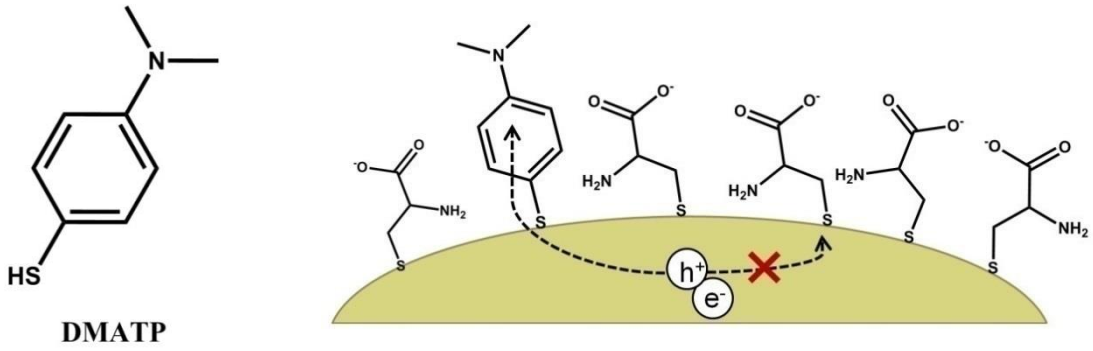

Figure 3-20. (Left) Structure of 4-dimethylaminothiophenol (DMATP); (right) scheme depicting hole transfer to DMATP rather than cysteine under illumination.

To investigate how the hole extracting abilities of DMATP might impact hydrogen evolution, the molecule was incorporated into a predominantly cysteine ligand shell for CdS QDs. Due to its hydrophobicity, the DMATP was pre-adsorbed to the QDs in chloroform ahead of phase transfer to water with cysteine. H_2 evolution was then conducted with these QDs and compared to an untreated control group from the same synthetic batch of QDs in combination with CoPyS as a co-catalyst. The results are shown in Figure 3-22.

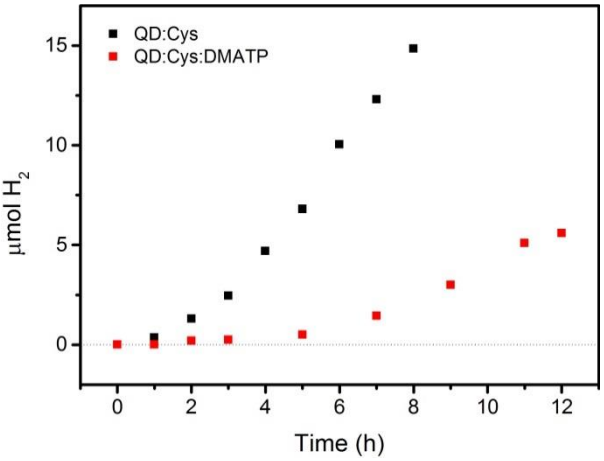

Figure 3-21. Comparison of hydrogen evolution in the presence of a CoPyS co-catalyst by QDs functionalised with cysteine ligands (black) or a mixed ligand shell of cysteine and DMATP (red).

Hydrogen was evolved by the control sample in a manner typical of this system, as demonstrated previously in this chapter. The increase in the rate of hydrogen production in the first 3-4 hours likely reflects both cobaloxime decomposition to form the active species and gradual oxidation of cysteine. In the DMATP-treated samples, the induction period is dramatically extended such that significant amounts of hydrogen are not observed until 5-6 hours of continuous illumination have elapsed. This behaviour is consistent with the protective effect of DMATP reported by Tan et al. through which holes are delocalised away from the QD core, which in the colloidal system slows oxidation of cysteine. It appears, however, that DMATP only delays the oxidation process. In an ideal case, the molecule would act as a conduit in a sort of "antenna" effect, channelling holes from the QD to acceptors in the surrounding solution to prevent loss of cysteine altogether. Despite the eventual aggregation of the QDs, this experiment showed that the introduction of hole-accepting molecules to the ligand shell had potential as a strategy for improving colloidal stability.

3.14 Conclusions

The results presented throughout this chapter suggest that, although photocatalytic hydrogen production was achieved, a true hybrid system composed of semiconductor nanocrystals and molecular catalysts was not realised. The nature of the

cobaloxime catalysts used for the study, in which the relatively labile ligand spheres were not synthetically stabilised (i.e. covalent attached to one another), meant that the complexes were prone to decomposition under redox cycling. While experimenting with these materials, a consensus appeared to develop in the literature that such simple cobaloximes were indeed unstable, and that rather than behaving as molecular catalysts, they act as pre-catalysts. The active species that develops on the QD surface following cobaloxime decomposition remains uncharacterised. It is possible that a complex possessing a macrocyclic ligand of higher denticity would be more stable upon adsorption to the QD surface and remain molecular.

Hydrogen evolution from a QD-based photocatalytic system was also found to be heavily dependent by the ligands used to colloidally stabilise the particles. Ligand oxidation and removal, while in principle a negative process in terms of the long-term stability of QDs, is actually an essential step before hydrogen evolution can begin. Comparing photocatalytic systems in which the QDs were stabilised by ligands with different susceptibilities to oxidation starkly illustrated the influence of ligands on overall activity. Colloidal stability and catalytic activity were therefore recognised as seemingly mutually exclusive properties to be reconciled. To address this dilemma, QD ligands could be chemically stripped before assembly of the photocatalyst, or the QDs could be additionally stabilised in-situ. Instead, a third strategy was pursued in which ligands actively promote transfer of holes from the QDs to scavengers. An initial experiment conducted with a hole-delocalising aromatic ligand, DMATP, suggested that tailoring the ligand shell to promote charge transfer might indeed be a viable strategy. This result motivated the work presented in the next chapter, where the mechanism underlying the observed effect of DMATP on ligand oxidation is investigated spectroscopically, and an effort is made to consolidate the functions of hole delocalisation and colloidal stabilisation into a single ligand.

3.15 References

(1) Wiberg, J.; Marinado, T.; Hagberg, D. P.; Sun, L.; Hagfeldt, A.; Albinsson, B. Effect of Anchoring Group on Electron Injection and Recombination Dynamics in Organic Dye-Sensitized Solar Cells. *J. Phys. Chem. B* **2009**, *113*, 3881–3886.

(2) Matta, S. K.; Kakiage, K.; Makuta, S.; Veamatahau, A.; Aoyama, Y.; Yano, T.; Hanaya, M.; Tachibana, Y. Dye-Anchoring Functional Groups on the Performance of Dye-Sensitized Solar Cells: Comparison between Alkoxysilyl and Carboxyl Groups. *J. Phys. Chem. C* **2014**, *118*, 28425–28434.

(3) Li, W.; Rego, L. G. C.; Bai, F.; Wang, J.; Jia, R.; Xie, L.-M.; Zhang, H.-X. What Makes Hydroxamate a Promising Anchoring Group in Dye-Sensitized Solar Cells? Insights from Theoretical Investigation. *J. Phys. Chem. Lett.* **2014**, *5*, 3992–3999.

(4) Schrauzer, G. N.; Windgassen, R. J. Alkylcobaloximes and Their Relation to Alkylcobalamins. *J. Am. Chem. Soc.* **1966**, *88*, 3738–3743.

(5) Schrauzer, G. N.; Windgassen, R. J. Cobalamin Model Compounds. Preparation and Reactions of Substituted Alkyl- and Alkenylcobaloximes and Biochemical Implications. *J. Am. Chem. Soc.* **1967**, *89*, 1999–2007.

(6) Schrauzer, G. N. Organocobalt Chemistry of Vitamin B12 Model Compounds (Cobaloximes). *Acc. Chem. Res.* **1968**, *1*, 97–103.

(7) Chao, T.-H.; Espenson, J. H. Mechanism of Hydrogen Evolution from Hydridocobaloxime. *J. Am. Chem. Soc.* **1978**, *100*, 129–133.

(8) Hawecker, J.; Lehn, J. M.; Ziessel, R. Efficient Homogeneous Photochemical Hydrogen Generation and Water Reduction Mediated by Cobaloxime or Macrocyclic Cobalt Complexes. *Nouv. J. Chim.* **1983**, *7*, 271–277.

(9) Connolly, P.; Espenson, J. H. Cobalt-Catalyzed Evolution of Molecular Hydrogen. *Inorg. Chem.* **1986**, *25*, 2684–2688.

(10) Razavet, M.; Artero, V.; Fontecave, M. Proton Electroreduction Catalyzed by Cobaloximes: Functional Models for Hydrogenases. *Inorg. Chem.* **2005**, *44*,

4786–4795.

(11) Hu, X.; Cossairt, B. M.; Brunschwig, B. S.; Lewis, N. S.; Peters, J. C. Electrocatalytic Hydrogen Evolution by Cobalt Difluoroboryl-Diglyoximate Complexes. *Chem. Commun.* **2005**, *1*, 4723–4725.

(12) Fihri, A.; Artero, V.; Razavet, M.; Baffert, C.; Leibl, W.; Fontecave, M. Cobaloxime-Based Photocatalytic Devices for Hydrogen Production. *Angew. Chem. Int. Ed. Engl.* **2008**, *47*, 564–567.

(13) Du, P.; Knowles, K.; Eisenberg, R. A Homogeneous System for the Photogeneration of Hydrogen from Water Based on a platinum(II) Terpyridyl Acetylide Chromophore and a Molecular Cobalt Catalyst. *J. Am. Chem. Soc.* **2008**, *130*, 12576–12577.

(14) Lazarides, T.; McCormick, T.; Du, P.; Luo, G.; Lindley, B.; Eisenberg, R. Making Hydrogen from Water Using a Homogeneous System without Noble Metals. *J. Am. Chem. Soc.* **2009**, *131*, 9192–9194.

(15) Lakadamyali, F.; Reisner, E. Photocatalytic H_2 Evolution from Neutral Water with a Molecular Cobalt Catalyst on a Dye-Sensitised TiO_2 Nanoparticle. *Chem. Commun.* **2011**, *47*, 1695–1697.

(16) Muresan, N. M.; Willkomm, J.; Mersch, D.; Vaynzof, Y.; Reisner, E. Immobilization of a Molecular Cobaloxime Catalyst for Hydrogen Evolution on a Mesoporous Metal Oxide Electrode. *Angew. Chem. Int. Ed. Engl.* **2012**, *51*, 12749–12753.

(17) Lakadamyali, F.; Kato, M.; Muresan, N. M.; Reisner, E. Selective Reduction of Aqueous Protons to Hydrogen with a Synthetic Cobaloxime Catalyst in the Presence of Atmospheric Oxygen. *Angew. Chem. Int. Ed. Engl.* **2012**, *51*, 9381–9384.

(18) Reynal, A.; Lakadamyali, F.; Gross, M. A.; Reisner, E.; Durrant, J. R. Parameters Affecting Electron Transfer Dynamics from Semiconductors to Molecular Catalysts for the Photochemical Reduction of Protons. *Energy Environ. Sci.* **2013**, *6*, 3291–3300.

(19) Reynal, A.; Willkomm, J.; Muresan, N. M.; Lakadamyali, F.; Planells, M.;

Reisner, E.; Durrant, J. R. Distance Dependent Charge Separation and Recombination in Semiconductor/Molecular Catalyst Systems for Water Splitting. *Chem. Commun.* **2014**, *50*, 12768–12771.

(20) Willkomm, J.; Muresan, N. M.; Reisner, E. Enhancing H_2 Evolution Performance of an Immobilised Cobalt Catalyst by Rational Ligand Design. *Chem. Sci.* **2015**, *6*, 2727–2736.

(21) Wen, F.; Yang, J.; Zong, X.; Ma, B.; Wang, D.; Li, C. Photocatalytic H_2 Production on Hybrid Catalyst System Composed of Inorganic Semiconductor and Cobaloximes Catalysts. *J. Catal.* **2011**, *281*, 318–324.

(22) Huang, J.; Mulfort, K. L.; Du, P.; Chen, L. X. Photodriven Charge Separation Dynamics in CdSe/ZnS Core/Shell Quantum Dot/Cobaloxime Hybrid for Efficient Hydrogen Production. *J. Am. Chem. Soc.* **2012**, *134*, 16472–16475.

(23) Gimbert-Suriñach, C.; Albero, J.; Stoll, T.; Fortage, J.; Collomb, M.-N.; Deronzier, A.; Palomares, E.; Llobet, A. Efficient and Limiting Reactions in Aqueous Light-Induced Hydrogen Evolution Systems Using Molecular Catalysts and Quantum Dots. *J. Am. Chem. Soc.* **2014**, *136*, 7655–7661.

(24) Meng, P.; Wang, M.; Yang, Y.; Zhang, S.; Sun, L. CdSe Quantum Dots/Molecular Cobalt Catalyst Co-Grafted Open Porous NiO Film as a Photocathode for Visible Light Driven H_2 Evolution from Neutral Water. *J. Mater. Chem. A* **2015**, *3*, 18852–18859.

(25) Wakerley, D. W.; Reisner, E. Development and Understanding of Cobaloxime Activity through Electrochemical Molecular Catalyst Screening. *Phys. Chem. Chem. Phys.* **2014**, 5739–5746.

(26) Connelly, N. G.; Geiger, W. E. Chemical Redox Agents for Organometallic Chemistry. *Chem. Rev.* **1996**, *96*, 877–910.

(27) Schrauzer, G. N. Bis(dimethylglyoximato)cobalt Complexes. *Inorg. Synth.* **1968**, *11*, 61–70.

(28) Du, P.; Schneider, J.; Luo, G.; Brennessel, W. W.; Eisenberg, R. Visible Light-Driven Hydrogen Production from Aqueous Protons Catalyzed by Molecular Cobaloxime Catalysts. *Inorg. Chem.* **2009**, *48*, 4952–4962.

(29) Dempsey, J. L.; Brunschwig, B. S.; Winkler, J. R.; Gray, H. B. Hydrogen Evolution Catalyzed by Cobaloximes. *Acc. Chem. Res.* **2009**, *42*, 1995–2004.

(30) Artero, V.; Chavarot-Kerlidou, M.; Fontecave, M. Splitting Water with Cobalt. *Angew. Chem. Int. Ed. Engl.* **2011**, *50*, 7238–7266.

(31) Li, W.; O'Dowd, G.; Whittles, T. J.; Hesp, D.; Gründer, Y.; Dhanak, V. R.; Jäckel, F. Colloidal Dual-Band Gap Cell for Photocatalytic Hydrogen Generation. *Nanoscale* **2015**, *7*, 16606–16610.

(32) Bard, A. J.; Faulkner, L. R. *Electrochemical Methods: Fundamentals and Applications*; 2nd ed.; John Wiley & Sons: New York, 2000.

(33) Berr, M. J.; Wagner, P.; Fischbach, S.; Vaneski, A.; Schneider, J.; Susha, A. S.; Rogach, A. L.; Jäckel, F.; Feldmann, J. Hole Scavenger Redox Potentials Determine Quantum Efficiency and Stability of Pt-Decorated CdS Nanorods for Photocatalytic Hydrogen Generation. *Appl. Phys. Lett.* **2012**, *100*, 223903.

(34) Liu, W.; Choi, H. S.; Zimmer, J. P.; Tanaka, E.; Frangioni, J. V; Bawendi, M. Compact Cysteine-Coated CdSe (ZnCdS) Quantum Dots for in Vivo Applications. *J. Am. Chem. Soc.* **2007**, *129*, 14530–14531.

(35) Berr, M.; Vaneski, A.; Susha, A. S.; Rodríguez-Fernández, J.; Döblinger, M.; Jäckel, F.; Rogach, A. L.; Feldmann, J. Colloidal CdS Nanorods Decorated with Subnanometer Sized Pt Clusters for Photocatalytic Hydrogen Generation. *Appl. Phys. Lett.* **2010**, *97*, 93108.

(36) Berr, M. J.; Vaneski, A.; Mauser, C.; Fischbach, S.; Susha, A. S.; Rogach, A. L.; Jäckel, F.; Feldmann, J. Delayed Photoelectron Transfer in Pt-Decorated CdS Nanorods under Hydrogen Generation Conditions. *Small* **2012**, *8*, 291–297.

(37) Yu, W. W.; Qu, L.; Guo, W.; Peng, X. Experimental Determination of the Extinction Coefficient of CdTe , CdSe , and CdS Nanocrystals. *Chem. Mater.* **2003**, *15*, 2854–2860.

(38) Chang, C. M.; Orchard, K. L.; Martindale, B. C. M.; Reisner, E. Ligand Removal from CdS Quantum Dots for Enhanced Photocatalytic H_2 Generation in pH Neutral Water. *J. Mater. Chem. A* **2016**, *4*, 2856–2862.

(39) Aldana, J.; Wang, Y. A.; Peng, X. Photochemical Instability of CdSe Nanocrystals Coated by Hydrophilic Thiols. *J. Am. Chem. Soc.* **2001**, *123*, 8844–8850.

(40) Jeong, S.; Achermann, M.; Nanda, J.; Ivanov, S.; Klimov, V. I.; Hollingsworth, J. A. Effect of the Thiol-Thiolate Equilibrium on the Photophysical Properties of Aqueous CdSe/ZnS Nanocrystal Quantum Dots. *J. Am. Chem. Soc.* **2005**, *127*, 10126–10127.

(41) Turo, M. J.; Macdonald, J. E. Crystal-Bound vs Surface-Bound Thiols on Nanocrystals. *ACS Nano* **2014**, *8*, 10205–10213.

(42) Anderson, N. C.; Hendricks, M. P.; Choi, J. J.; Owen, J. S. Ligand Exchange and the Stoichiometry of Metal Chalcogenide Nanocrystals: Spectroscopic Observation of Facile Metal-Carboxylate Displacement and Binding. *J. Am. Chem. Soc.* **2013**, *135*, 18536–18548.

(43) Trogler, W. C.; Stewart, R. C.; Epps, L. A.; Marzilli, L. G. Cis and Trans Effects on the Proton Magnetic Resonance Spectra of Cobaloximes. *Inorg. Chem.* **1974**, *13*, 1564–1570.

(44) Lakadamyali, F.; Reynal, A.; Kato, M.; Durrant, J. R.; Reisner, E. Electron Transfer in Dye-Sensitised Semiconductors Modified with Molecular Cobalt Catalysts: Photoreduction of Aqueous Protons. *Chemistry* **2012**, *18*, 15464–15475.

(45) Bakac, A.; Espenson, J. H. Unimolecular and Bimolecular Homolytic Reactions of Organochromium and Organocobalt Complexes. Kinetics and Equilibria. *J. Am. Chem. Soc.* **1984**, *106*, 5197–5202.

(46) Jacques, P.-A.; Artero, V.; Pécaut, J.; Fontecave, M. Cobalt and Nickel Diimine-Dioxime Complexes as Molecular Electrocatalysts for Hydrogen Evolution with Low Overvoltages. *Proc. Natl. Acad. Sci. U. S. A.* **2009**, *106*, 20627–20632.

(47) Andreiadis, E. S.; Jacques, P.-A.; Tran, P. D.; Leyris, A.; Chavarot-Kerlidou, M.; Jousselme, B.; Matheron, M.; Pécaut, J.; Palacin, S.; Fontecave, M.; *et al.* Molecular Engineering of a Cobalt-Based Electrocatalytic Nanomaterial for H_2 Evolution under Fully Aqueous Conditions. *Nat. Chem.* **2012**, *5*, 48–53.

(48) Cherdo, S.; Ghachtouli, S. El; Sircoglou, M.; Brisset, F.; Orio, M.; Aukauloo, A. A Nickel Dimethyl Glyoximato Complex to Form Nickel Based Nanoparticles for Electrocatalytic H_2 Production. *Chem. Commun.* **2014**, 13514–13516.

(49) Kaeffer, N.; Morozan, A.; Fize, J.; Martinez, E.; Guetaz, L.; Artero, V. The Dark Side of Molecular Catalysis: Diimine-Dioxime Cobalt Complexes Are Not the Actual Hydrogen Evolution Electrocatalyst in Acidic Aqueous Solutions. *ACS Catal.* **2016**, *6*, 3727–3737.

(50) Wuister, S. F.; Swart, I.; Driel, F. Van; Hickey, S. G.; Donega, C. D. M. Highly Luminescent Water-Soluble CdTe Quantum Dots. *Nano Lett.* **2003**, *3*, 503–507.

(51) Sambur, J. B.; Parkinson, B. A. CdSe/ZnS Core/Shell Quantum Dot Sensitization of Low Index TiO_2 Single Crystal Surfaces. *J. Am. Chem. Soc.* **2010**, *132*, 2130–2131.

(52) Kuehnel, M. F.; Wakerley, D. W.; Orchard, K. L.; Reisner, E. Photocatalytic Formic Acid Conversion on CdS Nanocrystals with Controllable Selectivity for H_2 or CO. *Angew. Chemie - Int. Ed.* **2015**, *54*, 9627–9631.

(53) Mora-Seró, I.; Giménez, S.; Moehl, T.; Fabregat-Santiago, F.; Lana-Villareal, T.; Gómez, R.; Bisquert, J. Factors Determining the Photovoltaic Performance of a CdSe Quantum Dot Sensitized Solar Cell: The Role of the Linker Molecule and of the Counter Electrode. *Nanotechnology* **2008**, *19*, 424007.

(54) Hines, D. A.; Kamat, P. V. Quantum Dot Surface Chemistry: Ligand Effects and Electron Transfer Reactions. *J. Phys. Chem.* **2013**, *117*, 14418–14426.

(55) Borghi, E. B.; Morando, P. J.; Blesa, M. A. Dissolution of Magnetite by Mercaptocarboxylic. *Langmuir* **1991**, *7*, 1652–1659.

(56) Forlano, P.; Olabe, J. A.; Magallanes, J. F.; Blesa, M. A. The Mechanism of Oxidation of 3-Mercaptopropionic Acid. *Can. J. Chem.* **1997**, *75*, 9–13.

(57) Li, W.; Lee, J. R.; Jäckel, F. Simultaneous Optimization of Colloidal Stability and Interfacial Charge Transfer Efficiency in Photocatalytic Pt/CdS Nanocrystals. *ACS Appl. Mater. Interfaces* **2016**, *8*, 29434–29441.

(58) Tan, Y.; Jin, S.; Hamers, R. J. Influence of Hole-Sequestering Ligands on the

Photostability of CdSe Quantum Dots. *J. Phys. Chem. C* **2013**, *117*, 313–320.

4. HYDROPHILIC AMINOTHIOLS AS LIGANDS FOR QDS

4.1 Overview

In the previous chapter, strategies were considered to address particle aggregation in QD-based systems during photocatalysis. One experiment investigated the effect of an aromatic thiol, 4-dimethylaminothiophenol (DMATP), on the activity of a colloidal CdS QD-based photocatalytic system. This molecule had previously been shown to delocalise holes from CdSe QDs during illumination, protecting the particles from photo-oxidation.[1] For colloidal CdS QDs, incorporation of DMATP into the ligand shell was found to dramatically delay the onset of hydrogen evolution, which was attributed to hole transfer from the QDs to the aromatic ligand and therefore a slowdown in oxidation of the cysteine stabilising ligands. This result showed that tailoring the ligand shell to promote hole transfer might be a viable strategy to reduce QD aggregration under illumination, and motivated further study of the DMATP and related molecules.

This chapter describes a study of several aminothiol molecules with the aim of identifying ligands that can promote hole transfer from QDs. Ultrafast transient absorption (TA) spectroscopy was used to explore the electronic effects of these ligands on QDs. To best utilise the transient absorption system available for this work, CdSe QDs were employed, which have spectral features within the most stable region of the white light continuum generated by the instrument. In the first section of this chapter, the mechanism underlying the protective effect of DMATP on QDs is investigated. A transient absorption study of this system did not exist in the literature, so it was hoped that the behaviour observed could be futher rationalised spectroscopically. Hole-delocalising properties similar to DMATP were then sought in an hydrophilic ligand, 4-aminothiophenol (ATP), in an attempt to consolidate hole extraction and QD stabilising functionalities in a single ligand. An aliphatic molecule bearing the same functional groups, 2-aminoethanethiol (AET), was also investigated to highlight the potential influence of conjugation in hole-delocaling ligands. To the best of our knowledge, no transient absorption studies of CdSe QDs stabilised in water by aminothiols exist in the literature, and until this year[2] we had not come across an example of ATP used as a ligand for colloidal semiconductor QDs in water.

4.2 Introduction

Aminothiols are infrequently used to stabilise group 10 chalcogenide nanocrystals in solution. Terminal amine ligands only impart solubility in water when the pH is sufficiently low (approaching the pK_a of the amine), such that the amine is protonated to form the positively charged ammonium species. This property restricts their useful pH range to relatively acidic conditions. When they are used as ligands, it is more often at an intermediate stage in material preparation, where the terminal amine is exploited for amide coupling reactions, rather than to provide colloidal stability; for example, this strategy is used to attach QDs to oxidised carbon nanotubes.[3,4] Aminothiols are also used in biological studies, where the QDs are employed as fluroescent sensors, or to conjugate QDs to DNA or proteins.[5–8] In all of these instances the thiol binds to the QD surface, leaving the terminal amine exposed to interact with a substrate. To the best of our knowledge, just three studies have been published that used aminothiols to colloidally stabilise Cd chalcogenide QDs in water: two photoluminescence studies by Wuister et al.[9,10] using CdTe QDs coated with 2-aminoethanethiol hydrochloride, and a paper[2] published since the work described herein was conducted, which used 4-aminothiophenol as a ligand for CdSe/ZnS core/shell QDs in acidic aqueous conditions.

Aromatic aminothiols have also been used to induce electronic changes in QDs, rather than to provide colloidal stability. Early transient spectroscopic studies of Cd chalcogenide QDs used 4-aminothiophenol as an electron-donating/hole-scavenging molecule to manipulate the relative populations of charge carriers in nanocrystals.[11,12] Aruda et al. included 4-aminothiophenol in a study of *para*-substituted thiophenols and their effect on CdSe QDs, finding that more electron donating substituents delocalised excitons to a greater extent from the QD core.[13] Work by Tan et al., referred to in Chapter 3 and at the beginning of this chapter, showed that 4-dimethylaminothiophenol protected CdSe QDs from oxidative degradation on porous TiO_2 electrodes under illumination.[1] In contrast, this study found that thiophenol and 1-dodecanethiol offered no such protection, demonstrating the significance of a conjugated moelecule and the amine functional group for hole delocalisation.

4.3 Features in Transient Absorption Spectra of CdSe QDs

The results in this chapter, as well as Chapter 5, consist primarily of transient absorption measurements of CdSe QDs. A brief overview of the significant features in the spectra of these materials, and their physical origins, is therefore provided here.

CdSe nanocrystals featured prominently in the early studies of quantum-confined semiconductors, and remain popular model absorbers for fundamental studies owing to their tuneable band gap in the visible region.[14,15] CdSe QDs were used to demonstrate the theoretical predictions of size-dependent optical spectra arising from quantum confinement and to assign the features to specific transitions.[16,17] Numerous in-depth transient absorption studies, notably by Klimov et al., have subsequently explored the charge carrier dynamics of excited CdSe QDs, and the physics underlying transient spectral features is now well established. These papers also introduced a naming convention for these features: A1, B1, B2, A2, B3, etc. as illustated below in Figure 4-1.[18,19] "A" refers to photoinduced absorptions with positive ΔA, while "B" refers to bleached absorptions with negative ΔA, while the numbering convention labels the signals within each group in ascending order by the energy at which the signal is found.

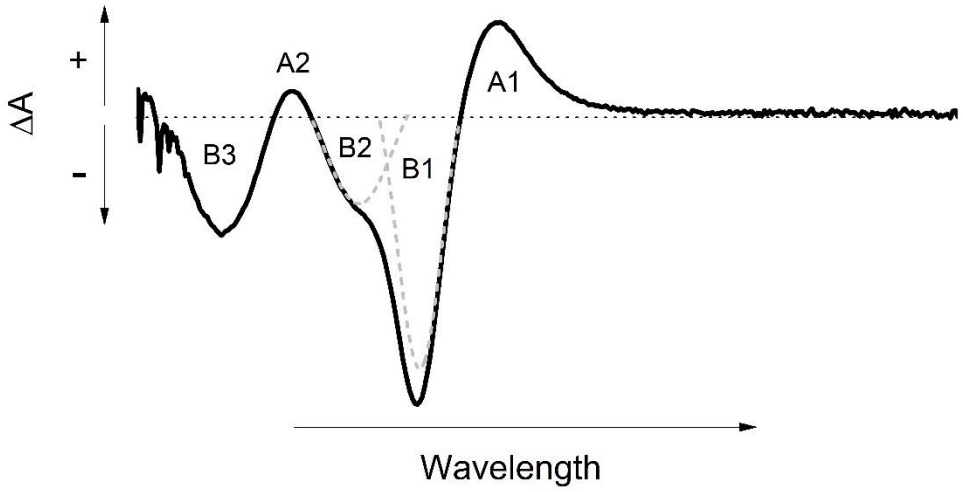

Figure 4-1. Illustration of the naming convention introduced by Klimov for transient features in TA spectra. The horizontal dotted line indicates ΔA = 0, while the dashed curves highlight the individual shapes of B1 and B2 when the overlapping signals are deconvoluted.

Transient absorption spectra of CdSe QDs consist of several typical features. Prominent negative signals at energies just above the band gap arise due to population of electronic excited states in the conduction band.[19,20] While these states are occupied, further transitions from the ground state are not possible, in accordance with the Pauli exclusion principle. This state filling manifests as bleaching of ground state transitions in the TA spectrum as probe light is no longer absorbed at these energies, hence a negative ΔA signal. As excited electrons depopulate the conduction band, the intensity of the ground state bleach signal diminishes. The kinetics of the ground state bleach signal can therefore be used to track the population of conduction band electrons over time.[11,21] Valence band holes do not contribute to the ground state bleach signal in CdSe QDs.[18,22]

Positive signals in TA spectra, referred to generally as photo-induced absorptions, correspond either to transitions that are newly accessible from populated energy levels within the electronically excited state or to red- or blue-shifted ground state transitions.[19,23] TA spectra of CdSe QDs also typically include a characteristic

photo-induced absorption which appears on the low energy edge of the ground state bleach. This feature, referred to frequently in the literature as "A1", is notable as it arises from biexcitons in CdSe QDs.[24] After the pump pulse has created an exciton in the QD, energy from the probe light can then be absorbed to create the biexciton, hence a positive ΔA. The red-shift of A1 reflects the biexciton binding energy, which as an attractive Coulomb potential reduces the overall energy of the biexciton relative to the energy of two non-interacting excitons. Finally, a broad, low intensity photo-induced absorption is sometimes observed in transient spectra of CdSe QDs and has been attributed to trapped holes based on electron and hole scavenging experiments.[21,25]

It should be noted that the transient spectra discussed throughout the remainder of this thesis are observed following single photon absorption by QDs. Given the extinction coefficient of the QDs at the pump wavelength and the energy density of the laser used to excite the samples, the excitation probability is estimated to be ~0.1 photons per QD. This ensures that contibutions to the overall spectra by doubly-excited QDs are minimised.

4.4 Influence of DMATP on CdSe QD Charge Charrier Dynamics

To investigate the underlying mechanism of the observed protective effect of DMATP, samples of CdSe QDs with average diameters of 3.7 nm were prepared with different amounts of the ligand adsorbed in chloroform. The as-synthesised QDs were compared to samples from the same batch that had been exposed to 1 and 5 molar equivalents of DMATP. Figure 4-2 details the extinction (a) and emission spectra (c) of the materials. DMATP does not affect the position of the excitonic peak, found at 575 nm in all samples, nor any other features in the spectrum. In contrast, the ligand has a significant impact on QD photoluminescence. As-synthesised CdSe QDs exhibited band edge emission centered at 590 nm, however exposure to the equivalent of just one DMATP molecule per QD reduced the emission yield by 50%. A concentration of five molecules per QD reduced the yield to roughly 5% of that observed for the control group.

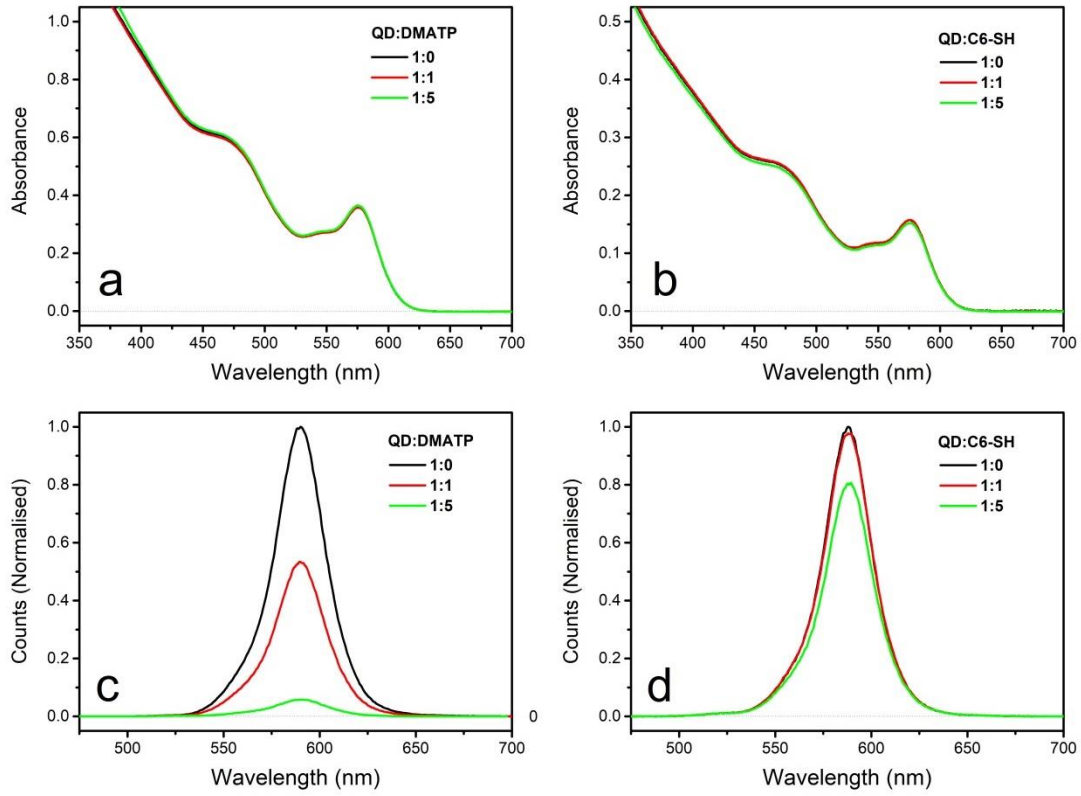

Figure 4-2. Extinction spectra of CdSe QDs functionalised with increasing QD:ligand ratios for (a) DMATP and (b) C6-SH in chloroform, along with emission spectra (c) and (d) of the respective QD materials (λ_{ex} = 450 nm). Emission spectra were normalised to the maximum number of counts detected for samples without thiol ligands (1:0).

Thiol functionalisation is known to reduce the yield of band edge photoluminesence in CdSe QDs by affecting the distribution of midgap trap states.[26] Nevertheless, the efficiency of quenching is striking at such low concentrations. To establish whether the observed effect on PL could simply be attributed to the thiol anchoring group of DMATP, parallel measurements using 1-hexanethiol (C6-SH) were performed. Adsorption of 1-hexanethiol does not affect the extinction spectrum of the QDs, as is evident from Figure 4-2(b). The emission spectra in Figure 4-2(d), however, show that 1-hexanethiol has a much more modest effect on the photoluminescence yield than DMATP at comparable concentrations. Even with 25 equivalents of this molecule present per QD, ~30% of the PL intensity observed in the unfuntionalised material

remained (data not shown). This result implies that DMATP efficiently suppresses the band edge emission of QDs, to a much greater extent than a simple thiol molecule. This behaviour is consistent with an additional mechanism of quenching, i.e. hole delocalisation from the QD onto the ligand, which interrupts the radiative recombination pathway.

A study by Sharma et al. comparing the effects of *n*-butylamine and *p*-phenylenediamine on the PL of CdSe QDs found that the aliphatic molecule passivated electron traps, enhancing the PL, but that the aromatic molecule could be oxidised by photo-generated holes which quenched the emission.[27] The nature of amine and thiol anchoring groups is obviously quite different, however the striking difference between aliphatic and aromatic ligands is relevant in the context of the effect of 1-hexanethiol compared to DMATP.

Following the steady-state characterisation of CdSe QDs with various DMATP loadings, transient absorption spectra were recorded. Samples were excited at 450 nm, which pumps the 1P(e)-$1P_{3/2}$(h) transition in the QDs.[28] This pump wavelength is also outside the range of the probe continuum (450 - 900 nm), and so eliminates unwanted contributions to the spectra. In Figure 4-3(a), a contour plot illustrates the evolution of the spectrum of as-synthesised QDs in the ~3 ns after initial excitation. The spectrum is dominated by a prominent negative signal at 575 nm with a clear shoulder at 550 nm (B1 and B2 respectively), and another negative signal at 475 nm, resulting from bleaching of the 1P(e)-$1P_{3/2}$(h) transition. The positive biexciton absorption (A1) on the low-energy edge of the bleach signal is also present, persisting on a comparable timescale to other signals in the spectrum.

Functionalisation with just one molecule of DMATP per QD induces significant changes to the spectral features, shown in Figure 4-3(b). The distinct B2 signal at 550 nm associated with the 1S(e)-$2S_{3/2}$(h) transition is no longer distinctly visible, apparently red-shifted so that it now overlaps the band edge signal at 575 nm. The energy of the 1P(e)-$1P_{3/2}$(h) transition at 475 nm in the control sample is red-shifted by ~10 nm in the presence of DMATP, with the intensity increasing with DMATP coverage. The B1 signal at 575 nm also red-shifts gradually with increasing ligand coverage. Notable changes occur in the A1 signal at ~620 nm, where adsorbed DMATP

results in a more intense signal that subsequently decays within 10 ps, in contrast to the long-lived (ns) A1 signal in the as-synthesised QDs. The spectral position of A1 does not shift appreciably.

Changes in the kinetics of bleach signals are also observed in DMATP-functionalised QDs. In Figure 4-4, B1 reaches its maximum intensity within 2 ps in the control group, followed by a fast initial relaxation over several picoseconds, while the same signal in DMATP QDs continues to grow in for the 10 ps following excitation. The B1 kinetics of all three samples, shown in Figure 4-5(a), converge after ~15 ps and decay at similar rates thereafter. The traces were fit to monoexponentials, which suggests a small acceleration in the kinetics based on the time constants, however the differences between samples are of similar magnitude to the errors on the fittings. The same analysis of the B3 kinetics in Figure 4-5(b) shows an acceleration of the bleach recovery upon adsorption of DMATP. Fit parameters for B1 and B3 kinetics are summarised in Table 4-1.

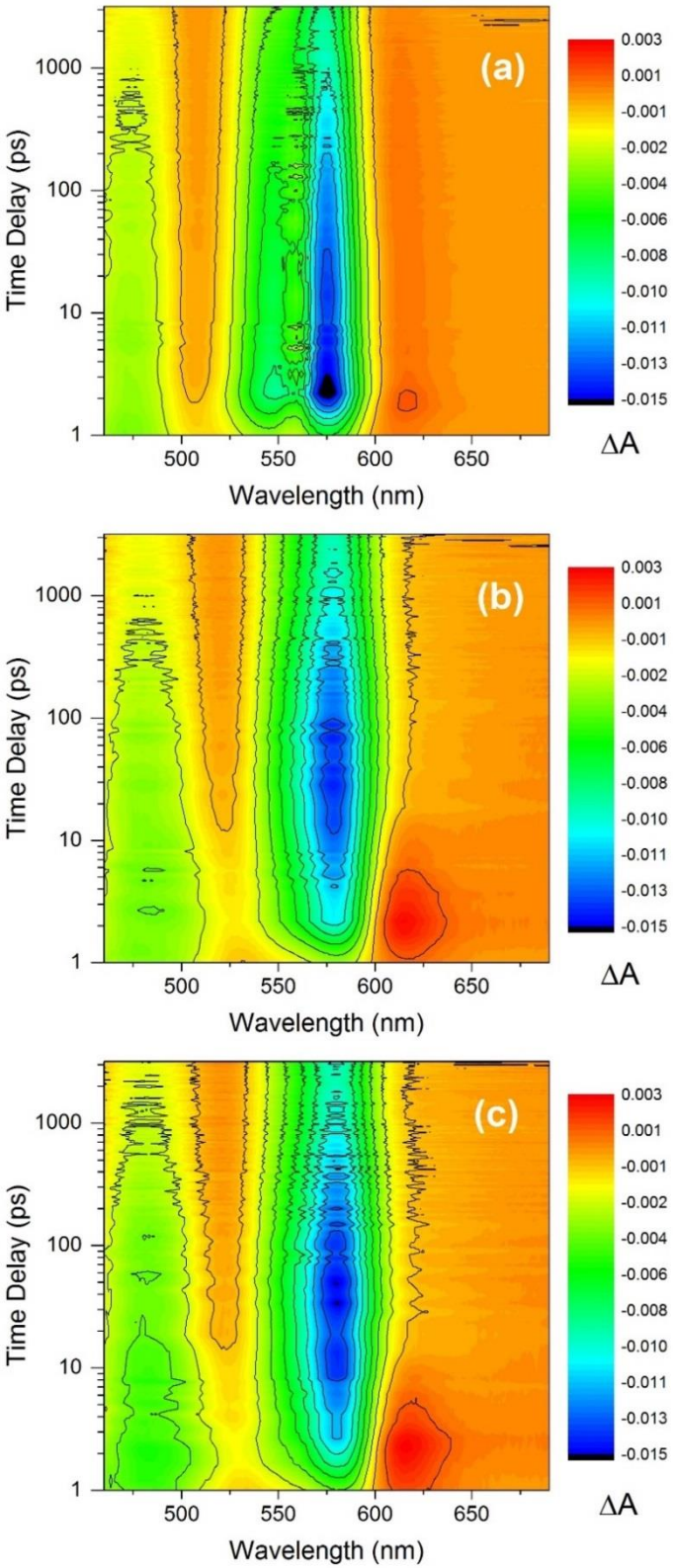

Figure 4-3. Transient absorption spectra (λex = 450 nm) of CdSe QDs, presented as contour plots on a logarithmic time scale. QD:DMATP ratios of (a) 1:0, (b) 1:1, (c) 1:5.

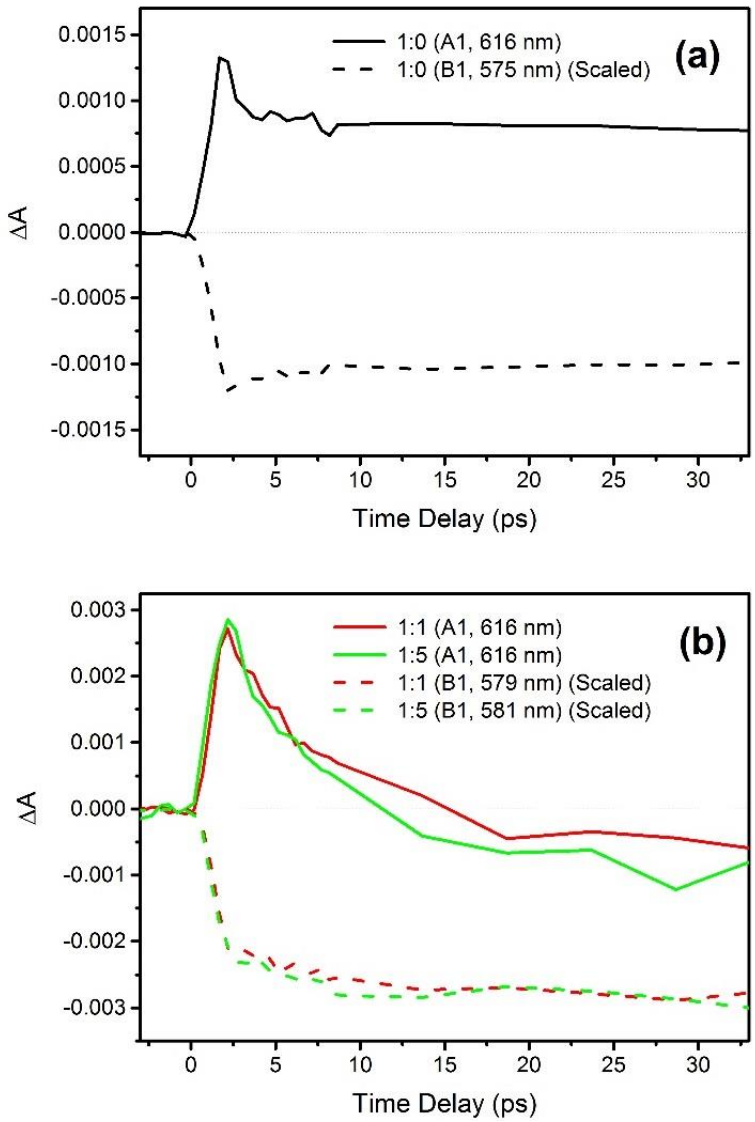

Figure 4-4. Kinetics of the A1 feature (solid lines) in the spectrum of CdSe QDs compared to the kinetics of the B1 feature (dashed lines, scaled for comparison). Legends indicate the spectral position of features. (a) 1:0, (b) 1:1 and 1:5 QD:DMATP ratios. In (b) the negative ΔA values in the kinetics of A1 (616 nm) after ~10 ps do not reflect bleaching but result from the broadening of the adjacent bleach signal region after decay of A1.

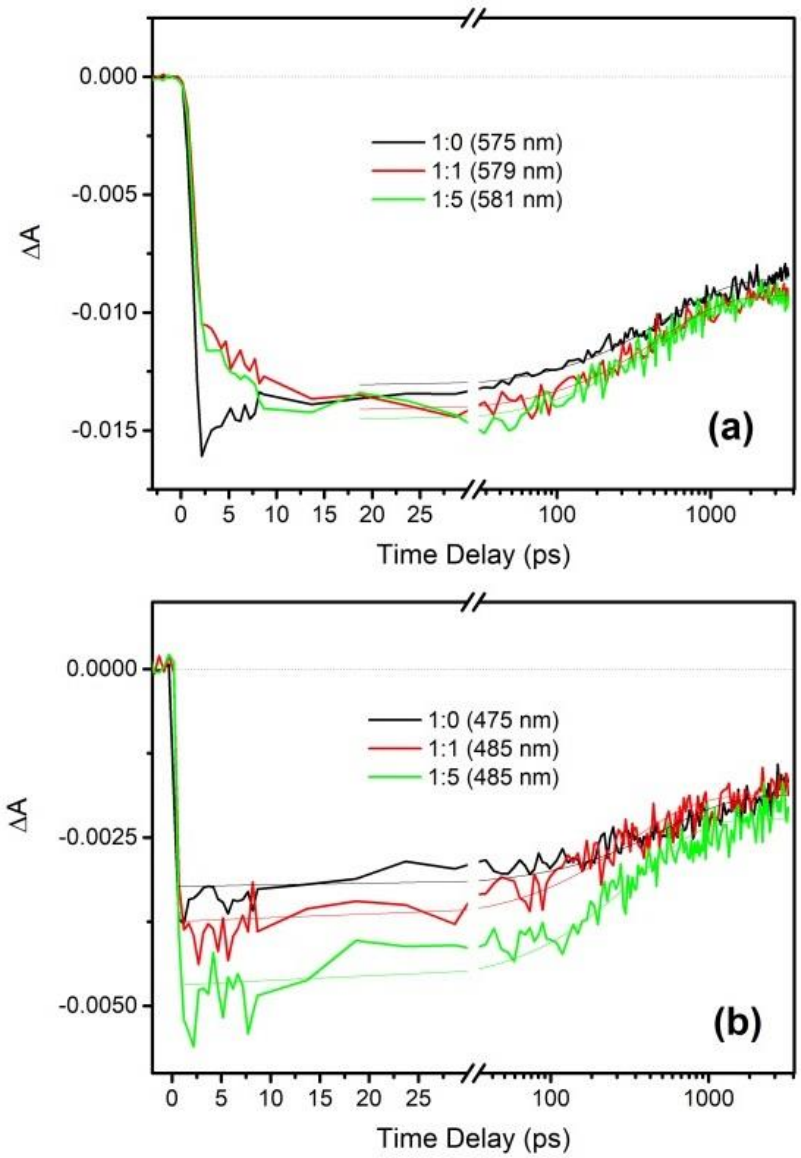

Figure 4-5. Kinetics of the (a) B1 and (b) B3 signals in CdSe QDs functionalised with varying amounts of DMATP, corresponding to relaxation of the excited 1S(e)-1S3/2(h) and 1P(e)-1P3/2(h) transitions, respectively. Exponential fits included, with tabulated fitting parameters.

		Equation: $y = A * \exp(-x/\tau) + y_0$		
		1:0	1:1	1:5
B1	y_0	-0.0086 ± 0.0001	-0.0093 ± 0.0001	-0.0093 ± 0.0001
	A	-0.0047 ± 0.0001	-0.0050 ± 0.0001	-0.0054 ± 0.0001
	τ	500 ± 20 ps	460 ± 20 ps	450 ± 30 ps
B3	y_0	-0.0019 ± 0.0001	-0.0019 ± 0.0001	-0.0022 ± 0.0001
	A	-0.0014 ± 0.0001	-0.0019 ± 0.0001	-0.0025 ± 0.0001
	τ	530 ± 50 ps	310 ± 20 ps	340 ± 20 ps

Table 4-1. Fitting parameters for the kinetics of the B1 and B3 signals plotted in Figure 4-5. Fitting windows begin at 1 ps for B1 and 18 ps for B3, and end at the final data point (3198 ps).

Based on the results of the transient absorption experiments, the charge carrier dynamics of CdSe QDs, with and without DMATP, are summarised as follows. The processes are illustrated schematically in Figure 4-6. The 1P(e)-$1P_{3/2}$(h) transition is excited by a pump pulse with energy greater than the band gap of the QDs, creating an exciton, Figure 4-6(a). The appearance of the B1/B2 bleach signals then implies population of 1S(e) states. In the case of the control sample without DMATP (Figure 4-6(b)), electrons begin to relax to the 1S state within ~2 ps, based on the onset rate of the B1 signal (see Figure 4-5(a)). This process evidently does not restore the 1P(e)-$1P_{3/2}$(h) transition, with the associated B3 bleach signal remaining in the spectra, which may indicate that the hole remains in the $1P_{3/2}$(h) state, as depicted in Figure 4-6. The B1 and B3 bleach signals then recover in parallel (Table 4-1). With excitons persisting on the order of nanoseconds, photons from the probe pulse can be absorbed to create biexcitons, resulting in the long-lived biexciton photo-induced absorption (A1) at ~620 nm.

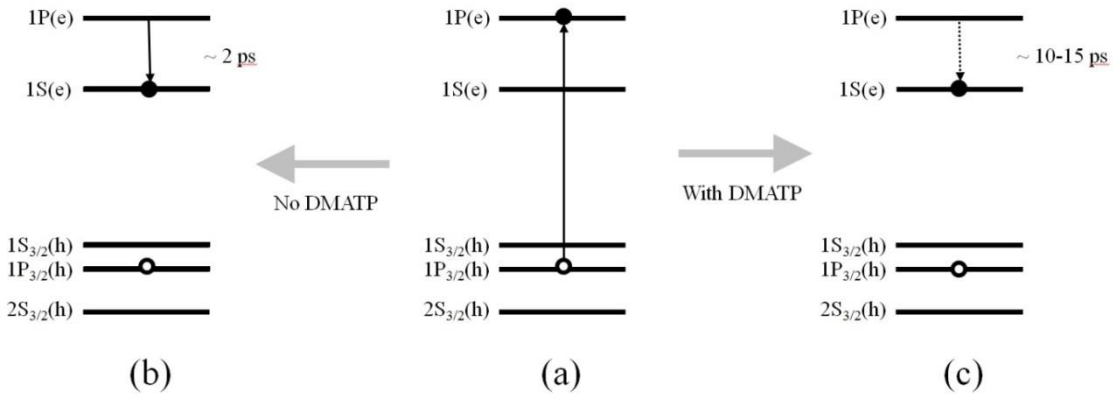

Figure 4-6. Schematic representation of charge carriers in CdSe QDs depicting (a) the initial excitation process and subsequent appearance of the B1 signal by electron cooling in the (b) absence and (c) presence of DMATP.

In samples with added DMATP it appears that the molecule retards electron cooling from the 1P(e) to 1S(e) state. The clearest manifestation of slower electron cooling is the more gradual rate of the B1 bleach signal onset (Figure 4-5(a)), which implies that electrons continue to relax into the 1S state in the 10-15 ps following excitation. In addition, the amplitude of the biexciton absorption (A1) is enhanced two-fold versus the as-synthesised QDs at early time delays. This may be due to different excitonic states interacting to establish biexcitons at early time delays in DMATP-functionalised QDs than in the as-synthesised QDs.[28,29]

The similarity in the timescales of the B1 onset and the A1 decay suggests that the two processes could be related. Spatially decoupling the hole has previously been shown to slow electron cooling in CdSe QDs.[32] The transient data presented here, however, do not offer direct evidence of hole transfer from the QDs to DMATP or for the delocalisation behaviour postulated by Tan et al.[1] In the absence of an exciton initially formed by the pump pulse, subsequent absorption of a probe photon would not create a biexciton. The decay of the A1 signal at early delay times might therefore indicate a mechanism induced by DMATP that disrupts the initially formed exciton, possibly as a result of new surface states or hybridised QD-ligand orbitals.

4.5 Hydrophilic Aminothiols as Ligands for CdSe QDs

Following the study of QDs in chloroform, work began to extend the behaviour of DMATP to an aqueous system by using an analogous hydrophilic ligand. Such a ligand could then compose the entire QD ligand shell, providing colloidal stability in addition to the desirable electronic effects, and possibly promote hole transfer to scavengers in solution. While amine functional groups are not sufficiently hydrophilic to stabilise QDs in water, under acidic conditions (approaching the pK_a of a given amine) protonation of amines occurs to generate positively-charged ammonium groups which are hydrophilic.

The dimethylamino group of DMATP itself could be protonated to form a water-soluble dimethylammonium group, however the cost of this material precluded its use for these experiments. We instead used 4-aminothiophenol (ATP), which preserved the essential structural features of DMATP, i.e. *para* thiol and amine groups, but is substantially more economical. For comparison, parallel batches of QDs were prepared using an alkyl ligand with the same functional groups, 2-aminoethanethiol (AET), which would impart solubility under the same pH conditions. The structures are shown in Figure 4-7. Typical carboxylic acid ligands (e.g. MPA) were not suitable for this purpose because the carboxylate group would protonate under such acidic conditions, causing the QDs to precipitate. The use of AET as a ligand was also intended to highlight any effects manifesting in the transient spectra of ATP-capped QDs due to conjugation of the thiol and amine groups. The ultrafast transient absorption spectra of semiconductor QDs stabilised by these ligands in water has not been reported.

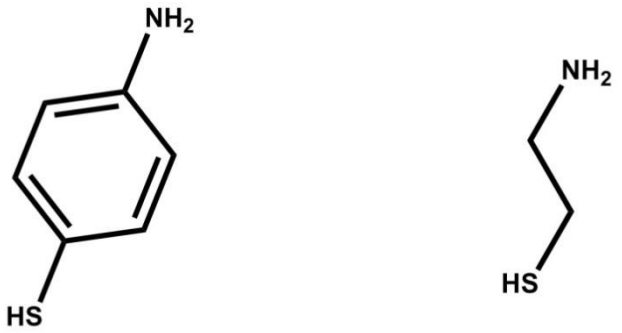

4-aminothiophenol (ATP) **2-aminoethanethiol (AET)**

Figure 4-7. Structures of aminothiol ligands used as ligands for CdSe QDs. Under acidic conditions, the amine groups can be protonated to form positively-charged ammonium groups which are hydrophilic.

ATP and AET have pK_a values of 4.3 and 8.6, respectively.[34,35] Under the experimental conditions used for the experiments described throughout this chapter (pH 3), the amine groups of both ligands will be protonated to form positively-charged ammonium groups which stabilise the QDs in water. In the case of ATP, protonation of the amine group will compromise the electron donating ability of the ligand relative to the DMATP ligand originally evaluated in organic solvent. Some of this character should be retained however by a small subpopulation of ATP that is not protonated at equilibrium.

The absorption and emission spectra of ATP- and AET-coated QDs are shown in Figure 4-8, compared to the as-synthesised QDs. Functionalisation with AET does not significantly change the spectrum of the QDs, however ATP induces a 6 nm redshift of the exciton absorption feature. This shift is consistent with that observed in the transient spectra upon adsorption of ~5 molecules of DMATP per CdSe QD, although an equivalent shift was not seen in the steady-state absorption spectra.

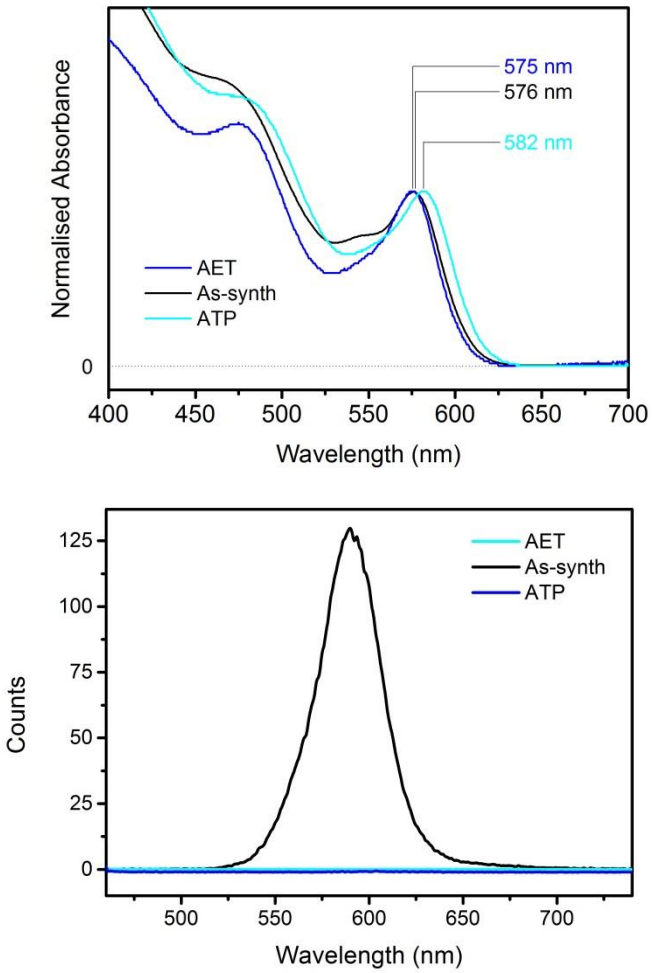

Figure 4-8. (Top) Extinction spectra and (bottom) emission spectra (λex = 450 nm) of CdSe QDs, comparing the as-synthesised QDs in chloroform to the QDs in water after ligand exchange with either AET or ATP. ATP spectrum Y-offset by -1 for visibility.

Band-edge emission with a maximum at 590 nm was observed in the as-synthesised QDs in chloroform. Ligand exchange with either aminothiol ligand completely quenched this emission. This result could be attributed to the extensive thiol coverage[26], however luminescence spectra of CdSe QDs functionalised with both ligands exist in the literature.[2,10] Li et al. recently reported aqueous ATP-coated CdSe QDs as a fluorescent pH probe, presenting emission data in the range of pH 3-6,[2] however in my experience, these materials aggregate above pH 4. The reason for these discrepancies remains unclear, however the ligand exchange procedures in these papers

involved addition of methanolic ligand solutions to the QDs in chloroform and hexane, as opposed to direct transfer to an aqueous ligand solution as done for this work. The two methods may passivate surface defects differently, resulting in preservation or quenching of QD emission.

Figure 4-9 illustrates the transient absorption spectra of (a) ATP- and (b) AET-capped CdSe QDs in water (pH 3) following excitation at 450 nm. The spectral features of both QD materials are similar, with prominent overlapping B1 and B2 bleach signals in the region of 550 – 600 nm. The redshift in the spectrum of ATP QDs observed in the steady-state absorption measurements is also seen in the TA spectrum (Figure 4-9(c)). This shift resolves the B3 feature at ~490 nm more clearly, whereas the equivalent signal is comparatively noisy in the spectrum of AET QDs due to its proximity to the edge of the probe continuum. Positive A2 signals are present in both spectra between 500 and 525 nm, while the biexciton absorption (A1) is present only at very early time delays (1-2 ps).

The B1 kinetics of ATP and AET QDs (monitored at 579 and 573 nm, respectively) are presented in Figure 4-10. Fit parameters quantifying the decay behaviour are tabulated in Table 4-2. Fitting to biexponential functions achieved minimal residuals (~1%) and yielded time constants of ~82 ps for the fast decay components of both materials, which reflects the coincidence of the kinetic traces in the first several hundred picoseconds. On longer timescales, however, the ground state bleach is seen to decay 2.5 times slower in ATP QDs than in AET QDs, with time constants of ~3600 ps and ~1500 ps, respectively. These decay rates mean that after 3 ns there are 50% more electrons residing in the 1S(e) conduction band state of ATP QDs compared to the population in AET QDs. Electron relaxation on this timescale (ns) has previously been attributed to recombination with trapped holes.[21,36] If electron-hole recombination is the primary relaxation pathway in these materials, the observed difference in B1 decay rate suggests that the ATP ligand disrupts this process somehow.

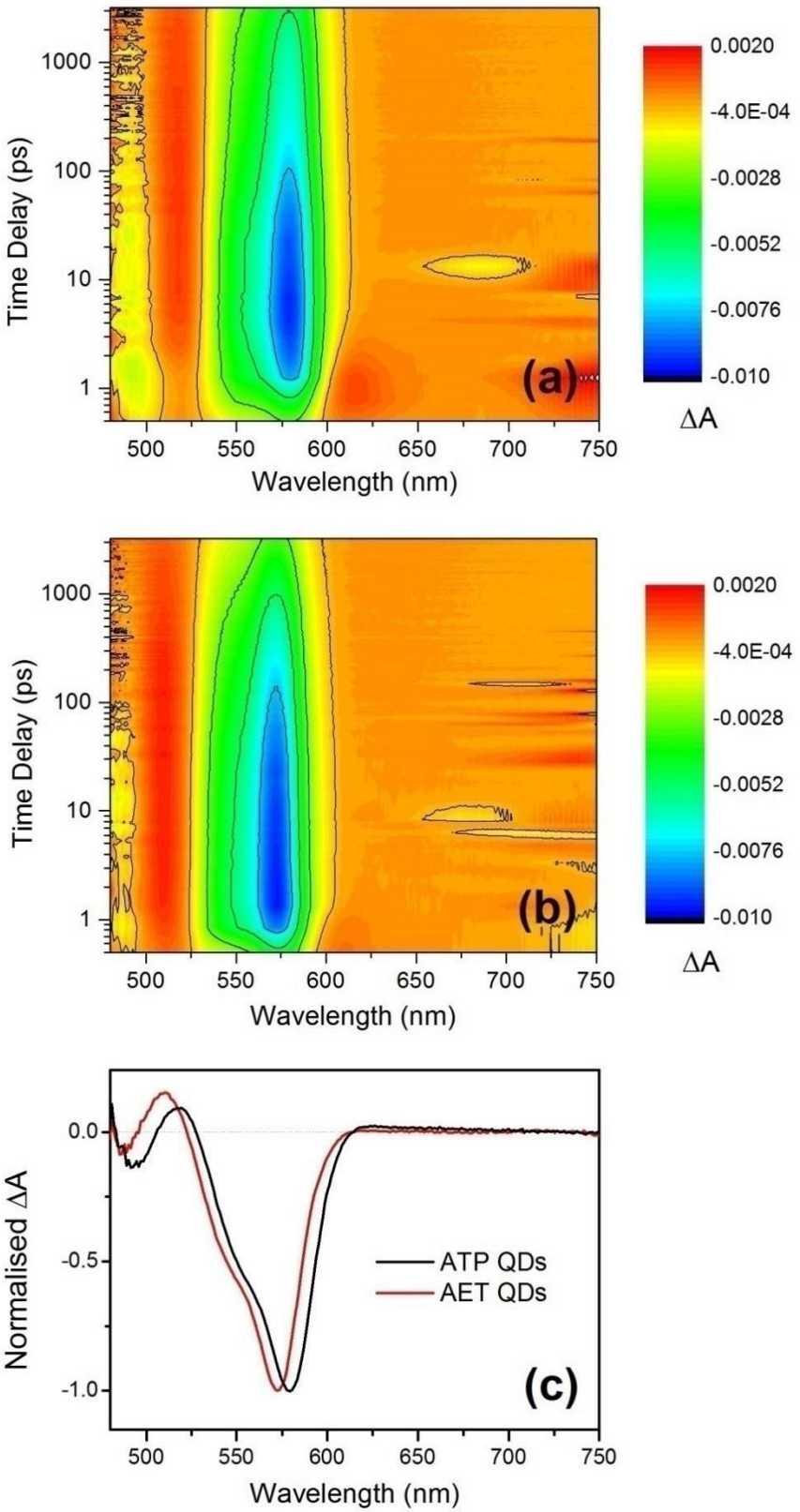

Figure 4-9. (a) ATP QDs, (b) AET QDs, (c) comparison of TA spectra of ATP and AET QDs at early time delay illustrating the red-shift of the QD spectrum due to the aromatic ligand.

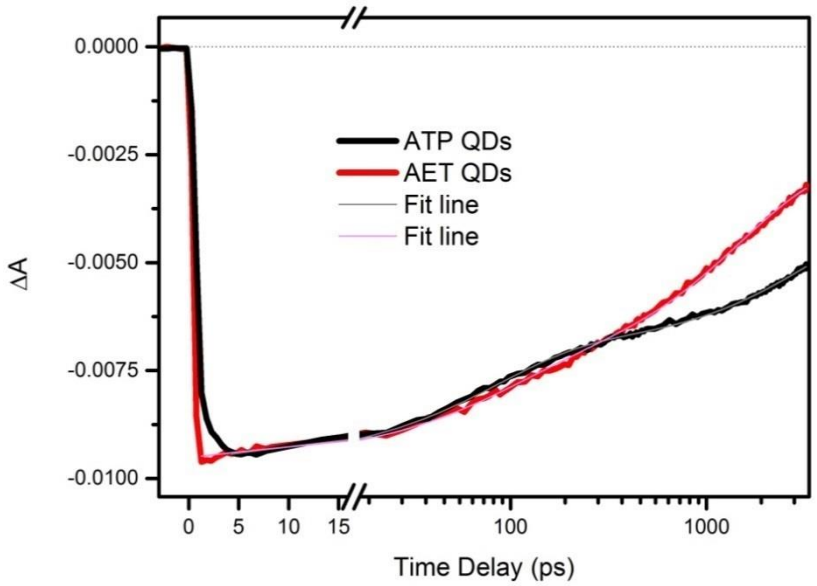

Figure 4-10. Kinetics of the B1 ground state bleach signals of ATP QDs and AET QDs, monitored at 579 and 573 nm, respectively.

	Equation: $y = A_1 * \exp(-x/\tau_1) + A_2 * \exp(-x/\tau_2) + y_0$	
	ATP QDs	AET QDs
y_0	-0.0038 ± 0.0001	-0.0027 ± 0.0001
A_1	-0.0032 ± 0.0001	-0.0049 ± 0.0001
τ_1	3600 ±300 ps	1500 ±30 ps
A_2	-0.0026 ± 0.0001	-0.0019 ± 0.0001
τ_2	82 ± 2 ps	82 ± 3 ps

Table 4-2. Fitting parameters for the kinetics of the B1 signals plotted in Figure 4-10. Fitting windows begin at the maximum initial amplitudes (at 4 ps for ATP QDs and 1 ps for AET QDs) and end at the final data point (3216 ps).

Another notable feature in the transient spectra of aminothiol-functionalised QDs is the difference in onset rates of the B1 signals, shown in detail in Figure 4-11. In AET QDs, ΔA reaches its maximum ~1 ps after excitation and immediately begins decaying. The equivalent signal in ATP QDs continues to increase in intensity for ~5 ps after excitation. A similar slowdown in the B1 onset rate was also seen to occur upon adsorption of DMATP to CdSe QDs in chloroform. This observation appears to confirm that ATP is indeed a functional analogue to DMATP in terms of its effect on the charge carrier dynamics of QDs, despite the structural and environmental differences between the two systems.

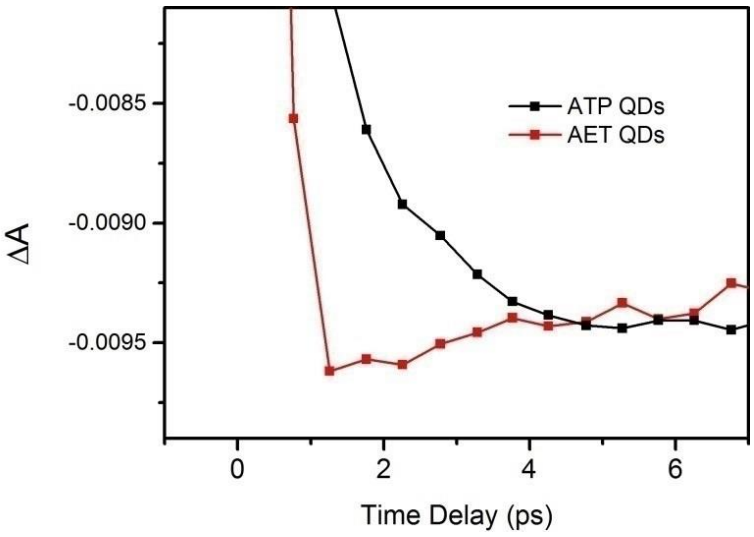

Figure 4-11. Detail of B1 signal at early time delays for ATP and AET QDs showing the difference in onset rate.

While both ligands slow the onset rate of the B1 signal, it appears that the effect is more pronounced for DMATP than ATP, with maximum ΔA values being reached in ~15 ps and ~5 ps, respectively. If the effect is related to the electron donation from the amines to the QDs as hypothesised, then the slower onset of B1 in DMATP-functionalised QDs is in line with expectations based on inductive electronic effects. The N-methyl groups in DMATP will contribute additional electron density to the nitrogen centre, resulting in a more electron donating substituent and hence molecule relative to ATP, which has only a primary amine. It is also possible that the protonated

amines donate less electron density; in this case, the observed behaviour could arise from the subset of unprotonated ligands that exist at any given time.

The photoinduced absorption denoted A2 appears in the spectra of ATP QDs at 517 nm, and at 510 nm in the spectra of AET QDs. The kinetics of this signal are shown in Figure 4-12. The A2 feature reflects population of the 1S(e) state, so the kinetics of the signal would be expected to correspond in some way with the B1 kinetics. The mechanisms giving rise to the bleach and positive signals are slightly different, however, the former being due to state filling, while the latter represents a transition newly accessible from the excited state. The B1 kinetics fit well to a biexponential function which suggested a process that occurs in both materials with a time constant of 82 ± 3 ps, and a slower process with time constants of 3600 ± 300 ps and 1500 ± 30 ps in ATP QDs and AET QDs, respectively. In the case of the A2 signals, only single exponentials resulted in sensible fitting parameters. There is good agreement in the time constants thus calculated for the B1 and A1 signals in AET QDs ($\tau \approx 1$ ns). The kinetics of the A2 signals show qualitatively the same behaviour as the B1 signal, with the signal in AET QDs decaying more rapidly on longer timescales. The initial relative intensities of the A2 signals differ by ~30%. The intensities of the B1 signals were almost identical. The reason for this difference is unclear.

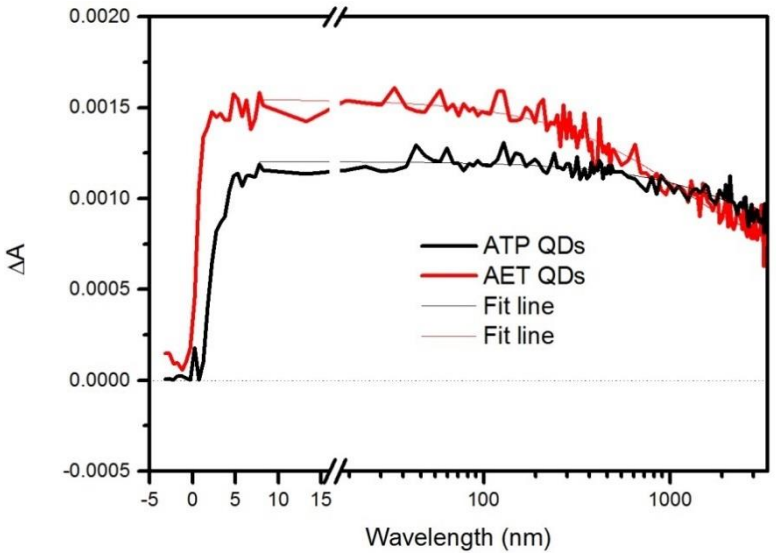

Figure 4-12. Kinetics of the A2 photoinduced absorption in ATP QDs and AET QDs, monitored at 517 nm and 510 nm, respectively.

	Equation: $y = A * \exp(-x/\tau) + y_0$	
	ATP QDs	AET QDs
y_0	3.8E-4 ± 3.7E-4	7.5E-4 ± 0.2E-4
A	8.3E-4 ± 3.6E-4	8.0-4 ± 0.2E-4
τ	6500 ± 3600 ps	1200 ± 100 ps

Table 4-3. Fitting parameters for the kinetics of the A2 signals plotted in Figure 4-12. Fitting windows begin at the maximum initial amplitudes (8 ps) and end at the final data point (3217 ps).

Finally, differences in the A1 photoinduced absorptions are observed in ATP QDs and AET QDs, shown in Figure 4-13. This signal arises due to biexciton absorption in the nanocrystals that occurs when probe pulses interact with QDs that contain excitons created by the pump pulse. In ATP QDs, the A1 feature is both more intense and longer lived than in AET QDs. The longer lifetime of the signal in ATP QDs suggests slower relaxation of the initially formed exciton. It is hypothesised, however, that the difference in the A1 signals arises from the changes to the charge carrier relaxation dynamics induced by the ATP ligand.

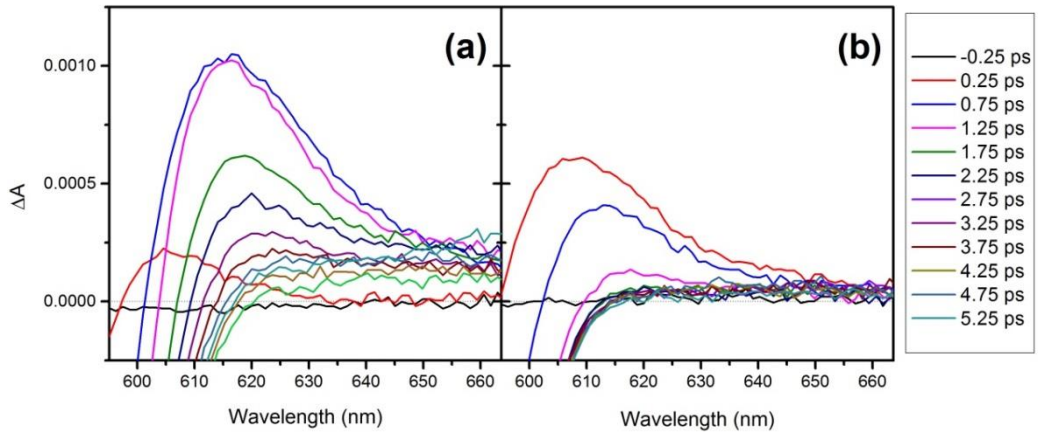

Figure 4-13. Detail of the A1 biexciton absorption feature in (a) ATP QDs at 616 nm, and (b) AET QDs at 614 nm.

The magnitude of the A1 feature is directly related to the biexciton binding energy.[20] Slower 1P(e)→1S(e) relaxation would mean that the initially created 1P(e)-$1P_{3/2}$(h) exciton persists longer in ATP QDs, whereas it would rapidly decay to 1S(e) in AET QDs. With different excitons present in ATP or AET QDs, the absorption of a probe pulse would therefore establish a different type of biexciton in the QDs, giving rise to a signal with different intensity.[28]

The transient absorption data suggests that ATP has a similar effect to that of DMATP on the charge carrier dynamics of CdSe QDs, manifesting on both picosecond and nanosecond timescales. ATP slows the onset of the B1 bleach signal and intensifies the A1 signal, which implies slower 1P(e)→1S(e) relaxation. On the nanosecond timescale, electrons reside for longer in the conduction band edge state, consistent with reduced recombination resulting from hole delocalisation from the QD core and into the ligand shell. No such changes were observed for AET QDs under the same experimental conditions which highlighted the importance of conjugation between the amine and thiol functional groups in ATP.

4.6 Transient Absorption of Aminothiol-Capped QDs in the Presence of Electron/Hole Scavengers

To further characterise the ligand shell of CdSe QDs capped with aminothiols, transient absorption measurements were performed in the presence of electron or hole scavengers. Methyl viologen (MV) was used as an electron acceptor, while methanol (MeOH) and ascorbic acid (AA) served as hole scavengers.

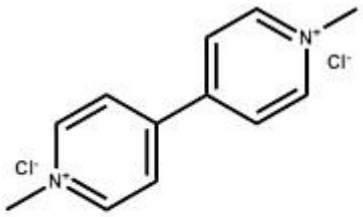

Methyl viologen

Aliquots of MV stock solution were added sequentially to the cuvette during the measurements, which reduced the concentration of QDs by ~10% each time. The ΔA signal is therefore expected to decrease proportionally scan-to-scan due to fewer QDs in the solution volume being probed.

The kinetics of the B1 signal of ATP QDs and AET QDs in the presence of 50 equivalents and 5000 equivalents of MV per QD are shown in Figure 4-14. Evidently, the presence of the electron scavenger has little discernible effect on the decay kinetics of either QD material. Fitting the traces to exponentials confirmed that the time constants are equal, within error, at all MV concentrations for these materials. For comparison, an equivalent set of measurements performed on MPA-functionalised QDs is also shown in Figure 4-14. The ground state bleach signal is completely quenched in the presence of 500 equivalents of MV in solution, as expected upon electron transfer from the conduction band to the viologen acceptor. In contrast, even a ten-fold higher concentration of MV had no effect on the B1 kinetics in aminothiol-capped QDs.

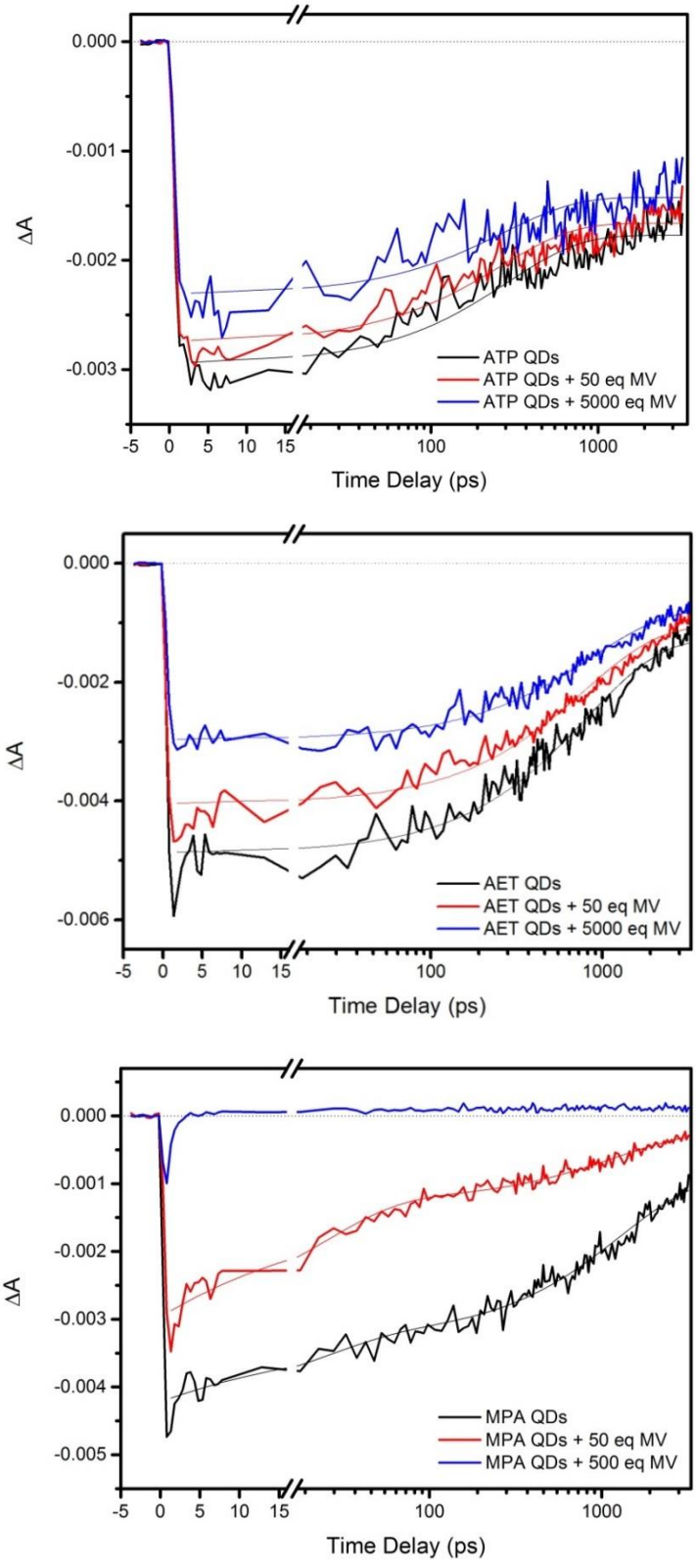

Figure 4-14. Kinetics of the B1 ground state bleach signals in ATP QDs, AET QDs, and MPA QDs in the presence of the electron scavenger methyl viologen.

		Equation: $y = A * \exp(-x/\tau) + y_0$		
		0 equiv. MV^{2+}	50 equiv. MV^{2+}	5000 equiv. MV^{2+}
ATP QDs	y_0	-0.0018 ± 0.0001	-0.0017 ± 0.0001	-0.0014 ± 0.0001
	A	-0.0012 ± 0.0001	-0.0011 ± 0.0001	-0.0010 ± 0.0001
	τ	290 ± 20 ps	260 ± 20 ps	270 ± 30 ps
AET QDs	y_0	-0.0013 ± 0.0001	-0.0011 ± 0.0001	-0.0010 ± 0.0001
	A	-0.0036 ± 0.0001	-0.0030 ± 0.0001	-0.0022 ± 0.0001
	τ	810 ± 40 ps	780 ± 30 ps	870 ± 40 ps

Table 4-4. Fitting parameters for the kinetics of the B1 signals of ATP QDs and AET QDs in the presence of methyl viologen, plotted in Figure 4-14. Fitting windows begin at the maximum initial amplitudes (at 3 ps for ATP QDs and at 2 ps for AET QDs) and end at the final data point (3198 ps).

		Equation: $y = A_1 * \exp(-x/\tau_1) + A_2 * \exp(-x/\tau_2) + y_0$		
		0 equiv. MV^{2+}	50 equiv. MV^{2+}	500 equiv. MV^{2+}
MPA QDs	y_0	-0.0010 ± 0.0001	-0.0002 ± 0.0001	--
	A_1	-0.0024 ± 0.0001	-0.0010 ± 0.0001	--
	τ_1	1300 ± 100 ps	1200 ± 200 ps	--
	A_2	-0.0010 ± 0.0001	-0.0017 ± 0.0001	--
	τ_2	24 ± 5 ps	24 ± 2 ps	--

Table 4-5. Fitting parameters for the kinetics of the B1 signals of MPA QDs in the presence of methyl viologen, plotted in Figure 4-14. Fitting windows begin at the maximum initial amplitudes (1 ps) and end at the final data point (3198 ps).

The reduction potential of methyl viologen is -0.446 V vs NHE in aqueous media and is independent of pH.[37] Based on reported conduction band edge energies (approx. -1.0 V vs NHE) of similarly-sized CdSe QDs[38–40], electron transfer to MV from CdSe QDs is energetically favourable, with a driving force of roughly 500 mV. A study by Knowles et al. using a series of benzoquinones demonstrated that the more sterically hindered analogues could not penetrate the oleic acid ligand shell of PbS QDs, and therefore showed no appreciable electron scavenging.[41] Rather than steric hindrance, we believe here that electrostatic repulsion of the methyl viologen dication by the positively-charge ammonium tail groups prevents the approach of MV to the QD surface and therefore electron scavenging does not proceed. Measurements using MPA QDs were performed at pH 11, significantly higher than for ATP and AET QDs, which increases the driving force for electron transfer to MV. A recent study showed, however, that sufficient driving force still exists for electron transfer to proceed from ~3 nm CdSe QDs to viologens at pH 4.[39]

Parallel measurements were performed in the presence of two common hole scavengers, methanol and ascorbic acid (AA), plotted below in Figure 4-15 and Figure 4-16, respectively. The kinetics of the B1 bleach were monitored, and fit to exponentials for comparison to the material in the absence of the scavenger, presented previously in the chapter. The methanol measurements fit well to a biexponential, and showed no change in decay kinetics relative to the QDs in water, within the error of the fitting; similarly, addition of ascorbic acid appeared to result in no kinetic change (Figures 4-15 and 4-16). In the latter case, the data could not be fit sensibly to a biexponential, so a single exponential to be able to compare AET to ATP QDs. The recovery of the ground state bleach is twice as fast in AET QDs, which is in line with the relative rates deduced from fits for the materials in water

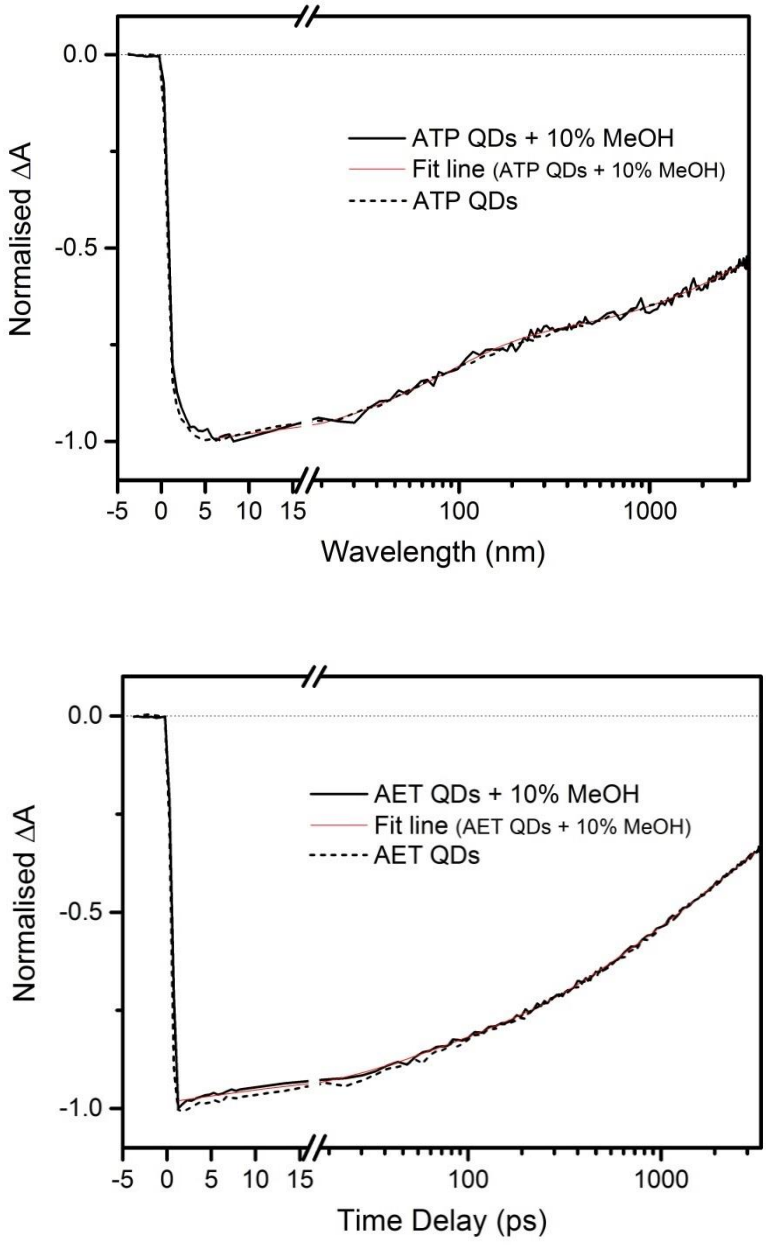

Figure 4-15. Kinetics of the B1 ground state bleach signals of ATP QDs and AET QDs in the presence of the hole scavenger methanol.

	Equation: $y = A_1 * \exp(-x/\tau_1) + A_2 * \exp(-x/\tau_2) + A_3 * \exp(-x/\tau_3) + y_0$	
	ATP QDs + 10% MeOH	AET QDs + 10% MeOH
y_0	-0.43 ± 0.03	-0.24 ± 0.02
A_1	-0.28 ± 0.01	-0.18 ± 0.02
τ_1	80 ± 4 ps	330 ± 50 ps
A_2	-0.31 ± 0.02	-0.46 ± 0.01
τ_2	3100 ± 400 ps	2100 ± 200 ps
A_3	--	-0.11 ± 0.01
τ_3	--	40 ± 4 ps

Table 4-6. Fitting parameters for the kinetics of the B1 signals of ATP QDs and AET QDs in the presence of the hole scavenger methanol, plotted in Figure 4-15. Fitting windows begin at the maximum initial amplitudes (at 6 ps for ATP QDs and at 1 ps for AET QDs) and end at the final data point (3217 ps).

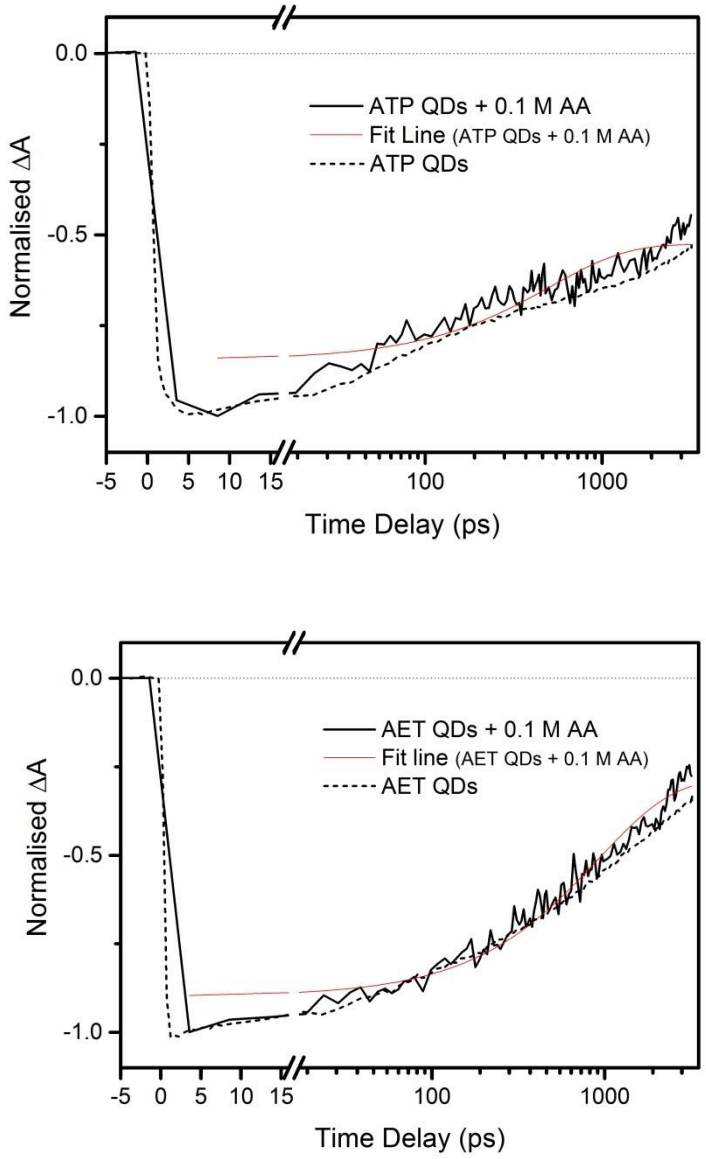

Figure 4-16. Kinetics of the B1 ground state bleach signals of ATP QDs and AET QDs in the presence of the hole scavenger ascorbic acid (AA).

	Equation: $y = A_1 * \exp(-x/\tau_1) + y_0$	
	ATP QDs + 0.1 M AA	AET QDs + 0.1 M AA
y_0	-0.53 ± 0.01	-0.29 ± 0.01
A_1	-0.32 ± 0.01	-0.62 ± 0.01
τ_1	500 ± 50 ps	900 ± 50 ps

Table 4-7. Fitting parameters for the kinetics of the B1 signals of ATP QDs and AET QDs in the presence of the hole scavenger ascorbic acid (AA), plotted in Figure 4-16. Fitting windows begin at the maximum initial amplitudes (at 8 ps for ATP QDs and at 4 ps for AET QDs) and end at the final data point (at 3165 ps for ATP QDs and at 3178 ps for AET QDs).

The pK_a of ascorbic acid is 4.17, so at pH 3 the acid exists predominantly in its neutral, protonated state. This may reduce the effectiveness of scavenging compared to ascorbate. Methanol is not charged, so electrostatic repulsion should be an issue in either case. In CdSe nanocrystals, transient bleach signals arise primarily from population of electron states.[28,29] Electron scavenging, e.g. by methyl viologen, therefore has a pronounced effect on the spectra and kinetics; hole scavenging, on the other hand, is only indirectly observed as a slower bleach recovery rate due to reduced recombination.[42]

4.7 Conclusions

The effect of small amounts of a hole-delocalising ligand, DMATP, on the charge carrier dynamics of CdSe QDs were investigated, following observations of a protective effect exerted by the molecule on colloidal CdS QDs under photocatalytic conditions. Transient absorption measurements revealed that this ligand appears to affect intraband 1P→1S electron relaxation. Interruption of this process is consistent with interaction of DMATP with QD hole states[33], and may lend support to the assertion by Tan et al. that the ligand can partially delocalise holes away from the QD core.[1] Direct evidence for hole transfer from the QDs to DMATP was not observed in the transient spectra, however.

The behaviour exhibited by DMATP was then extended to aqueous conditions, towards improving hole scavenging in photocatalytic systems. Similar charge carrier dynamics were observed in QDs stabilised by ATP at low pH to those seen for DMATP-functionalised QDs, in particular a slower onset rate of the ground state bleach. Comparing QDs stabilised by ATP to those coated with an analogous alkyl ligand with the same functional groups, electron relaxation was considerably slower in QDs bearing the aromatic ligand. Extended conduction band electron lifetimes are potentially beneficial to photocatalytic systems for reductive chemistry, extending the time frame for electron transfer from the QD to an acceptor.

Despite the kinetic changes induced by ATP stabilising ligands, addition of electron or hole scavengers to the QDs showed no indication of facilitated charge transfer. While the conjugated ligand can influence the dynamics of charge carriers in the QD core, it appears to hinder the approach of redox species to the nanocrystal surface in the same way as conventional ligands such as MPA or cysteine.

4.8 References

(1) Tan, Y.; Jin, S.; Hamers, R. J. Influence of Hole-Sequestering Ligands on the Photostability of CdSe Quantum Dots. *J. Phys. Chem. C* **2013**, *117*, 313–320.

(2) Li, D.; Xu, H.; Li, D.; Wang, Y. *p*-Aminothiophenol-Coated CdSe/ZnS Quantum Dots as a Turn-on Fluorescent Probe for pH Detection in Aqueous Media. *Talanta* **2017**, *166*, 54–62.

(3) Haremza, J. M.; Hahn, M. A.; Krauss, T. D.; Chen, S.; Calcines, J. Attachment of Single CdSe Nanocrystals to Individual Single-Walled Carbon Nanotubes. *Nano Lett.* **2002**, *2*, 1253–1258.

(4) Ravindran, S.; Chaudhary, S.; Colburn, B.; Ozkan, M.; Ozkan, C. S. Covalent Coupling of Quantum Dots to Multiwalled Carbon Nanotubes for Electronic Device Applications. *Nano Lett.* **2003**, *3*, 447–453.

(5) Zhang, F.; Ali, Z.; Amin, F.; Feltz, A.; Oheim, M.; Parak, W. J. Ion and pH Sensing with Colloidal Nanoparticles: Influence of Surface Charge on Sensing and Colloidal Properties. *ChemPhysChem* **2010**, *11*, 730–735.

(6) Silvi, S.; Credi, A. Luminescent Sensors Based on Quantum Dot-Molecule Conjugates. *Chem. Soc. Rev.* **2015**, *44*, 4275–4289.

(7) Parak, W. J.; Gerion, D.; Zanchet, D.; Woerz, A. S.; Pellegrino, T.; Micheel, C.; Williams, S. C.; Seitz, M.; Bruehl, R. E.; Bryant, Z.; *et al.* Conjugation of DNA to Silanized Colloidal Semiconductor Nanocrystalline Quantum Dots. *Chem. Mater.* **2002**, *14*, 2113–2119.

(8) Xiao, Q.; Zhou, B.; Huang, S.; Tian, F.; Guan, H.; Ge, Y.; Liu, X.; He, Z.; Liu, Y. Direct Observation of the Binding Process between Protein and Quantum Dots by in Situ Surface Plasmon Resonance. *Nanotechnology* **2009**, *20*, 325101.

(9) Wuister, S. F.; Swart, I.; Driel, F. Van; Hickey, S. G.; Donega, C. D. M. Highly Luminescent Water-Soluble CdTe Quantum Dots. *Nano Lett.* **2003**, *3*, 503–507.

(10) Wuister, S. F.; Donega, C. D. M.; Meijerink, A. Influence of Thiol Capping on the Exciton Luminescence and Decay Kinetics of CdTe and CdSe Quantum Dots.

2004, 17393–17397.

(11) Burda, C.; Link, S.; Mohamed, M.; El-Sayed, M. The Relaxation Pathways of CdSe Nanoparticles Monitored with Femtosecond Time-Resolution from the Visible to the IR: Assignment of the Transient Features by Carrier Quenching. *J. Phys. Chem. B* **2001**, *105*, 12286–12292.

(12) Yagi, I.; Mikami, K.; Ebina, K.; Okamura, M.; Uosaki, K. Size-Dependent Carrier Dynamics in CdS Nanoparticles by Femtosecond Visible-Pump/IR-Probe Measurements. *J. Phys. Chem. B* **2006**, *110*, 14192–14197.

(13) Aruda, K. O.; Amin, V. A.; Thompson, C. M.; Lau, B.; Nepomnyashchii, A. B.; Weiss, E. A. Description of the Adsorption and Exciton Delocalizing Properties of *p*-Substituted Thiophenols on CdSe Quantum Dots. *Langmuir* **2016**, *32*, 3354–3364.

(14) Steigerwald, M. L.; Brus, L. Semiconductor Crystallites: A Class of Large Molecules. *Acc. Chem. Res.* **1990**, *23*, 183–188.

(15) Bawendi, M. G.; Wilson, W. L.; Rothberg, L.; Carroll, P. J.; Jedju, T. M.; Steigerwald, M. L.; Brus, L. E. Electronic Structure and Photoexcited-Carrier Dynamics in Nanometer-Size CdSe Clusters. *Phys. Rev. Lett.* **1990**, *65*, 1623–1626.

(16) Norris, D. J.; Bawendi, M. G. Measurement and Assignment of the Size-Dependent Optical Spectrum in CdSe Quantum Dots. *Phys. Rev. B* **1996**, *53*, 16338–16346.

(17) Norris, D.; Efros, A.; Rosen, M.; Bawendi, M. Size Dependence of Exciton Fine Structure in CdSe Quantum Dots. *Phys. Rev. B* **1996**, *53*, 16347–16354.

(18) Klimov, V. I. Optical Nonlinearities and Ultrafast Carrier Dynamics in Semiconductor Nanocrystals. *J. Phys. Chem. B* **2000**, *104*, 6112–6123.

(19) Klimov, V. I.; McBranch, D. W.; Leatherdale, C. A.; Bawendi, M. G. Electron and Hole Relaxation Pathways in Semiconductor Quantum Dots. *Phys. Rev. B* **1999**, *60*, 13740–13749.

(20) Sewall, S. L.; Cooney, R. R.; Anderson, K. E. H.; Dias, E. A.; Kambhampati, P.

State-to-State Exciton Dynamics in Semiconductor Quantum Dots. *Phys. Rev. B* **2006**, *74*, 235328.

(21) Schnitzenbaumer, K. J.; Labrador, T.; Dukovic, G. Impact of Chalcogenide Ligands on Excited State Dynamics in CdSe Quantum Dots. *J. Phys. Chem. C* **2015**, *119*, 13314–13324.

(22) Hunsche, S.; Dekorsy, T.; Klimov, V. I.; Kurz, H. Ultrafast Dynamics of Carrier-Induced Absorption Changes in Highly-Excited CdSe Nanocrystals. *Appl. Phys. B Laser Opt.* **1996**, *62*, 3–10.

(23) Klimov, V. I.; Mikhailovsky, A. A.; McBranch, D. W. Mechanisms for Intraband Energy Relaxation in Semiconductor Quantum Dots: The Role of Electron-Hole Interactions. **2000**, *61*, 349–352.

(24) Burda, C.; Link, S.; Green, T. C.; El-Sayed, M. A. New Transient Absorption Observed in the Spectrum of Colloidal CdSe Nanoparticles Pumped with High-Power Femtosecond Pulses. *J. Phys. Chem. B* **1999**, *103*, 10775–10780.

(25) Huang, J.; Huang, Z.; Jin, S.; Lian, T. Exciton Dissociation in CdSe Quantum Dots by Hole Transfer to Phenothiazine. *J. Phys. Chem. C* **2008**, *112*, 19734–19738.

(26) Baker, D. R.; Kamat, P. V. Tuning the Emission of CdSe Quantum Dots by Controlled Trap Enhancement. *Langmuir* **2010**, *26*, 11272–11276.

(27) Sharma, S. N.; Pillai, Z. S.; Kamat, P. V. Photoinduced Charge Transfer between CdSe Quantum Dots and *p*-Phenylenediamine. *J. Phys. Chem. B* **2003**, *107*, 10088–10093.

(28) Kambhampati, P. Unraveling the Structure and Dynamics of Excitons in Semiconductor Quantum Dots. *Acc. Chem. Res.* **2011**, *44*, 1–13.

(29) Klimov, V. I. Spectral and Dynamical Properties of Multiexcitons in Semiconductor Nanocrystals. *Annu. Rev. Phys. Chem.* **2007**, *58*, 635–673.

(30) Talapin, D. V; Lee, J.-S.; Kovalenko, M. V; Shevchenko, E. V. Prospects of Colloidal Nanocrystals for Electronic and Optoelectronic Applications. *Chem. Rev.* **2010**, *110*, 389–458.

(31) Peterson, M. D.; Cass, L. C.; Harris, R. D.; Edme, K.; Sung, K.; Weiss, E. A. The Role of Ligands in Determining the Exciton Relaxation Dynamics in Semiconductor Quantum Dots. *Annu. Rev. Phys. Chem.* **2014**, *65*, 317–339.

(32) Guyot-Sionnest, P.; Wehrenberg, B.; Yu, D. Intraband Relaxation in CdSe Nanocrystals and the Strong Influence of the Surface Ligands. *J. Chem. Phys.* **2005**, *123*, 74709.

(33) Guyot-Sionnest, P.; Shim, M.; Matranga, C.; Hines, M. Intraband Relaxation in CdSe Quantum Dots. **1999**, *60*, 2181–2184.

(34) Bryant, M. A.; Crooks, R. M. Determination of Surface pKa Values of Surface-Confined Molecules Derivatized with pH-Sensitive Pendant Groups. *Langmuir* **1993**, *9*, 385–387.

(35) Mezyk, S. P. Rate Constant Determination for the Reaction of Sulfhydryl Species with the Hydrated Electron in Aqueous Solution. *J. Phys. Chem.* **1995**, *99*, 13970–13975.

(36) Knowles, K. E.; Mcarthur, E. A.; Weiss, E. A. A Multi-Timescale Map of Radiative and Nonradiative Decay Pathways for Excitons in CdSe Quantum Dots. *ACS Nano* **2011**, *5*, 2026–2035.

(37) Bird, C. L.; Kuhn, A. T. Electrochemistry of the Viologens. *Chem. Soc. Rev.* **1981**, *10*, 49.

(38) Zheng, K.; Žídek, K.; Abdellah, M.; Zhang, W.; Chábera, P.; Lenngren, N.; Yartsev, A.; Pullerits, T. Ultrafast Charge Transfer from CdSe Quantum Dots to p-Type NiO: Hole Injection vs Hole Trapping. *J. Phys. Chem.* **2014**, *118*, 18462–18471.

(39) Chen, J.; Wu, K.; Rudshteyn, B.; Jia, Y.; Ding, W.; Xie, Z. X.; Batista, V. S.; Lian, T. Ultrafast Photoinduced Interfacial Proton Coupled Electron Transfer from CdSe Quantum Dots to 4,4′-Bipyridine. *J. Am. Chem. Soc.* **2016**, *138*, 884–892.

(40) Wang, Y. F.; Wang, H. Y.; Li, Z. S.; Zhao, J.; Wang, L.; Chen, Q. D.; Wang, W. Q.; Sun, H. B. Electron Extraction Dynamics in CdSe and CdSe/CdS/ZnS Quantum Dots Adsorbed with Methyl Viologen. *J. Phys. Chem. C* **2014**, *118*,

17240–17246.

(41) Knowles, K. E.; Tagliazucchi, M.; Malicki, M.; Swenson, N. K.; Weiss, E. A. Electron Transfer as a Probe of the Permeability of Organic Monolayers on the Surfaces of Colloidal PbS Quantum Dots. *J. Phys. Chem. C* **2013**, *117*, 15849–15857.

(42) Huang, J.; Mulfort, K. L.; Du, P.; Chen, L. X. Photodriven Charge Separation Dynamics in CdSe/ZnS Core/shell Quantum Dot/cobaloxime Hybrid for Efficient Hydrogen Production. *J. Am. Chem. Soc.* **2012**, *134*, 16472–16475.

5. Hydrophilic Dithiocarbamates as Ligands for QDs

5.1 Overview

In Chapter 3, the photo-oxidation and loss of surface ligands was recognised as a necessary step before hydrogen evolution begins in a colloidal QD-based system, but which eventually leads to aggregation of the QDs and precipitation from solution. To address this issue, ligands that could transfer holes from the QD core to scavengers in solution were sought. Aromatic aminothiol ligands were investigated for this purpose in Chapter 4. Transient absorption spectroscopy showed that conduction band electrons persist for longer in QDs functionalised with ATP than with AET, but direct evidence for hole delocalisation by these materials was not observed. Changes in the QDs' spectra that might suggest facilitated hole transfer from the nanocrystals were not observed upon exposing the materials to different hole scavengers.

This chapter reports work conducted using hydrophilic dithiocarbamate (DTC) molecules as stabilising ligands for CdSe QDs in water, with a view to facilitating hole scavenging from the particles during photocatalysis. After a protocol for functionalising QDs with DTC ligands had been established, a size-dependence study was conducted to assess the changes in the transient absorption spectra induced by the ligands. The findings from this study informed the subsequent work which evaluated hole scavenging from DTC-functionalised QDs in water, the results of which were published in *The Journal of Physical Chemistry C* in an article entitled "Hydrophilic, hole-delocalizing ligand shell to promote charge transfer from colloidal CdSe quantum dots" (Appendix 1).[1] Transient absorption measurements provided evidence for hole scavenging from QDs stabilised by an aromatic DTC ligand, resulting in a dramatic prolongation of the lifetime of electrons in the conduction band. These results should inform the future assembly of QD-based photocatalysts with ligand shells that dynamically transfer charge to and from the core to achieve both activity and colloidal stability under illumination.

5.2 Introduction

The interactions of dithiocarbamates and semiconductor surfaces have been studied since at least the 1980s.[2,3] Early work by Kamat sought to address photocorrosion of CdS nanocrystals in acetonitrile through functionalisation with diethyldithiocarbamate.[3] The colloidal nanocrystals were synthesised by a precipitation

route commonly employed at that time which does not introduce stabilising ligands to the particles, leaving them prone to rapid degradation. Much later, as hot-injection methods were being established for the synthesis of colloidally stable nanocrystals, a 2007 paper by Dubois and co-workers reported ligand exchange with dithiocarbamates as a versatile strategy for functionalising QDs with both hydrophobic and hydrophilic molecules.[4] Numerous authors subsequently reported systems in which dithiocarbamates were used to stabilise semiconductor QDs in aqueous conditions.[5–8]

Dithiocarbamates are readily synthesised by reacting a primary or secondary amine with carbon disulfide in the presence of a base. The resulting functional group is electron donating and readily chelates to metal ions and surfaces.[9,10] This property has been exploited to prepare precursors for metal sulfide thin films and has recently been used for semiconductor nanoparticle synthesis.[11] The strong binding of dithiocarbamates to most transition metal ions also means that these materials have utility in post-synthetic nanoparticle ligand exchange where they can readily displace native ligands.[9,12] Given their straightforward synthesis and the diversity of amine precursors available, dithiocarbamates provide a means to introduce a wide range of functionalities to nanocrystal surfaces.

In some of the aforementioned studies, a red-shift of up to tens of nanometres in the absorption spectra of QDs is apparent, but the origin of this phenomenon was not addressed at the time.[4,7] A 2010 paper from the Weiss group at Northwestern University investigated the effect of phenyldithiocarbamate (PTC) on CdSe QDs and ascribed the resulting red shift of the absorption spectrum to exciton delocalisation from the nanocrystal core into the ligand shell.[13] A detailed follow-up study extended that work to include CdS and PbS QDs, in addition to the CdSe QDs originally used, to elucidate the mechanism of the spectral red-shift induced by the PTC ligand.[14] In the case of CdSe, the authors were able to determine that hole delocalisation was specifically responsible for the observed behaviour, which was facilitated by the energetic proximity of the QD valence band and HOMO of the PTC ligand (Figure 5-1). The same authors published a further study supporting this hypothesis in which the energy of the ligand HOMO was modulated relative to the QD valence band by varying the *para*-substituent with a series of phenyldithiocarbamates.[15] Closer energetic resonance between QD and

PTC levels led to greater orbital mixing which resulted in the most significant degree of hole delocalisation, as quantified by the magnitude of the induced spectral shift.

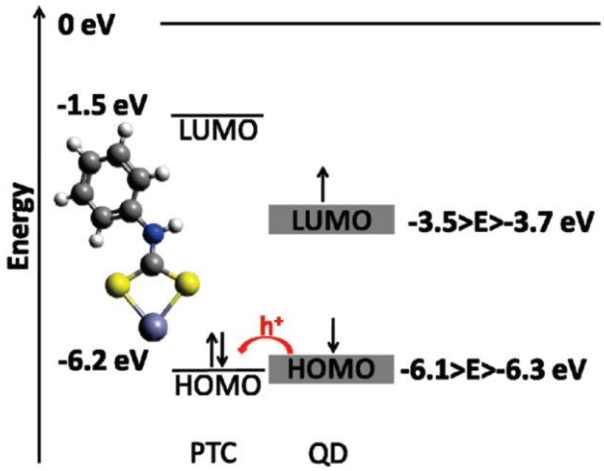

Figure 5-1. Energy level diagram of the molecular orbitals of phenyldithiocarbamate (PTC) relative to the frontier orbitals of CdSe QDs. Reproduced from [13].

Several studies have used dithiocarbamate anchoring groups to promote charge transfer between semiconductor nanocrystals and adsorbed molecular acceptors or donors. A conjugated bis(dithiocarbamate) molecule adsorbed to a CdSe QD via one DTC group and coordinated to the metal centre of a Zn porphyrin via the other was found to enhance the quantum yield of electron injection from the photoexcited porphyrin to the QD by a factor of 5 compared to direct interaction between the porphyrin and QD.[16] Lian et al. prepared phenothiazine derivatives with either carboxylate or dithiocarbamate anchoring groups and found that the latter enhanced the rate of hole transfer from CdS QDs to the acceptor by a factor of 20, such that it occurred within ~300 fs.[17] Earlier this year, a very interesting paper was published by La Croix and co-workers in which CdSe/CdS nanorods were functionalised with a bipyridyl dithiocarbamate ligand; subsequent treatment with $Fe(acac)_3$ led to chelation of the iron centre by the DTC-anchored bipyridine.[18] While the DTC precursor ligand itself delocalised holes from the semicondutor, the surface-assembled complex was shown to be significantly more efficient.

Much of the literature pertaining to the effects of dithiocarbamate ligands on charge carriers in QDs is built upon photoluminescence measurements. Few studies exist that utilise transient absorption spectroscopy to investigate these systems. The paper by Lian et al. mentioned above used TA to monitor the kinetics of a signal associated with the phenothiazine radical cation that appears following hole transfer from CdS, but the carrier dynamics of the QDs themselves were not examined.[17] Xie and co-workers did focus on the semiconductor charge carrier kinetics of molecule-like CdSe clusters with diameters of 1.6 nm functionalised with PTC, reporting hot hole transfer to the ligands from the valence band.[19] A more in-depth approach was taken by Azzarro et al. to study CdSe QDs with PTC ligands, using the state-specific excitation method pioneered by Kambhampati[20] to study carrier cooling rates and hole delocalisation.[21] This study provided further evidence for the specific interaction of DTC ligands with holes by showing that the rate of hole cooling was reversibly accelerated by adsorption of PTC, while electron cooling rates were unaffected. Given the general sparsity of the literature and the lack of any reported studies in aqueous media – the conditions in which these ligands would be applied in a photocatalytic system – a transient absorption study of hydrophilic dithiocarbamates as ligands for QDs was therefore of interest.

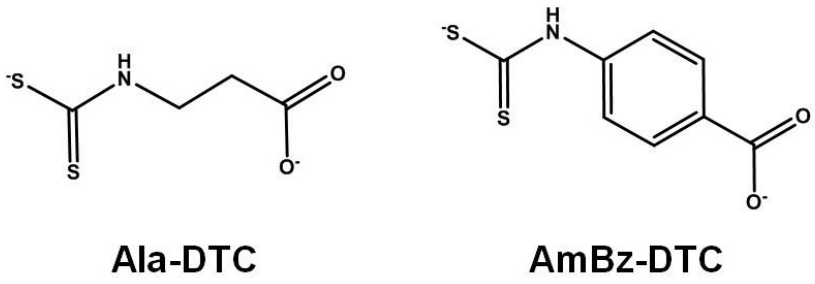

Figure 5-2. Structures of the hydrophilic dithiocarbamate ligands used in this study, derived fromβ-alanine (left) and 4-aminobenzoic acid (right).

For this work, we employed an alkyl and aromatic dithiocarbamate ligand, derived from β-alanine (3-aminopropionic acid) and 4-aminobenzoic acid, respectively (Figure 5-2). These molecules are referred to as Ala-DTC and AmBz-DTC throughout this chapter. Previous studies that had explicitly examined the hole delocalising or

charge transfer properties of dithiocarbamates had all made use of phenyldithiocarbamates, so this combination of ligands allowed the impact of conjugation to be investigated. This comparison was of particular interest in the context of hole scavenging by an acceptor in solution, where a conjugated ligand might serve as a conduit between the QD and scavenger. Given that transient data of such materials did not appear in the literature, samples of MPA-functionalised QDs were prepared from the same synthetic nanocrystal batches and measured alongside the DTC QDs under the same conditions to provide some context for the observed behaviour.

5.3 Size-Dependent Changes Induced by DTC Ligands in the Spectra of CdSe QDs

The experimental and theoretical work of Frederick et al.[13] motivated an initial size-dependence study of changes induced by dithiocarbamate ligands in the transient absorption spectra of CdSe QDs. These authors synthesised QDs with a range of sizes and quantified the magnitude of the red shift of the optical spectrum of each batch after treatment with PTC in terms of ΔR, the hypothetical physical increase of the QD radius that would achieve an equivalent red shift. The radii were calculated using the empirical formula developed by Yu et al. for determining QD size according to peak positions in absorption spectra.[22] For CdSe QDs, Frederick et al. observed saturation of ΔR for QDs with radii less than ~1.9 nm, shown in a plot from their paper, reproduced below in Figure 5-3.

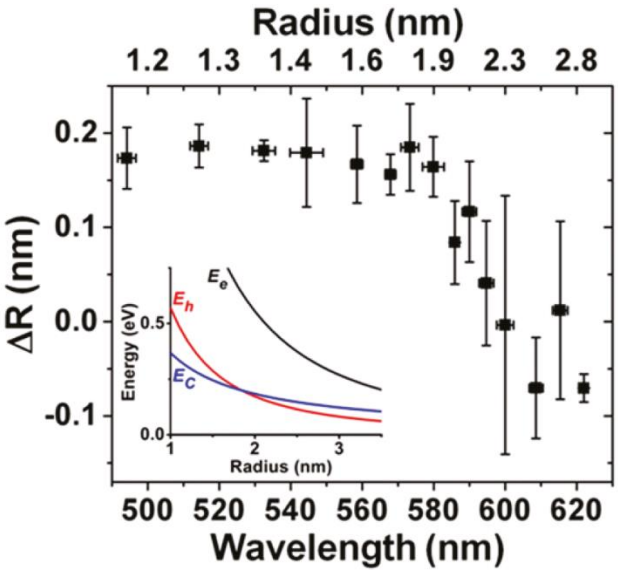

Figure 5-3. Plot reproduced from [14] illustrating saturation of the apparent change in QD radius, ΔR, upon adsorption of PTC for strongly confined nanocrystals with decreasing physical radius. The inset compares the electron (E_e) and hole (E_h) kinetic energies to the Coulomb energy (E_C) as a function of QD radius.

The authors identified the inflection point in the plot of ΔR vs R as being a result of the transition from a size regime of weak quantum confinement to one of strong confinement in CdSe, where the kinetic energies of the charge carriers are larger than the Coulomb potential.[23,24] Indeed, by using a core-shell particle-in-a-sphere model and calculating the kinetic energies of electrons (E_e) and holes (E_h) and comparing them to the Coulomb energy (E_C), the authors found that the kinetic energy of holes in CdSe equals the Coulomb energy for particles with radii of ~1.9 nm (Figure 5-3, inset). For smaller QDs, the kinetic energy of the hole exceeds the Coulomb energy (i.e. strongly confined) and the carrier is therefore capable of spatially delocalising beyond the QD core. Interestingly, the model also showed that the electron kinetic energy exceeds the Coulomb energy across the entire radius range studied, implying that electron delocalisation does not contribute to the observed spectral shifts in CdSe QDs upon dithiocarbamate functionalisation.

Three sizes of CdSe QDs were used for the size-dependent transient absorption study described herein, encompassing the different hole confinement regimes identified by Frederick et al. QDs with diameters of 2.5, 3.5 and 4.5 nm were synthesised to investigate the influence of DTC ligands on strongly, intermediately, and weakly confined holes, respectively.

The absorption spectra of the as-synthesised QDs before ligand exchange with dithiocarbamates are shown in Figure 5-4, with the peak maximum used to calculate the QD size included.[22] In Figure 5-5, the absorption spectra of QDs from each batch are shown after ligand exchange with Ala-DTC, AmBz-DTC, or MPA. The peak maxima of QDs of all sizes were blue-shifted by 2-5 nm after treatment with MPA, suggesting that slight etching of the QDs occurred, probably as a result of using the same alkaline conditions as used for DTC ligand exchange; the protocol was subsequently modified to avoid this.

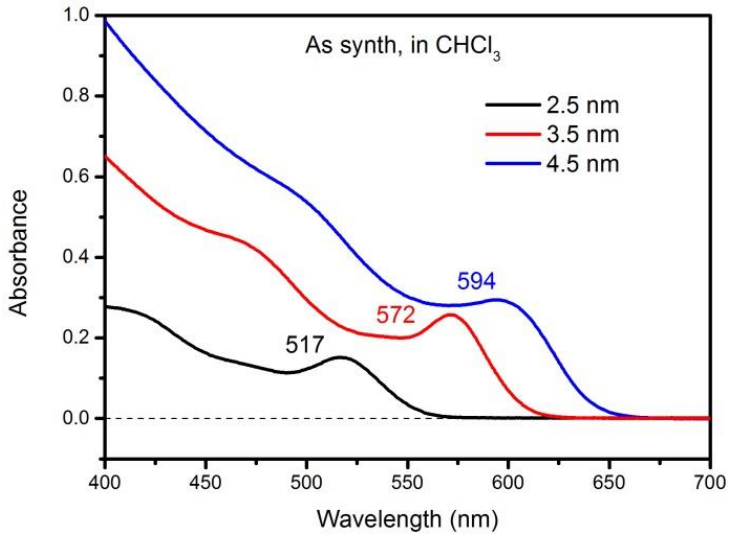

Figure 5-4. Extinction spectra of the different sizes of CdSe QDs synthesised for the size-dependence study of dithiocarbamate ligands.

Ligand exchange with dithiocarbamates results in red-shifted absorption spectra for all QD sizes. For weakly and intermediately confined QDs with diameters of 4.5 and 3.5 nm, respectively, the red shifts are modest, in the range of 3-5 nm. More significant red shifts of 14-18 nm are observed for the strongly confined 2.5 nm QDs.

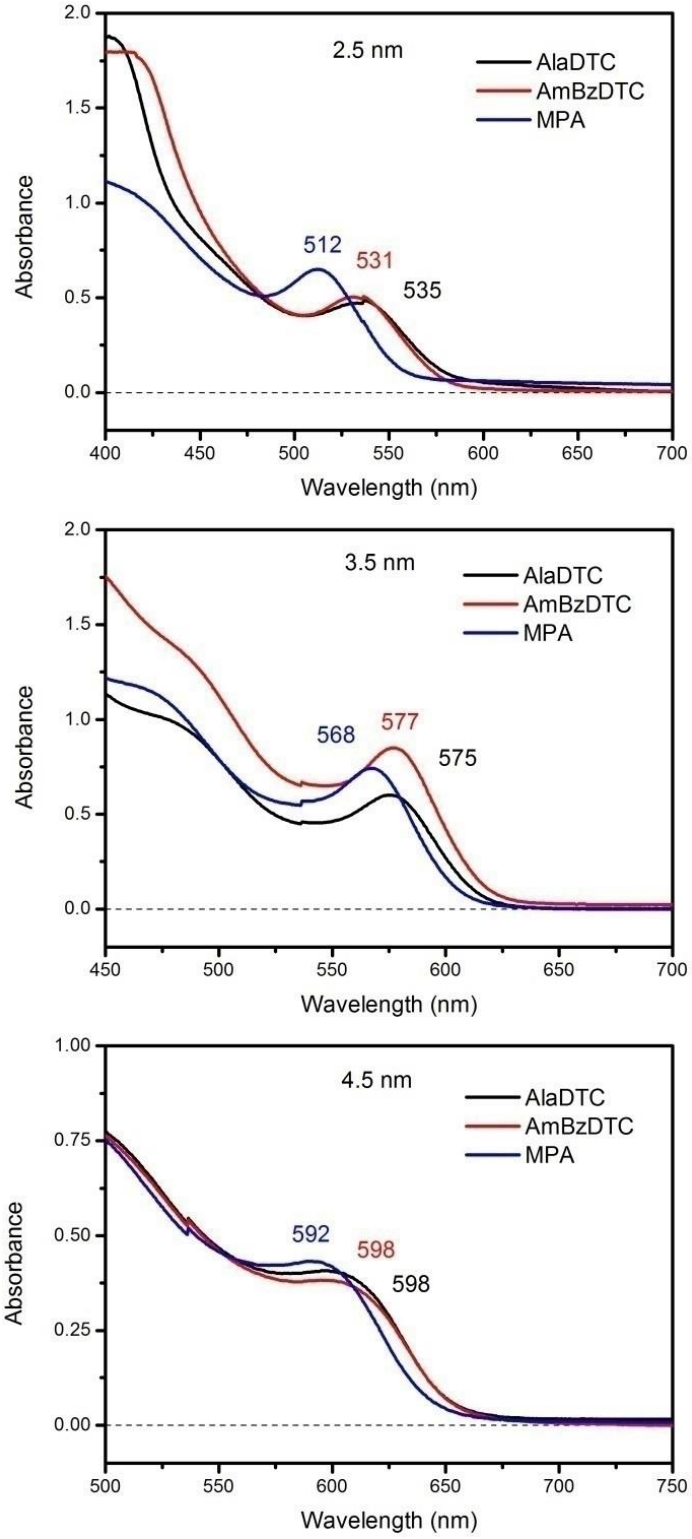

Figure 5-5. Extinction spectra of the different sizes of QDs, functionalised with Ala-DTC, AmBz-DTC, or MPA.

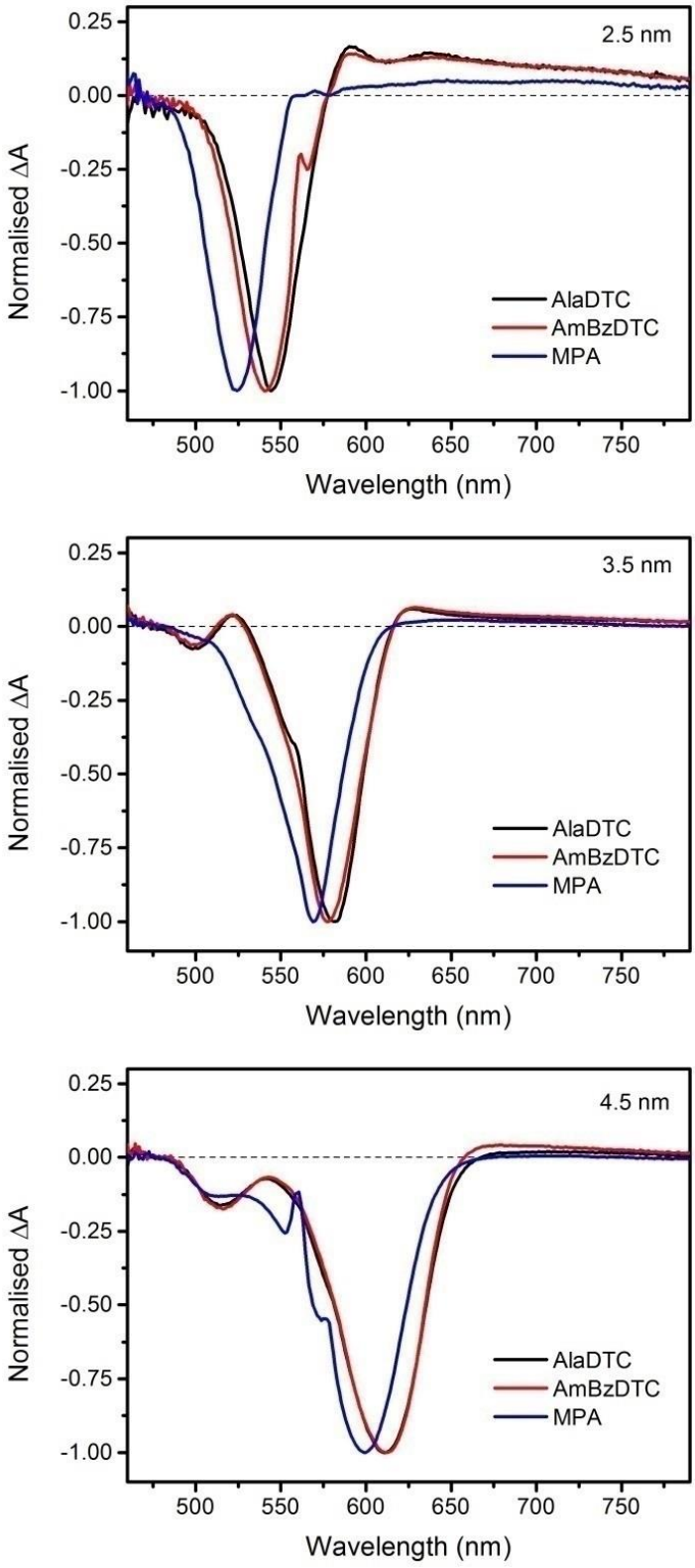

Figure 5-6. Difference spectra of CdSe QDs measured 1 ps after excitation at 450 nm. Discontinuities in 2.5 nm AmBz-DTC and 4.5 nm MPA spectra are believed to be due to partial detector saturation.

After performing steady-state absorption measurements, transient absorption spectra were collected for each QD material. All samples were excited at 450 nm to avoid obscuring the probe spectrum. As a result of the range of QD sizes studied, however, it should be noted that using the same excitation wavelength for each QD size introduces an experimental inconsistency. The initially created excitonic states of the QDs differ slightly, such that the larger QDs were pumped into a higher excited state relative to the smaller QDs. For the purpose of these experiments – exploring potentially size-dependent differences in spectral features and kinetics on the pico- to nanosecond timescale – this inconsistency is not expected to significantly affect the analysis, as carrier cooling from hot states to the band edges occurs on the femtosecond timescale.[21,25]

In Figure 5-6, the difference spectra recorded 1 ps after initial excitation are illustrated for the three QD sizes with either dithiocarbamate or MPA ligands. All spectra are dominated by negative signals arising from bleaching of the QD ground state. These signals are comprised of overlapping B1 and B2 signals; B3 bleach signals are also visible for 3.5 and 4.5 nm samples at higher energies (~500-520 nm), but are outside the probe range in the 2.5 nm QDs. The maxima of the bleach signals for each QD material are tabulated in Table 5-1, below. Adsorption of Ala-DTC appears to result in a slightly larger red-shift than AmBz-DTC in the smaller particles, while the shifts induced by the dithiocarbamates are equal for 4.5 nm QDs. Electronic coupling between adjacent PTC molecules adsorbed to CdS QDs has previously been shown to enhance the hole-delocalising effect of the ligands.[26] Ala-DTC is smaller and less rigid than AmBz-DTC, so may be able to form a slightly denser layer on the surface of QDs. Closer proximity of Ala-DTC ligands might therefore account for the larger red-shift induced by these molecules.

QD Diameter	Ala-DTC	AmBz-DTC	MPA
2.5 nm	544 nm	541 nm	524 nm
3.5 nm	581 nm	577 nm	568 nm
4.5 nm	612 nm	612 nm	600 nm

Table 5-1. Wavelengths of the maxima of ground state bleach signals in the transient spectra of CdSe QDs functionalised with DTC or MPA ligands.

Perhaps the most striking feature of the difference spectra is the pronounced positive signal that extends from the low-energy edge of the ground state bleach in 2.5 nm QDs functionalised with Ala-DTC and AmBz-DTC, at wavelengths above 575 nm. This signal is absent in the spectra of 3.5 and 4.5 nm QDs bearing the same ligands, which suggests that it arises as a result of the particular interaction between dithiocarbamates and QDs in which photo-generated holes are strongly confined. The nature of this signal is addressed in greater detail later in this chapter.

In Figure 5-7, the bleach recovery kinetics of each QD material are plotted, which represent the population of conduction band edge states by excited electrons. Note that the plots are grouped by ligand to highlight size-dependent effects, rather than by QD size as above. All kinetic traces were fit to biexponential functions to quantify the rates of decay, the results of which are summarised in Table 5-2. Evidently, DTC ligands affect the QDs almost identically in terms of their impact on the bleach recovery, with electrons depopulating the conduction band progressively faster as the size of the QDs decreases. For the smallest QDs, the bleach signal recovers completely in ~100 ps. The kinetics of the MPA-coated QDs are significantly slower. The same trend with QD size appears at early time delays, but the traces converge at ~50 ps, after which point faster decay is observed for larger QDs.

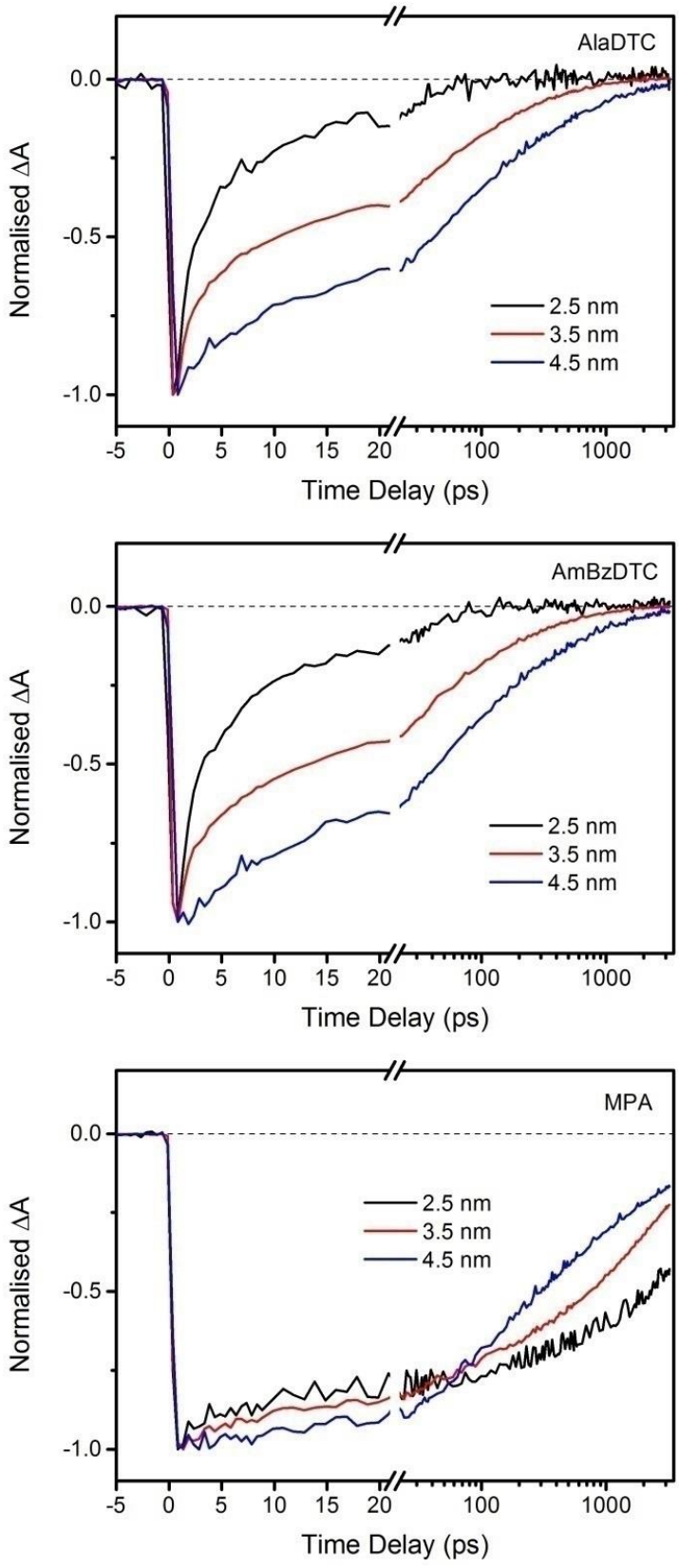

Figure 5-7. Kinetics monitored at the wavelength of the initial maximum of the bleach signals.

		2.5 nm	3.5 nm	4.5 nm
Ala-DTC	A_1	-0.80 ± 0.02	-0.56 ± 0.01	-0.50 ± 0.01
	τ_1	1.9 ± 0.1 ps	5.3 ± 0.3 ps	23 ± 1 ps
	A_2	-0.37 ± 0.02	-0.41 ± -0.01	-0.41 ± 0.01
	τ_2	20 ± 1 ps	127 ± 5 ps	330 ± 13 ps
	y_0	0.006 ± 0.001	-0.015 ± 0.002	-0.034 ± 0.002
AmBz-DTC	A_1	-0.90 ± 0.3	-0.52 ± 0.01	-0.55 ± 0.01
	τ_1	1.9 ± 0.1 ps	8.8 ± 0.5 ps	24 ± 1 ps
	A_2	-0.41 ± 0.02	-0.39 ± 0.01	-0.41 ± 0.01
	τ_2	19 ± 1 ps	145 ± 7 ps	323 ± 12 ps
	y_0	0.002 ± 0.001	-0.016 ± 0.003	-0.032 ± 0.002
MPA	A_1	-0.19 ± 0.01	-0.24 ± 0.01	-0.40 ± 0.01
	τ_1	9.7 ± 1.4 ps	36 ± 2 ps	96 ± 4 ps
	A_2	-0.37 ± 0.01	-0.55 ± 0.01	-0.43 ± 0.01
	τ_2	1417 ± 141 ps	1440 ± 51 ps	951 ± 47 ps
	y_0	-0.41 ± 0.02	-0.18 ± 0.01	-0.16 ± 0.01

Table 5-2. Time constants from fits of the B1 signal kinetics, plotted in Figure 5-7. Fitting windows begin at the maximum initial amplitudes (1 ps) and end at the final data point (3195 ps).

The trend in the recovery kinetics of DTC-functionalised QDs is consistent with a mechanism involving surface states. Smaller particles have a higher surface-to-volume ratio, so ligand-induced effects would likely have greater influence on the overall behaviour as the particle size decreases. While a similar behaviour seems to be present at early time delays in MPA-functionalised CdSe QDs, the trend in relaxation kinetics is reversed at longer timescales. Recombination of electrons with trapped holes is believed to be the dominant pathway for depopulation of the conduction band in these materials,

typically occurring on a nanosecond timescale.[25] While adsorption of MPA is known to create surface traps, states in the QD core (e.g. defects) can also serve as trapping sites.[27,28] The faster relaxation observed in MPA-coated QDs with increasing size, on the hundreds of picoseconds to nanosecond timescale, might be related to a greater proportion of core states that exist in the larger particles contributing to recombination.

Performing a size-dependence study of the effects of dithiocarbamate ligands on CdSe QDs provided some useful results to guide further work. The appearance of the broad, low-energy photoinduced absorption in the transient spectra of only the smallest QDs upon DTC-functionalisation potentially offered a spectral signature for hybridised QD-DTC states. This signal, combined with the trend in bleach recovery kinetics, confirmed the theoretical expectation that the effects of dithiocarbamate ligands would be most pronounced in smaller QD in which holes are strongly confined.

5.4 Hole-Scavenging from Dithiocarbamate-Functionalised CdSe QDs

Based on the results of the size-dependence study of dithiocarbamate-functionalised QDs, an investigation of the potential for DTC ligands to facilitate charge transfer to and from CdSe QDs was undertaken. To maximise the hole delocalising effects of these ligands, 2.5 nm QDs were employed for this study. As previously, MPA-coated QDs were measured in parallel to highlight the effects of the dithiocarbamates.

Figure 5-8 illustrates the absorption spectra of the CdSe QDs before and after ligand exchange. The as-synthesised QDs in chloroform have an absorption maximum at 520 nm. Ligand exchange with MPA red-shifted this peak by 8 nm, while functionalisation with dithiocarbamates resulted in a dramatic shift of 35-45 nm, visibly changing the colour of the QDs. The red shift induced by the DTC ligands in this instance is larger than that observed in the previous section for nominally the same materials. Batch-to-batch inconsistencies in the magnitude of the red shift upon DTC adsorption has been reported in the literature, and attributed to differences in surface coverage and spatial distribution of ligands.[26]

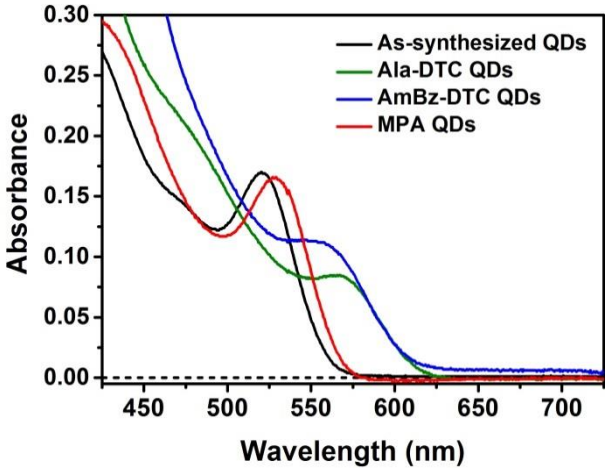

Figure 5-8. Extinction spectra of CdSe QDs before and after ligand exchange with DTC or MPA ligands.

Figure 5-9(a) shows the emission spectrum (red) overlaid with the absorption spectrum (black) of the as-synthesised QDs. The emission spectra of the QDs after ligand exchange are presented in Figure 5-9(b). Adsorption of MPA reduced the band edge emission to ~4% of its initial intensity, while emission at longer wavelengths arising from newly formed trap states appeared to increase slightly, consistent with previous observations of MPA-coated QDs.[27] Emission was completely quenched upon functionalisation with both Ala-DTC and AmBz-DTC.

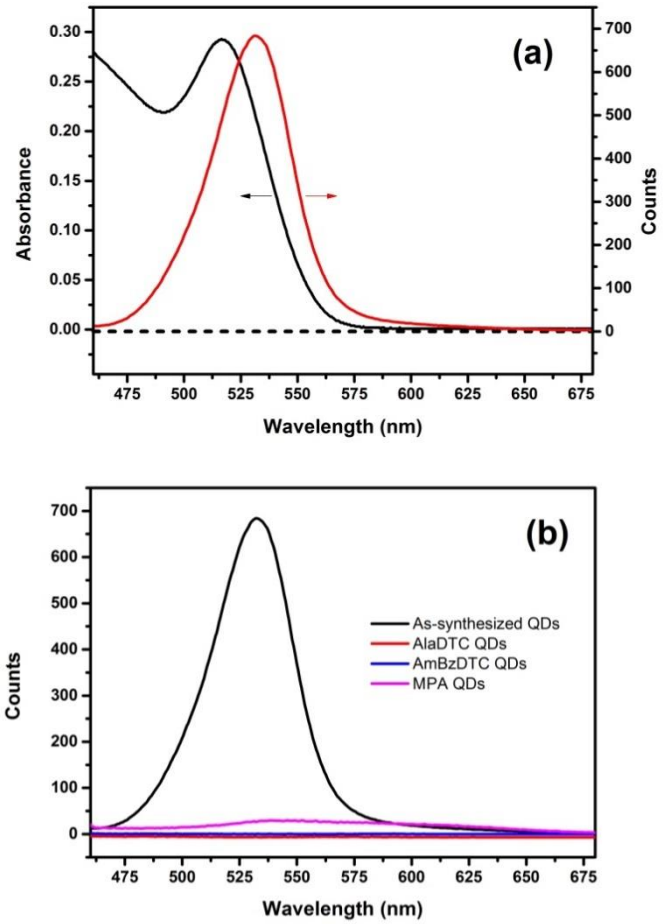

Figure 5-9. (a) Band edge emission of as-synthesised CdSe QDs in chloroform, relative to the excitonic extinction spectrum. (b) Emission spectra of CdSe QDs before and after ligand exchange with Ala-DTC, AmBz-DTC, or MPA. Ala-DTC spectrum Y-offset by -7 for visibility.

Dithiocarbamate ligands have previously been observed to quench QD photoluminescence. Jin et al. showed that treatment of CdSe QDs in dichloromethane with phenyldithiocarbamate (PTC) reduced the PL quantum yield by 95%, but that subsequent treatment with Cd^{2+} not only restored the initial yield, but enhanced it by a factor of two.[29] The authors ascribed this behaviour to two mechanisms: (i) passivation of undercoordinated selenium surface sites, and (ii) precipitation of free or loosely-bound PTC upon complexation with the cadmium cations, which are thought to introduce non-radiative exciton decay pathways. Azzarro et al. drew similar conclusions from studying the same system, suggesting that the absorption and emission behaviour

was due to subsets of PTC ligands bound in different geometries.[21] Monodentate PTC was likely to trap holes, given the presence of a lone pair on the unbound sulfur atom, whereas bidentate PTC was responsible for the exciton delocalisation and resulting optical shifts. Computational studies support the distinction between dithiocarbamates with various binding geometries as having different electronic effects on QDs.[30,31] Interestingly, Dubois et al. also reported that emission from CdSe QDs was quenched after ligand exchange with a dithiocarbamate, but that emission from CdSe/ZnS core/shell QDs was unaffected by functionalisation with the same ligand.[32] The authors did not comment on the mechanism, but it is likely to be a consequence of the energetic barrier to hole delocalisation established by the ZnS shell, which confines the hole to the CdSe core such that it eventually recombines radiatively with the electron.

Following steady-state characterisation of the QD materials, we collected transient absorption spectra of the QD materials after excitation at 450 nm. Difference spectra of each material at selected time delays are presented in Figure 5-10. The spectra are qualitatively the same as those obtained in the size-dependence study in terms of features, with the prominent photoinduced absorption in the DTC-functionalised samples again present. As before, the recovery of the ground state bleach signal is also accelerated by the DTC ligands.

Figure 5-11 illustrates the photoinduced absorption feature in greater detail at various time delays for the three QD materials. The A1 feature associated with biexciton interactions, discussed previously in Chapter 4, appears as the relatively well-defined peak on the low-energy edge of the bleach signal, visible at all time delays in MPA QDs (Figure 5-11(c)). At 1 ps after excitation, the A1 signal is present in the spectra for DTC QDs but disappears at later delay times. A similarly rapid decay of A1 is apparent in spectra published by Xie et al. of CdSe nanoclusters functionalised with PTC.[33] The short lifetime of A1 in these materials suggests that excitons created upon absorption of pump pulses do not persist in the QDs, possibly as a result of hole delocalisation beyond the QD core.

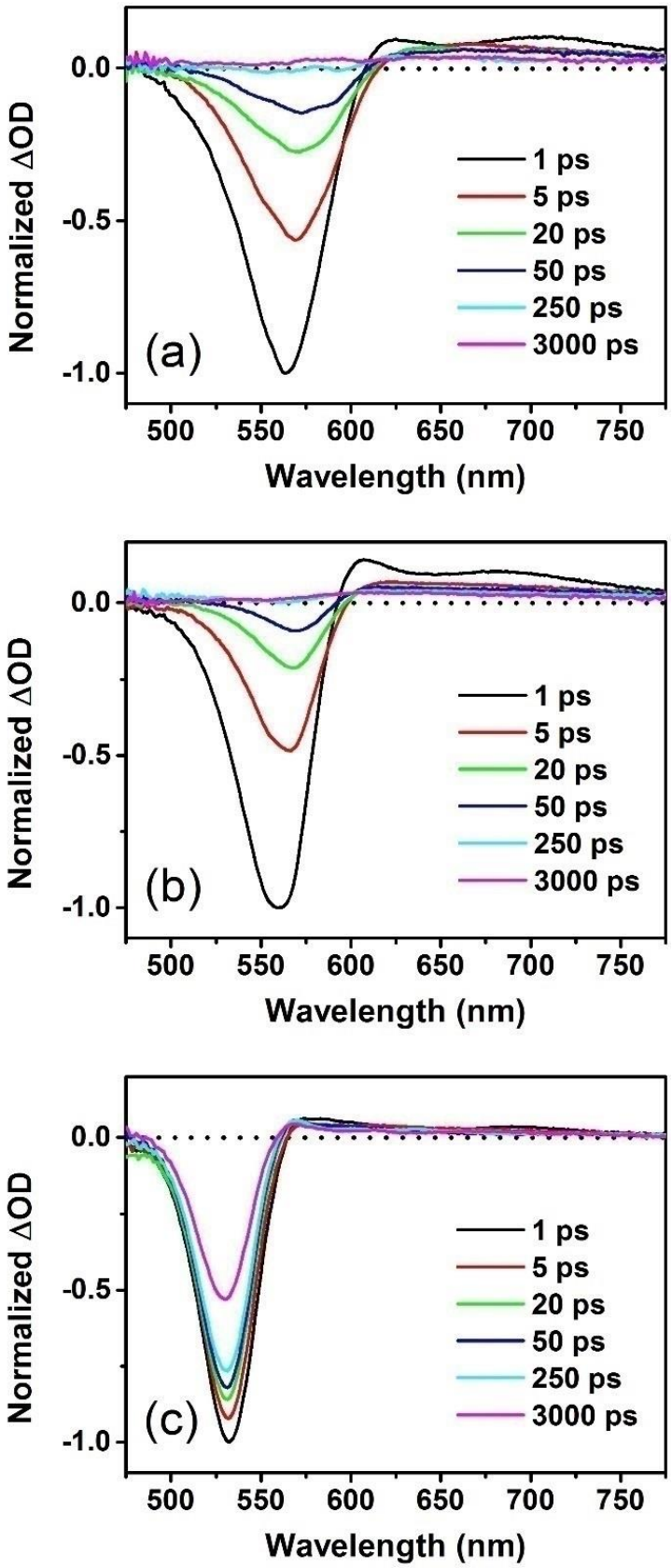

Figure 5-10. Difference spectra of CdSe QDs functionalised with (a) Ala-DTC, (b) AmBz-DTC or (c) MPA at selected time delays after excitation at 450 nm.

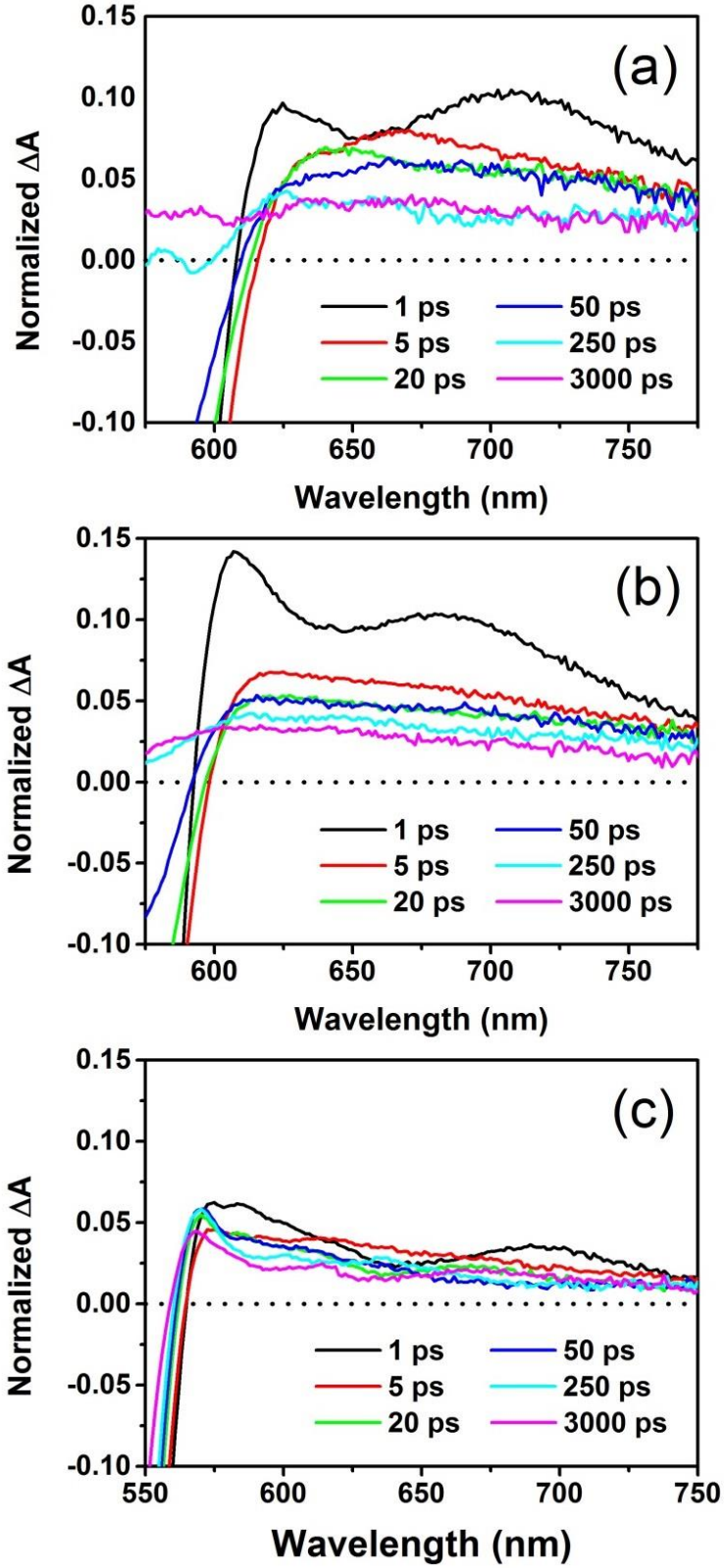

Figure 5-11. Detail of the photoinduced absorptions in the spectra of CdSe QDs functionalised with (a) Ala-DTC, (b) AmBz-DTC or (c) MPA.

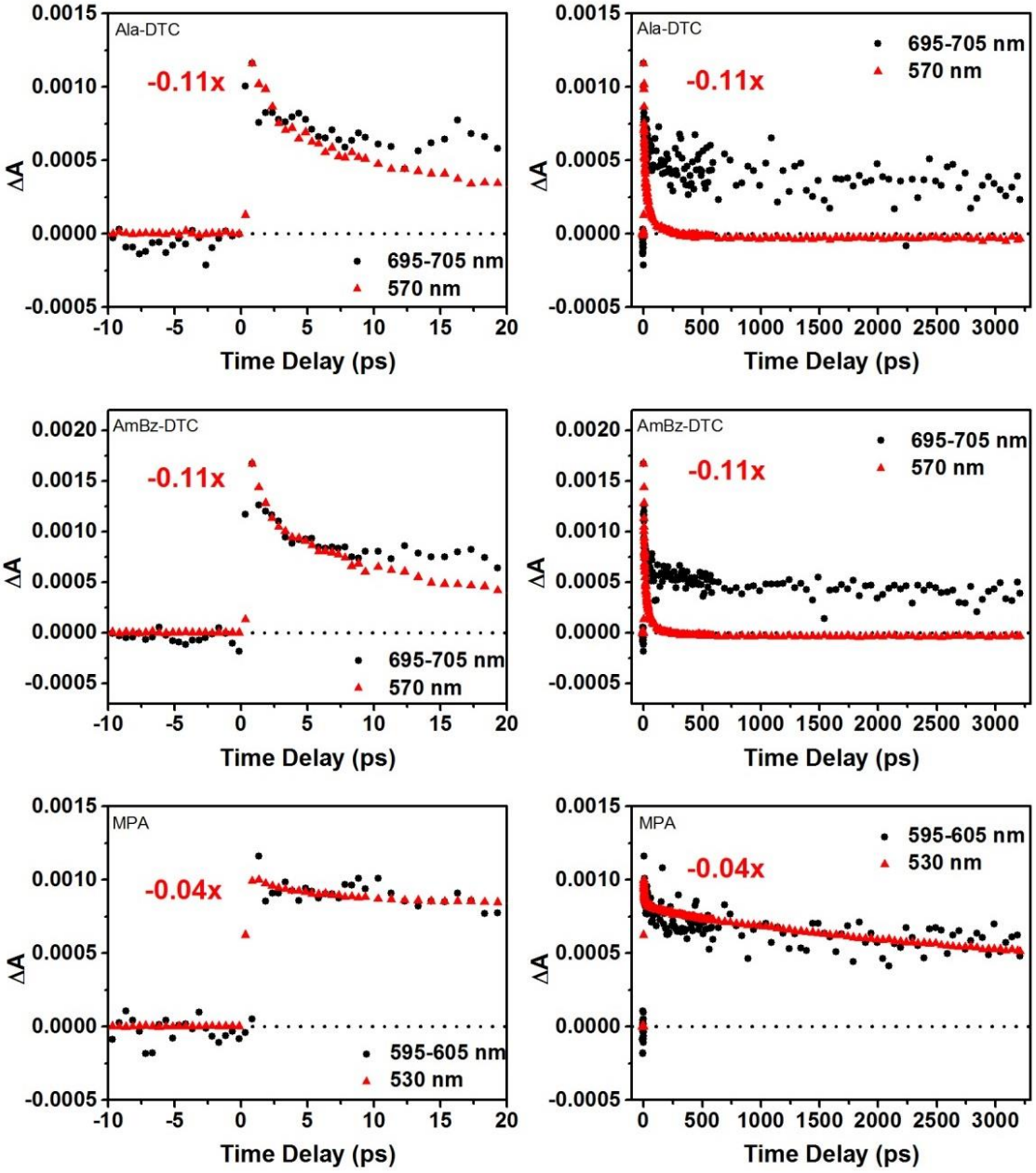

Figure 5-12. Kinetic of the PA signal monitored at the indicated wavelength range, compared with the kinetics of the B1 signal which have been scaled to match the initial intensity of the PA signal by the factor indicated.

The broader component of the photoinduced absorption, which extends towards the near-IR in the spectra, has previously been attributed to lattice- and surface-trapped holes in CdSe QDs.[25,34] This feature will be referred to hence as the "PA" (photoinduced absorption). In Figure 5-12, the kinetics of this signal are plotted (black dots) at early time delays (left column) and over the full timeframe of the measurement (right column). Due to the low intensity of the signal, values were averaged across a ten-nanometre portion of the spectrum at each time delay to improve the signal-to-noise ratio. The kinetics of the ground state bleach have been overlaid (red dots) and scaled to match the initial intensity of the PA signal. It should be noted that the magnitude of the signal in DTC QDs is roughly twice that observed in the same region for MPA QDs relative to the bleach signal intensity.

For MPA-functionalised QDs, excellent correspondence is observed between the kinetics of the bleach and PA signals over the 3.2 ns period of the transient measurement. This result would appear to support the conclusions of other authors that the PA signal is related to trapped holes, and that recombination of conduction band electrons with trapped holes is the dominant relaxation mechanism in MPA-coated CdSe QDs.[25] In DTC-functionalised QDs, however, the correlation between the decay of the PA signal and the ground state bleach recovery exists only in the first ~10 ps after excitation. Beyond this time, the PA signal is relatively stable, whereas the intensity of the bleach signal continues to decrease rapidly to zero. The picosecond decay pathway for electrons induced by DTC ligands appears to affect only a fraction of initially trapped holes. Abdellah et al. identified the presence of both shallow and deep traps in CdSe QDs; while holes in the former can de-trap, holes trapped in so-called deep traps can remain localised for up to microseconds.[35] It may be that dithiocarbamate ligands only affect holes in shallow traps, perhaps by facilitating de-trapping or recombination with electrons.

To assess the potential for dithiocarbamate ligands to promote hole scavenging from CdSe QDs, we recorded transient absorption spectra in the presence of 0.1 M sodium sulfite. In Figure 5-13, the spectra are presented as a series of contour plots focusing on the ground state bleach region. The upper frames show the spectra of the QDs, while the lower frames show the spectra in the presence of the hole scavenger. All samples were excited at 450 nm. Evidently, sulfite only induced significant changes in

the transient spectrum of AmBz-DTC QDs. Interestingly, the effect of the scavenger appears to manifest differently at different wavelengths, suggesting that sulfite interacts with discrete states in the QD-ligand complex, rather than affecting the material uniformly.

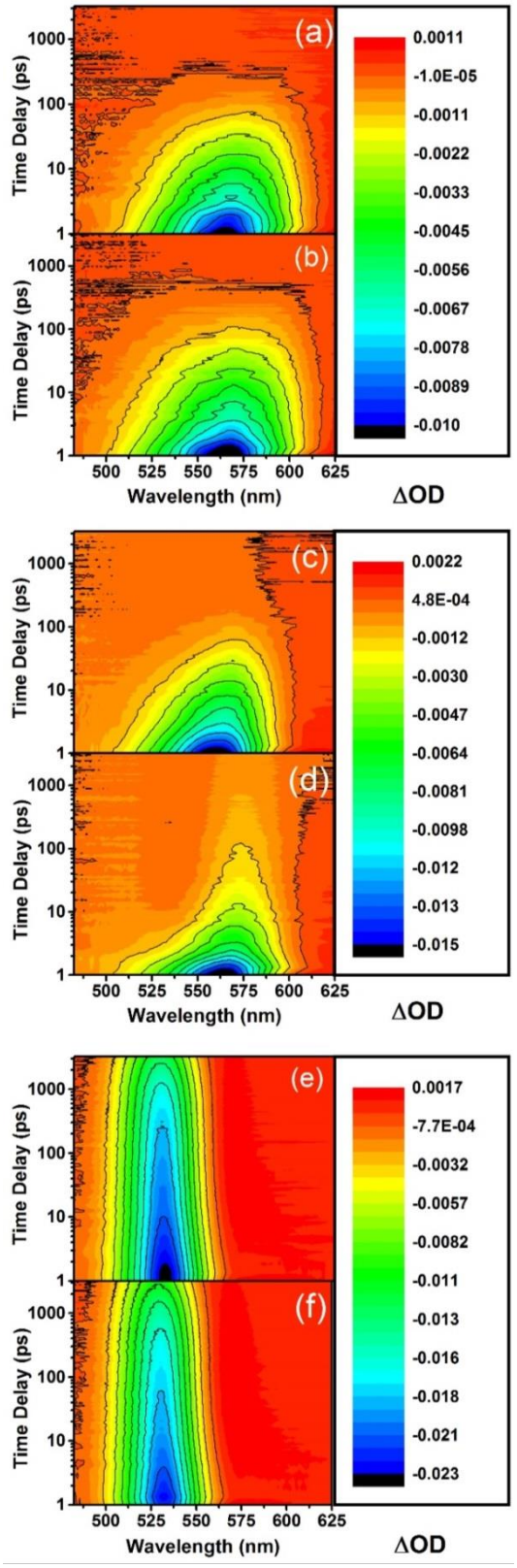

Figure 5-13. Contour plots of CdSe QDs functionalised with Ala-DTC (top), AmBz-DTC (middle), or MPA (bottom), recorded in the absence (a, c, e) and presence (b, d, f) of the hole scavenger sodium sulfite.

Due to the quantisation of energy levels in nanocrystals, individual spectral features can be assigned to specific transitions between states in the valence and conduction bands.[20,36] In CdSe QDs of the dimensions studied here, the band edge $1S_{3/2}$(h)–1S(e) transition and the higher energy $2S_{3/2}$(h)–1S(e) transition are separated by 100-150 meV.[37] These transitions combine to form the characteristic low-energy absorption peak in steady-state absorption spectra, while pumping them produces the B1 bleach feature in transient spectra. The kinetics of the QD materials could therefore be evaluated at specific wavelengths corresponding these transitions: 535 and 575 nm for the DTC QDs, and at 515 and 545 nm for the MPA QDs. These wavelengths are consistent with the theoretical energetic spacing of the transitions, and take into account the greater separation on the wavelength scale in the red-shifted DTC QD spectra.[25,38]

Figure 5-14 plots the kinetics of the ground state bleach recovery for the different QDs in the absence (hollow dots) and presence (solid dots) of sulfite at wavelengths corresponding to the $1S_{3/2}$(h)–1S(e) and $2S_{3/2}$(h)–1S(e) transitions. The kinetics were fit to triexponentials to extract time constants, which are summarised in Table 5-3. Some differences exist in the relative rates of $1S_{3/2}$(h)–1S(e) and $2S_{3/2}$(h)–1S(e) bleach recovery among the samples even in the absence of the hole scavenger. In Ala-DTC QDs, these transitions recover at nearly identical rates, whereas the higher energy transition recovers roughly twice as fast in AmBz-DTC QDs. The availability of additional vibrational modes associated with the aromatic ring in AmBz-DTC might contribute to this difference in relaxation rate, as suggested by computational work by Swenson et al.[39] It is also possible that some variation exists in the binding geometries adopted by the smaller Ala-DTC and the larger, more rigid AmBz-DTC molecules in ligand shells, which would affect the relaxation rates.[21,30,31] In contrast to the dithiocarbamate materials, the bleach recovery in MPA QDs is at least 10 times slower, with the $1S_{3/2}$(h)–1S(e) recovering marginally faster.

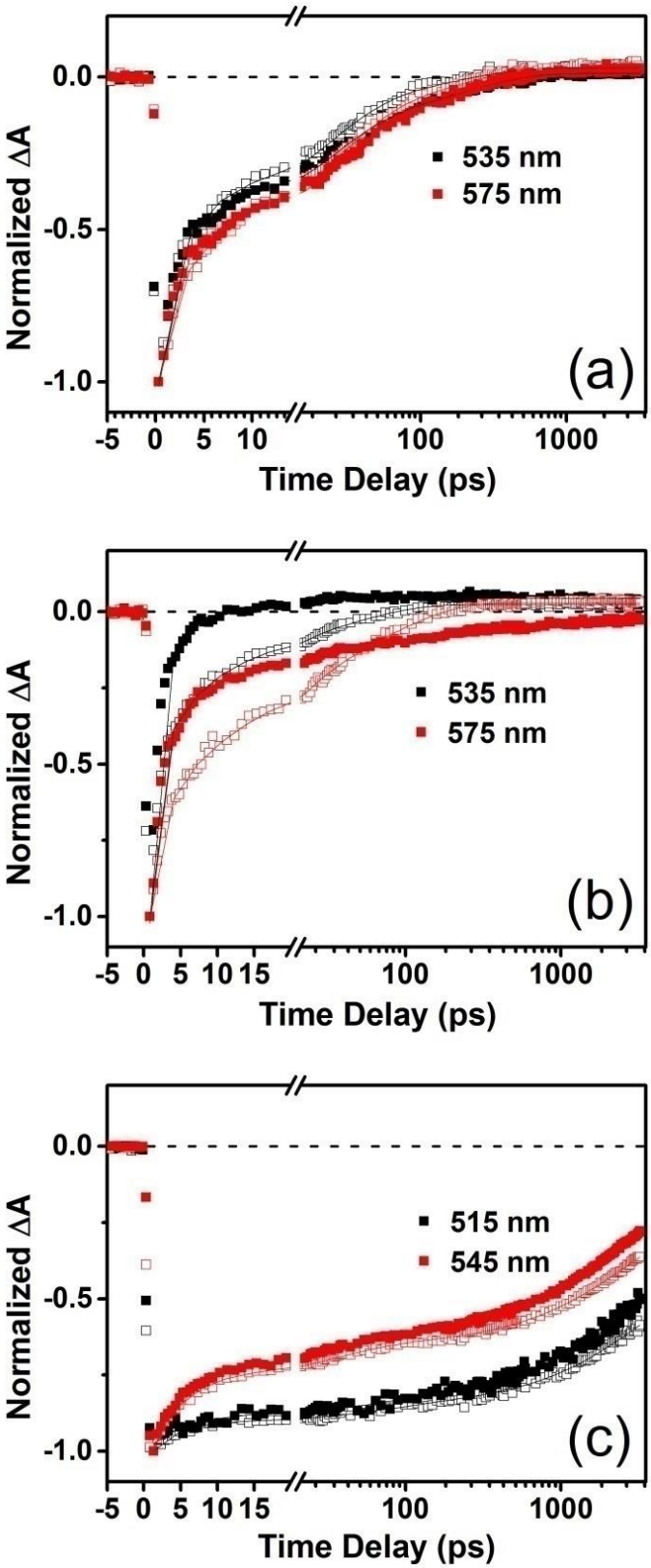

Figure 5-14. Kinetics of the ground state bleach of CdSe QDs functionalised by (a) Ala-DTC, (b) AmBz-DTC, or (c) MPA, monitored at the wavelengths indicated, in the absence (open markers) and presence (solid markers) of 0.1 M sodium sulfite.

	Equation: $y = y_0 + A_1 * \exp(-x/\tau_1) + A_2 * \exp(-x/\tau_2) + A_3 * \exp(-x/\tau_3)$				
		535 nm		575 nm	
		Without SO_3^-	With SO_3^-	Without SO_3^-	With SO_3^-
Ala-DTC	y_0	-0.029 ± 0.001	0.011 ± 0.002	-0.032 ± 0.002	0.021 ± 0.001
	A_1	-0.598 ± 0.013	-0.616 ± 0.015	-0.480 ± 0.014	-0.506 ± 0.013
	τ_1 (ps)	1.9 ± 0.1	1.5 ± 0.1	2.4 ± 0.1	1.7 ± 0.1
	A_2	-0.415 ± 0.011	-0.375 ± 0.011	-0.465 ± 0.014	-0.428 ± 0.001
	τ_2 (ps)	22.4 ± 1.3	23.4 ± 1.4	25.7 ± 1.6	25.3 ± 1.2
	A_3	-0.115 ± 0.012	-0.157 ± 0.011	-0.155 ± 0.015	-0.180 ± 0.010
	τ_3 (ps)	180 ± 20	211 ± 18	184 ± 18	216 ± 14
		535 nm		575 nm	
		Without SO_3^-	With SO_3^-	Without SO_3^-	With SO_3^-
AmBz-DTC	y_0	-0.024 ± 0.001	0.043 ± 0.001	-0.030 ± 0.001	-0.031 ± 0.001
	A_1	-1.149 ± 0.027	-0.210 ± 0.130	-0.584 ± 0.028	-1.097 ± 0.024
	τ_1 (ps)	1.0 ± 0.1	0.9 ± 0.1	1.4 ± 0.1	1.5 ± 0.1
	A_2	-0.406 ± 0.012	-0.154 ± 0.212	-0.464 ± 0.014	-0.288 ± 0.014
	τ_2 (ps)	7.7 ± 0.5	3.3 ± 4.2	12.9 ± 1.0	12.2 ± 0.9
	A_3	-0.163 ± 0.012	-1.834 ± 0.155	-0.289 ± 0.018	-0.089 ± 0.004
	τ_3 (ps)	45.6 ± 3.2	8.7 ± 4.5	78.3 ± 4.7	310 ± 30
		515 nm		545 nm	
		Without SO_3^-	With SO_3^-	Without SO_3^-	With SO_3^-
MPA	y_0	-0.422 ± 0.032	-0.310 ± 0.060	-0.242 ± 0.012	-0.174 ± 0.008
	A_1	-0.430 ± 0.030	-0.117 ± 0.018	-0.293 ± 0.009	-0.317 ± 0.008
	τ_1 (ps)	3.3 ± 0.5	4.3 ± 1.2	3.5 ± 0.2	3.3 ± 0.2
	A_2	-0.129 ± 0.013	-0.065 ± 0.009	-0.139 ± 0.007	-0.155 ± 0.007
	τ_2 (ps)	65.5 ± 13.0	75.6 ± 25.1	31.1 ± 2.2	28.7 ± 1.7
	A_3	-0.056 ± 0.005	-0.516 ± 0.054	-0.414 ± 0.011	-0.452 ± 0.007
	τ_3 (ps)	3300 ± 400	3300 ± 600	2630 ± 130	2270 ± 80

Table 5-3. Summary of fitting parameters extracted from the kinetic traces in Figure 5-14. Fitting windows begin at the maximum initial amplitudes (1 ps) and end at the final data point (3190 ps).

Upon addition of sulfite to the AmBz-DTC QDs, the recovery of the bleached $2S_{3/2}(h)–1S(e)$ transition at 535 nm is accelerated ~~by an order of magnitude~~, such that the signal decays in ~10 ps. The band edge transition at 575 nm also decays rapidly at early time delays, but slows markedly at longer timescales, manifesting as a four-fold increase in the τ_3 time constant. This asymmetric effect on the kinetics is absent for Ala-

DTC and MPA QDs, where only modest changes on the order of the standard errors of the exponential fits are observed.

The fact that excitation of the $1S_{3/2}(h)$–1S(e) and $2S_{3/2}(h)$–1S(e) transitions populates the same conduction band state suggests that the discrepancy in their bleach recovery rates might arise as a result of different dynamics in their respective hole states. State-specificity involving the $2S_{3/2}(h)$ state in CdSe QDs has been observed previously upon adsorption of phenyldithiocarbamate[33] as well as hole-accepting catechols[40] and thiols[41]. Evidence for the involvement of the $2S_{3/2}(h)$ state in hole transfer can also be seen in TA and PL spectra reported for CdSe QDs adsorbed to NiO films using MPA as a linker, where holes are transferred to the p-type semiconductor.[42] Hot hole transfer from the $2S_{3/2}(h)$ state may cause the electron in the associated 1S(e) state to localise, depopulating the conduction band and leading to the accelerated decay of the bleach signal observed in the presence of sulfite.

The most significant outcome of this experiment is highlighted in Figure 5-15, in which the kinetics of AmBz-DTC QDs are plotted on a linear scale. In the presence of sulfite, the bleaching of the band edge transition at 575 nm now persists on the nanosecond timescale, indicating a substantial increase in the lifetime of conduction band electrons for the $1S_{3/2}(h)$–1S(e) transition. In isolation, the extended B1 lifetime suggests that AmBz-DTC can facilitate hole transfer from CdSe QDs through the ligand shell to the hole scavenger in the surrounding solution, which would eliminate the recombination pathway through which conduction band electrons can relax and manifest in the transient absorption spectra as the observed longer-lived ground state bleach signal. The complete recovery of the B2 bleach at 535 nm, however, associated with the $2S_{3/2}(h)$–1S(e) transition, is difficult to reconcile with this simple model. The rapid recovery of the B2 bleach implies that conduction band electrons actually *depopulate* the 1S(e) states within several picoseconds in the presence of the hole scavenger. It may be that the extensive hybridisation between the QD and ligand interfacial orbitals leads to a decoupling of the upper states of the $1S_{3/2}(h)$–1S(e) and $2S_{3/2}(h)$–1S(e) transitions, but this is highly speculative. At present, a comprehensive model that rationalises the apparently contradictory behaviour of the B1 and B2 signals has not been formulated.

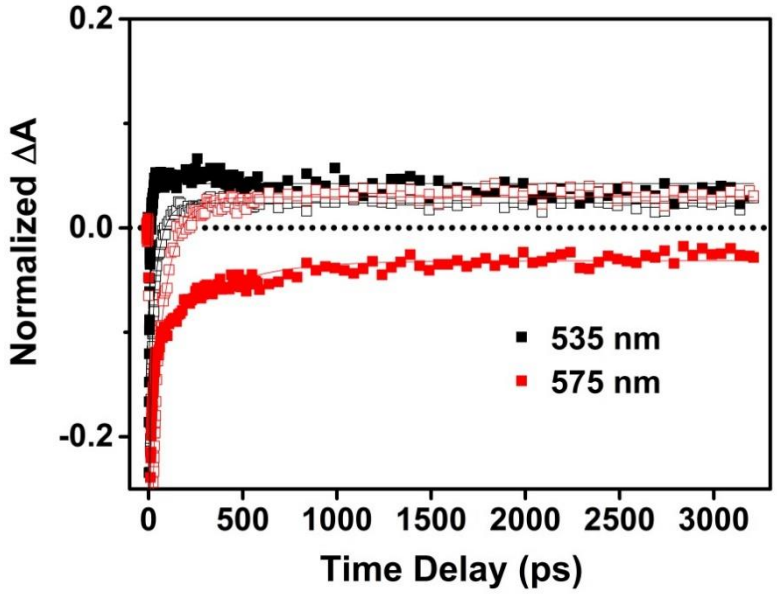

Figure 5-15. Linear plot of the kinetics of the ground state bleach signals in CdSe QDs coated with AmBz-DTC in the absence (open markers) and presence (closed markers) of 0.1 M sodium sulfite.

The use of Ala-DTC as a ligand for the QDs under the same experimental conditions provides a useful point of comparison from which to explore the possible mechanism operating in the AmBz-DTC QD system. The two ligands adsorb to CdSe via the same functional group, which results in the similar red shifts of their excitonic peaks observed in the absorption spectra and induces the accelerated bleach recovery kinetics observed in the transient spectra. Calculations by Azpiroz and De Angelis have shown that the orbitals into which hole density primarily delocalises when PTC is used as a ligand for CdSe QDs are located on the dithiocarbamate group, not the aryl group.[30] It follows that qualitatively similar behaviour should be observed after functionalising QDs with either the alkyl or aromatic DTC ligand.

The aromatic ring in AmBz-DTC does however result in a conjugated molecule, whereas the alkyl chain effectively isolates the dithiocarbamate group of Ala-DTC at the QD interface. Jin et al. previously reported that a conjugated bis-dithiocarbamate linker promoted electron transfer from photoexcited porphyrins to CdSe QDs.[16] Work from the same group showed that hole transfer to a phenothiazine bound to CdS QDs

via a conjugated dithiocarbamate moiety was accelerated 20-fold relative to a carboxylate-bound analogue.[17] Perhaps most pertinently, a study of CdSe QD films by Zotti et al. found that a conjugated bis-dithiocarbamate linker enhanced the extracted photocurrent by a factor of 5 compared to the alkyl analogue.[43] Similarly, it is thought the conjugation of the AmBz-DTC ligand facilitates hole transfer from the QD to sulfite, represented schematically in Figure 5-16.

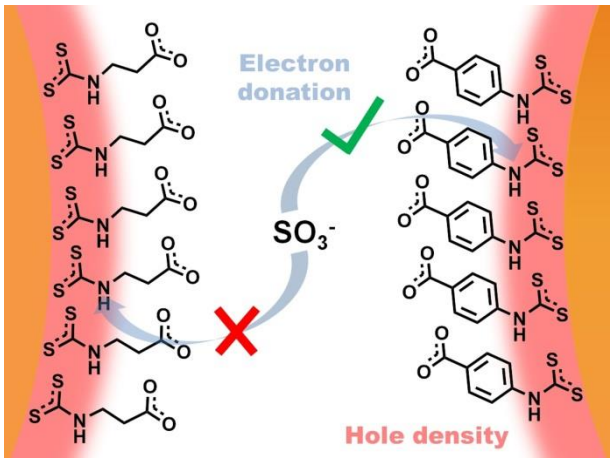

Figure 5-16. Schematic representation of Ala-DTC and AmBz-DTC adsorbed to the surface of CdSe QDs.

Based on the spectroscopic features discussed, several processes appear to govern the charge carrier dynamics of the dithiocarbamate-functionalised QDs, which are summarised in Figure 5-17. Following photoexcitation, electron-hole pairs are created in the CdSe QDs, populating 1S(e) conduction band states which are of primarily QD character.[30] This process establishes the ground state bleach signal in transient spectra, which decays on the order of tens of picoseconds as electrons begin to depopulate the conduction band. Concurrently, valence band holes created by photoexcitation are trapped at lattice or surface sites within ~1 ps, giving rise to the PA signal. Hybridised QD-DTC states are also accessible to the initially created holes, providing for delocalisation beyond the volume of the core in strongly confined QDs. This hole delocalisation is thought to induce electron migration from states in the core towards the surface of the QD as a result of Coulomb drag.[44] This process would bring

electrons into closer proximity with surface-trapped holes, with which they could recombine, leading to the picosecond decay of the PA observed in DTC QDs. The electrons could also be trapped themselves in surface states arising from QD-DTC interactions, also leading to depopulation of the conduction band.[21] The exact nature of the acceptor states for electrons leaving the conduction band is not known, but they are believed to arise through the extensive hybridisation of QD valence band and ligand HOMO orbitals identified by other authors.[15,30]

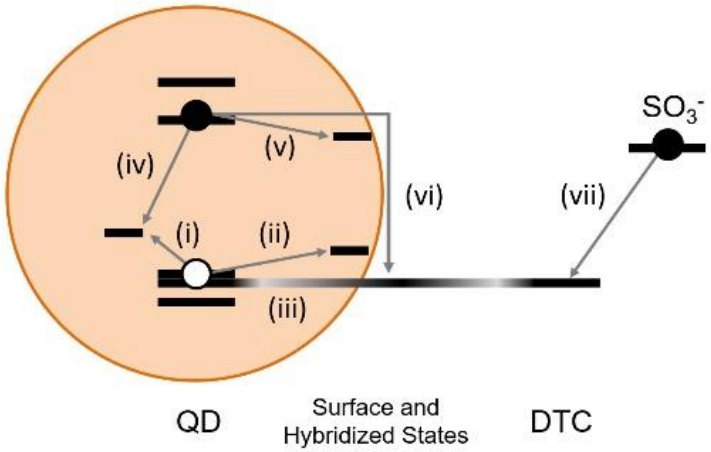

Figure 5-17. Scheme summarising the processes governing the observed behaviour of CdSe QDs functionalised with AmBz-DTC. (i) Hole trapping to core states; (ii) hole trapping to surface states; (iii) hole delocalization into hybridized QD-DTC states; (iv) hole trap-mediated recombination, governs relaxation in MPA QDs; (v) electron trapping; (vi) electron−hole recombination via hybridized QD-DTC states; (vii) electron transfer (hole scavenging) by sulfite in solution.

It should be noted that an alternative mechanism has been proposed to explain the red shifts observed in optical spectra of CdSe QDs functionalised with dithiocarbamates. Grenland et al. suggested in a very recent paper that the behaviour attributed to hole delocalisation into the ligand shell could also be explained by the presence of thin layers of CdS on the QD surface that form due to dithiocarbamate decomposition and reaction with excess cadmium.[45] The band alignments between CdSe and CdS are such that the electron could delocalise into the CdS, with the resulting decrease in confinement leading to the observed shift of the exciton to lower

energies. The study relies on Raman spectroscopy which shows the appearance of a peak at 273 cm^{-1} in the spectra of CdSe QDs after either functionalisation with a dithiocarbamate or intentional growth of a CdS shell on the QDs. An NMR study by Munro et al. is also cited prominently by the authors in which a pre-synthesised dithiocarbamate was shown to decompose rapidly under specific ligand exchange conditions.[46]

Although the study by Grenland et al. was performed on QD films, not colloidal QDs, it still raises interesting questions about the results discussed earlier in this chapter. Electron transfer from CdSe to surface domains of CdS could result in depopulation of the conduction band and a decay of the bleach signal. In other transient absorption studies, however, growth of CdS shells on CdSe QD cores has not been shown to accelerate the ground state bleach recovery, but does shift the excitonic absorption to lower energies.[47,48] The impact of Ala-DTC and AmBz-DTC on the bleach recovery kinetics of CdSe QDs was among the most striking consequences of ligand exchange with these molecules; the fact that this behaviour is not reproduced by CdS shells suggests that there are additional electronic effects of the dithiocarbamate ligands acting on the QDs.

The appearance of Raman peaks with the same shift upon either dithiocarbamate adsorption or CdS shell growth might simply be due to the Cd–S bonds that form between the ligand and cadmium sites on the QD surface. Frederick et al. have noted that the geometry of the dithiocarbamate group upon chelating cadmium closely approximates the atomic positions and bond lengths of the CdS crystal lattice.[49]

Finally, while the study by Munro et al. demonstrated rapid dithiocarbamate decomposition, nonaqueous conditions in which the process were studied are of limited relevance to the work presented in this chapter. Under the aqueous alkaline conditions used for Ala-DTC and AmBz-DTC ligand exchanges, the respective precursor amines would not be capable of displacing the native ligands and binding to the as-synthesised QDs to effect phase transfer from chloroform. After transfer to water, degradation of ligands is of course possible, however the QDs would eventually precipitate after breakdown of a sufficient amount of ligands. For these reasons, it is believed that intact Ala-DTC and AmBz-DTC molecules were the stabilising ligands for the CdSe QDs in

the experiments discussed herein. Thin layers of CdS may be present, as proposed by Grenland et al., but would not account for the behaviour observed.

5.5 Conclusions

In this chapter, the results of experiments using hydrophilic dithiocarbamates as stabilising ligands for CdSe QDs in aqueous conditions were presented. The ligands Ala-DTC and AmBz-DTC were shown to induce a red shift in the absorption spectra of QDs. By preparing samples using QDs of different sizes, the magnitude of the induced red shift was shown to vary with QD size and was correlated to the degree of quantum confinement in the QDs. Transient absorption spectra of these materials were collected and reported for the first time, showing an acceleration of the ground state bleach recovery in dithiocarbamate-functionalised QDs, the extent of which was also found to be size dependent. A photoinduced absorption of enhanced intensity was observed in strongly confined QDs upon adsorption of dithiocarbamates but was not definitively assigned.

Additionally, the aromatic ligand AmBz-DTC appears to facilitate hole scavenging from CdSe QDs. In the presence of the hole scavenger sodium sulfite the lifetime of conduction band electrons, as measured at the wavelength of the lowest energy band edge transition, was prolonged from tens of picoseconds to nanoseconds. This result has relevance in applications that rely on charge transfer to and from semiconductor nanocrystals, such as quantum dot-sensitised solar cells and nanocrystal-based photocatalytic systems, where efficient extraction of holes could increase quantum efficiency by reducing recombination losses. These findings should enable to development of a QD-based photocatalyst that is both colloidally stable and catalytically active.

5.6 References

(1) Lee, J. R.; Li, W.; Cowan, A. J.; Jäckel, F. Hydrophilic, Hole-Delocalizing Ligand Shell to Promote Charge Transfer from Colloidal CdSe Quantum Dots in Water. *J. Phys. Chem. C* **2017**, *121*, 15160–15168.

(2) Thackeray, J. W.; Natan, M. J.; Ng, P.; Wrighton, M. S. Interaction of Diethyldithiocarbamate with n-Type Cadmium Sulfide and Cadmium Selenide: Efficient Photoelectrochemical Oxidation to the Disulfide and Flat-Band Potential of the Semiconductor as a Function of Adsorbate Concentration. *J. Am. Chem. Soc.* **1986**, *108*, 3570–3577.

(3) Kamat, P. V.; Dimitrijevic, N. M. Photoelectrochemistry in Semiconductor Particulate Systems. 13. Surface Modification of Cadmium Sulfide Semiconductor Colloids with Diethyldithiocarbamate. *J. Phys. Chem.* **1989**, *93*, 4259–4263.

(4) Dubois, F.; Mahler, B.; Dubertret, B.; Doris, E.; Mioskowski, C. A Versatile Strategy for Quantum Dot Ligand Exchange. *J. Am. Chem. Soc.* **2007**, *129*, 482–483.

(5) Wang, J.; Xu, J.; Goodman, M. D.; Chen, Y.; Cai, M.; Shinar, J.; Lin, Z. A Simple Biphasic Route to Water Soluble Dithiocarbamate Functionalized Quantum Dots. *J. Mater. Chem.* **2008**, *18*, 3270.

(6) Zhang, Y.; Schnoes, A. M.; Clapp, A. R. Dithiocarbamates as Capping Ligands for Water-Soluble Quantum Dots. *ACS Appl. Mater. Interfaces* **2010**, *2*, 3384–3395.

(7) Yuwen, L.; Lu, H.; He, Y.; Chen, L.; Hu, M.; Bao, B.; Boey, F.; Zhang, H.; Wang, L. A Facile Low Temperature Growth of CdTe Nanocrystals Using Novel Dithiocarbamate Ligands in Aqueous Solution. *J. Mater. Chem.* **2010**, *20*, 2788–2793.

(8) Drozd, M.; Pietrzak, M.; Kalinowska, D.; Grabowska-Jadach, I.; Malinowska, E. Glucose Dithiocarbamate Derivatives as Capping Ligands of Water-Soluble CdSeS/ZnS Quantum Dots. *Colloids Surfaces A Physicochem. Eng. Asp.* **2016**,

509, 656–665.

(9) Hulanicki, A. Complexation Reactions of Dithiocarbamates. *Talanta* **1967**, *14*, 1371–1392.

(10) Zhao, Y.; Perez-Segarra, W.; Shi, Q.; Wei, A. Dithiocarbamate Assembly on Gold. *J. Am. Chem. Soc.* **2005**, *127*, 7328–7329.

(11) van Embden, J.; Chesman, A. S. R.; Jasieniak, J. J. The Heat-Up Synthesis of Colloidal Nanocrystals. *Chem. Mater.* **2015**, *27*, 2246–2285.

(12) Hogarth, G. Metal-Dithiocarbamate Complexes: Chemistry and Biological Activity. *Mini Rev. Med. Chem.* **2012**, *12*, 1202–1215.

(13) Frederick, M. T.; Weiss, E. A. Relaxation of Exciton Confinement in CdSe Quantum Dots by Modification with a Conjugated Dithiocarbamate Ligand. *ACS Nano* **2010**, *4*, 3195–3200.

(14) Frederick, M. T.; Amin, V. A.; Cass, L. C.; Weiss, E. A. A Molecule to Detect and Perturb the Confinement of Charge Carriers in Quantum Dots. *Nano Lett.* **2011**, *11*, 5455–5460.

(15) Frederick, M. T.; Amin, V. A.; Swenson, N. K.; Ho, A. Y.; Weiss, E. A. Control of Exciton Confinement in Quantum Dot−Organic Complexes through Energetic Alignment of Interfacial Orbitals. *Nano Lett.* **2013**, *13*, 287–292.

(16) Jin, S.; Tagliazucchi, M.; Son, H.-J.; Harris, R. D.; Aruda, K. O.; Weinberg, D. J.; Nepomnyashchii, A. B.; Farha, O. K.; Hupp, J. T.; Weiss, E. A. Enhancement of the Yield of Photoinduced Charge Separation in Zinc Porphyrin–Quantum Dot Complexes by a Bis(dithiocarbamate) Linkage. *J. Phys. Chem. C* **2015**, *119*, 5195–5202.

(17) Lian, S.; Weinberg, D. J.; Harris, R. D.; Kodaimati, M. S.; Weiss, E. A. Subpicosecond Photoinduced Hole Transfer from a CdS Quantum Dot to a Molecular Acceptor Bound Through an Exciton-Delocalizing Ligand. *ACS Nano* **2016**, *10*, 6372–6382.

(18) La Croix, A. D.; O'Hara, A.; Reid, K. R.; Orfield, N. J.; Pantelides, S. T.; Rosenthal, S. J.; Macdonald, J. E. Design of a Hole Trapping Ligand. *Nano Lett.*

2017, *17*, 909–914.

(19) Xie, Y.; Teunis, M. B.; Pandit, B.; Sardar, R.; Liu, J. Molecule-like CdSe Nanoclusters Passivated with Strongly Interacting Ligands: Energy Level Alignment and Photoinduced Ultrafast Charge Transfer Processes. *J. Phys. Chem. C* **2015**, *119*, 2813–2821.

(20) Kambhampati, P. Unraveling the Structure and Dynamics of Excitons in Semiconductor Quantum Dots. *Acc. Chem. Res.* **2011**, *44*, 1–13.

(21) Azzaro, M. S.; Babin, M. C.; Stauffer, S. K.; Henkelman, G.; Roberts, S. T. Can Exciton-Delocalizing Ligands Facilitate Hot Hole Transfer from Semiconductor Nanocrystals? *J. Phys. Chem. C* **2016**, *120*, 28224–28234.

(22) Yu, W. W.; Qu, L.; Guo, W.; Peng, X. Experimental Determination of the Extinction Coefficient of CdTe , CdSe , and CdS Nanocrystals. *Chem. Mater.* **2003**, *15*, 2854–2860.

(23) Takagahara, T. Biexciton States in Semiconductor Quantum Dots and Their Nonlinear Optical Properties. *Phys. Rev. B* **1989**, *39*, 10206–10231.

(24) Achermann, M.; Hollingsworth, J. A.; Klimov, V. I. Multiexcitons Confined within a Sub-Excitonic Volume: Spectroscopic and Dynamical Signatures of Neutral and Charged Biexcitons in Ultrasmall Semiconductor Nanocrystals. *Phys. Rev. B* **2003**, *68*, 245302.

(25) Schnitzenbaumer, K. J.; Labrador, T.; Dukovic, G. Impact of Chalcogenide Ligands on Excited State Dynamics in CdSe Quantum Dots. *J. Phys. Chem. C* **2015**, *119*, 13314–13324.

(26) Harris, R. D.; Amin, V. A.; Lau, B.; Weiss, E. A. Role of Interligand Coupling in Determining the Interfacial Electronic Structure of Colloidal CdS Quantum Dots. *ACS Nano* **2016**, *10*, 1395–1403.

(27) Baker, D. R.; Kamat, P. V. Tuning the Emission of CdSe Quantum Dots by Controlled Trap Enhancement. *Langmuir* **2010**, *26*, 11272–11276.

(28) Peterson, M. D.; Cass, L. C.; Harris, R. D.; Edme, K.; Sung, K.; Weiss, E. A. The Role of Ligands in Determining the Exciton Relaxation Dynamics in

Semiconductor Quantum Dots. *Annu. Rev. Phys. Chem.* **2014**, *65*, 317–339.

(29) Jin, S.; Harris, R. D.; Lau, B.; Aruda, K. O.; Amin, V. A.; Weiss, E. A. Enhanced Rate of Radiative Decay in CdSe Quantum Dots upon Adsorption of an Exciton-Delocalizing Ligand. *Nano Lett.* **2014**, 0–5.

(30) Azpiroz, J. M.; De Angelis, F. Ligand Induced Spectral Changes in CdSe Quantum Dots. *ACS Appl. Mater. Interfaces* **2015**, *7*, 19736–19745.

(31) Swenson, N. K.; Ratner, M. A.; Weiss, E. A. Computational Study of the Influence of the Binding Geometries of Organic Ligands on the Photoluminescence Quantum Yield of CdSe Clusters. *J. Phys. Chem. C* **2016**, *120*, 6859–6868.

(32) Dubois, F.; Mahler, B.; Dubertret, B.; Doris, E.; Mioskowski, C. A Versatile Strategy for Quantum Dots Ligand Exchange. **2005**, 183–184.

(33) Xie, Y.; Teunis, M. B.; Pandit, B.; Sardar, R.; Liu, J. Molecule-like CdSe Nanoclusters Passivated with Strongly Interacting Ligands: Energy Level Alignment and Photoinduced Ultrafast Charge Transfer Processes. *J. Phys. Chem. C* **2015**, *119*, 2813–2821.

(34) Huang, J.; Huang, Z.; Jin, S.; Lian, T. Exciton Dissociation in CdSe Quantum Dots by Hole Transfer to Phenothiazine. *J. Phys. Chem. C* **2008**, *112*, 19734–19738.

(35) Abdellah, M.; Karki, K. J.; Lenngren, N.; Zheng, K.; Pascher, T.; Yartsev, A.; Pullerits, T. Ultra Long-Lived Radiative Trap States in CdSe Quantum Dots. *J. Phys. Chem. C* **2014**, *118*, 21682–21686.

(36) Klimov, V. I. Spectral and Dynamical Properties of Multiexcitons in Semiconductor Nanocrystals. *Annu. Rev. Phys. Chem.* **2007**, *58*, 635–673.

(37) Klimov, V. I.; McBranch, D. W.; Leatherdale, C. A.; Bawendi, M. G. Electron and Hole Relaxation Pathways in Semiconductor Quantum Dots. *Phys. Rev. B* **1999**, *60*, 13740–13749.

(38) Norris, D. J.; Bawendi, M. G. Measurement and Assignment of the Size-Dependent Optical Spectrum in CdSe Quantum Dots. *Phys. Rev. B* **1996**, *53*,

16338–16346.

(39) Swenson, N. K.; Ratner, M. A.; Weiss, E. A. Computational Study of the Enhancement of Raman Signals of Ligands Adsorbed to CdSe Clusters through Photoexcitation of the Cluster. *J. Phys. Chem. C* **2016**, *120*, 20954–20960.

(40) Singhal, P.; Ghosh, H. N. Hot-Hole Extraction from Quantum Dot to Molecular Adsorbate. *Chem. - A Eur. J.* **2015**, *21*, 4405–4412.

(41) Singhal, P.; Ghorpade, P. V.; Shankarling, G. S.; Singal, N.; Jha, S. K.; Tripathi, R. M.; Ghosh, H. N. Exciton Delocalization and Hot Hole Extraction in CdSe QDs and CdSe/ZnS Type 1 Core Shell QDs Sensitized with Newly Synthesized Thiols. *Nanoscale* **2016**, *8*, 1823–1833.

(42) Zheng, K.; Žídek, K.; Abdellah, M.; Zhang, W.; Chábera, P.; Lenngren, N.; Yartsev, A.; Pullerits, T. Ultrafast Charge Transfer from CdSe Quantum Dots to p-Type NiO: Hole Injection vs Hole Trapping. *J. Phys. Chem.* **2014**, *118*, 18462–18471.

(43) Zotti, G.; Vercelli, B.; Berlin, A.; Virgili, T. Multilayers of CdSe Nanocrystals and Bis(dithiocarbamate) Linkers Displaying Record Photoconduction. *J. Phys. Chem. C* **2012**, *116*, 25689–25693.

(44) Mauser, C.; Da Como, E.; Baldauf, J.; Rogach, A. L.; Huang, J.; Talapin, D. V.; Feldmann, J. Spatio-Temporal Dynamics of Coupled Electrons and Holes in Nanosize CdSe-CdS Semiconductor Tetrapods. *Phys. Rev. B* **2010**, *82*, 81306.

(45) Grenland, J. J.; Lin, C.; Gong, K.; Kelley, D. F.; Kelley, A. M. Resonance Raman Investigation of the Interaction between Aromatic Dithiocarbamate Ligands and CdSe Quantum Dots. *J. Phys. Chem. C* **2017**, *121*, 7056–7061.

(46) Munro, A. M.; Chandler, C.; Garling, M.; Chai, D.; Popovich, V.; Lystrom, L.; Kilina, S. Phenyldithiocarbamate Ligands Decompose During Nanocrystal Ligand Exchange. **2016**.

(47) Maity, P.; Debnath, T.; Ghosh, H. N. Ultrafast Charge Carrier Delocalization in CdSe/CdS Quasi-Type II and CdS/CdSe Inverted Type I Core-Shell: A Structural Analysis through Carrier-Quenching Study. *J. Phys. Chem. C* **2015**, *119*, 26202–26211.

(48) Jia, Y.; Chen, J.; Wu, K.; Kaledin, A.; Musaev, D. G.; Xie, Z.; Lian, T. Enhancing Photo-Reduction Quantum Efficiency Using Quasi-Type II Core/shell Quantum. *Chem. Sci.* **2016**, *7*, 4125–4133.

(49) Frederick, M. T.; Amin, V. A.; Weiss, E. A. Optical Properties of Strongly Coupled Quantum Dot–Ligand Systems. *J. Phys. Chem. Lett.* **2013**, *4*, 634–640.

6. Conclusions and Future Work

This thesis attempted to incorporate semiconductor nanocrystals into a hybrid photocatalytic system with a molecular cobaloxime catalyst. Due to the poor stability of the chosen catalysts, a hybrid system was unfortunately not realised. The nanocrystals were however shown to be effective for harvesting light to drive hydrogen evolution. Judicious selection of a more robust coordination complex as the molecular catalyst, for example with a multi-dentate ligand, would probably allow a hybrid system to be assembled. The observation that surface ligands can dictate the activity of a colloidal QD-based photocatalysts was perhaps the most valuable insight to come out of the experiments targeting hybrid systems.

The most significant result from this work was the demonstration of hole scavenging promoted by the hydrophilic dithiocarbamate ligand, AmBz-DTC. Surface ligands need not be a passive component of a colloidal QD-based system. This work has shown that ligands can potentially play an active role in charge transfer at the QD/solution interface to enhance the activity of the system.

Building on the results presented in this chapter, there are several avenues of investigation to pursue. Extending the use of the AmBz-DTC ligand to a nanocrystal-based photocatalytic system to produce hydrogen is a logical next step. A metal co-catalyst would be the most straightforward, however to isolate the influence of the ligand on the system, the metal should be deposited on nanocrystals before ligand exchange with the dithiocarbamate. Typical photodeposition routes in water would be strongly influenced by the choice of stabilising ligand and would muddle experimental observations. Chemical reduction of a metal to form clusters on nanocrystals would be ideal, allowing the same nominal catalyst to be present before ligand exchange to isolate the effect of the ligands.

Another interesting application of AmBz-DTC would be the preparation of p-type photocathodes, either for QD-sensitised solar cells or for photoelectrochemical hydrogen production. Using AmBz-DTC as a linker to anchor QDs to a nanoporous NiO could potentially promote hole injection to the oxide; a co-catalyst on the QDs could subsequently evolve hydrogen, or the photo-generated electrons could reduce the redox couple in a solar cell.

Finally, measurement of the Raman spectrum of the intact dithiocarbamate on the QD surface would help to clarify the debate in the literature surrounding the origin of the induced red shift. We have collected preliminary spectra by adsorbing CdSe QDs bearing AmBz-DTC ligands to the surface of silica-coated gold nanoparticles to plasmonically enhance the ligand signal. Work is ongoing to assign these signals.

7. APPENDIX

THE JOURNAL OF PHYSICAL CHEMISTRY C

Article

pubs.acs.org/JPCC

Hydrophilic, Hole-Delocalizing Ligand Shell to Promote Charge Transfer from Colloidal CdSe Quantum Dots in Water

Jonathan R. Lee,[†,‡] Wei Li,[†,‡,∥] Alexander J. Cowan,[‡,§] and Frank Jäckel*[,†,‡]

[†]Department of Physics, University of Liverpool, Oxford Street, Liverpool L69 7ZE, United Kingdom

[‡]Stephenson Institute for Renewable Energy, University of Liverpool, Peach Street, Liverpool L69 7ZF, United Kingdom

[§]Department of Chemistry, University of Liverpool, Crown Street, Liverpool L69 7ZD, United Kingdom

Supporting Information

ABSTRACT: Colloidal cadmium chalcogenide nanocrystals are usually stabilized in polar solvents by functionalizing the surface with a layer of hydrophilic ligands. While these ligands protect against aggregation, they also present a steric barrier that hinders surface access. In applications that require charge transfer to and from nanocrystals, colloidal stability and surface access for redox species are therefore difficult to reconcile. This work assesses the possibility of a more dynamic ligand shell that not only provides stability to nanocrystals but also promotes charge transfer without the need for ligand removal. We use transient absorption spectroscopy to study CdSe quantum dots functionalized with hydrophilic, hole-delocalizing dithiocarbamate ligands in water for the first time, and find that a conjugated ligand facilitates charge transfer to redox species in solution.

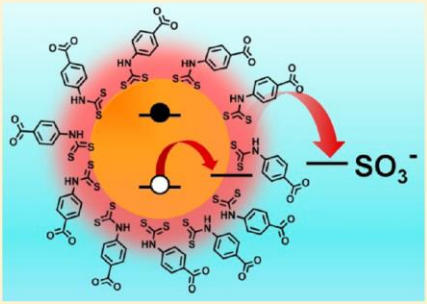

INTRODUCTION

Energy conversion technologies incorporating semiconductor nanocrystals depend critically on the ability to separate and extract both the electrons and holes that are generated upon photoexcitation. Quantum dot (QD)-sensitized solar cells are limited by the rate at which redox mediators in the electrolyte remove holes from the QDs after electron injection into the oxide scaffold.[1,2] Similarly, in photocatalytic systems, the rate of hole removal from nanocrystals by scavengers dictates the rate of product formation, quantum efficiency.[3−5] An additional concern is that accumulation of holes in nanocrystals eventually results in oxidative degradation, either by ligand removal followed by particle aggregation or by oxidation of the material itself.[3,6]

Increasingly, researchers have begun to focus on the fundamental mechanisms of hole transfer to improve the performance of nanocrystal-based energy systems. Cadmium chalcogenide nanocrystals have been widely investigated and are therefore frequently employed as model light absorbers to which hole acceptors can be covalently bound to control proximity. Tethered ferrocene derivatives attached to CdSe/CdS core/shell nanocrystals by thiol anchoring groups have been used by the Alivisatos group to establish hole transfer rates based on driving force.[7−9] Thiophenols bound to cadmium chalcogenides have been reported to delocalize holes, enhancing QD photostability and extending the lifetime of excited charge carriers.[10−13] The Weiss group has published numerous in-depth studies describing hole delocalization into the ligand shell of QDs, and identified the dithiocarbamate (DTC) functional group as having a particular ability to hybridize extensively with valence band orbitals of cadmium and lead chalcogenides.[14−16] Recently, these authors reported enhanced charge transfer to and from molecular acceptors bound to nanocrystal surfaces via dithiocarbamate linkages.[17,18] Dithiocarbamate functionalization has also been reported to improve photostability of QDs on TiO_2 and to increase the photoconductivity of QD films.[19,20]

Aqueous photocatalytic systems composed of colloidal nanocrystals present a particular challenge in terms of hole removal. Differences in the passivation of surface traps by various hydrophilic ligands have been shown to significantly influence the quantum efficiency of hydrogen evolution by a CdS/Au photocatalyst.[21] Surface ligands that stabilize individual particles against aggregation and impart solubility also create a barrier that hinders the approach of redox species to the surface. Recent work by our group demonstrated that hydrogen evolution by a CdS/Pt photocatalyst is not observed until the ligand shell is partially compromised through photooxidation, and that the duration of hydrogen evolution can subsequently be extended by replacing these ligands in situ with a loosely bound stabilizer that allows hole scavengers to access the nanocrystal surface.[6] Alternatively, postsynthetic ligand stripping has been shown to enhance activity in nanocrystal-based photocatalysts, but leads to significant particle aggregation in water.[22] A ligand that could promote charge transfer across the nanocrystal/solution interface while bound

Received: March 28, 2017
Revised: May 20, 2017
Published: June 21, 2017

DOI: 10.1021/acs.jpcc.7b02949
J. Phys. Chem. C 2017, 121, 15160−15168

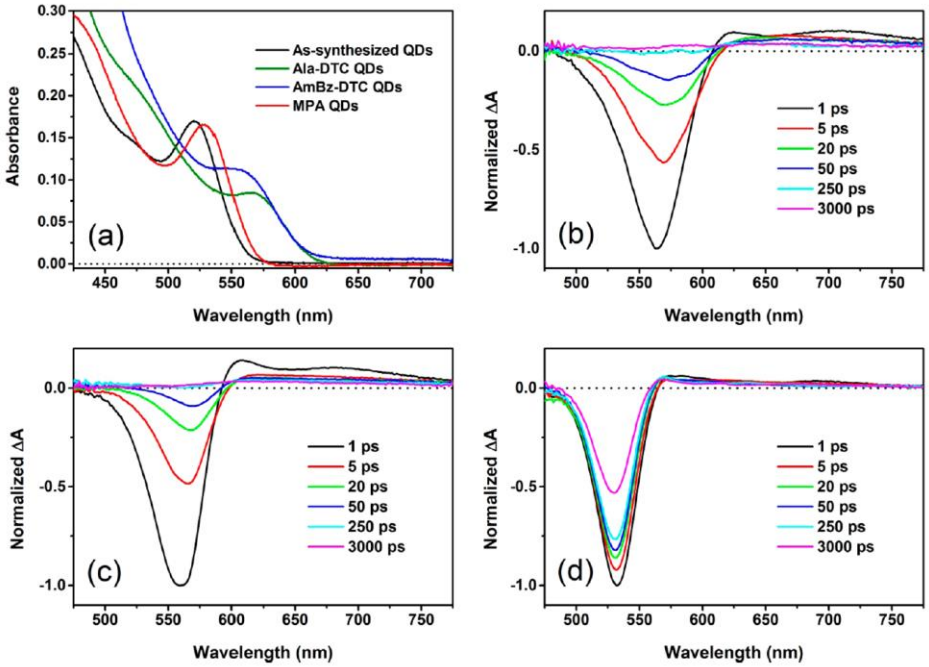

Figure 1. (a) Extinction spectra of as-synthesized QDs in chloroform, and of Ala-DTC, AmBz-DTC, and MPA QDs in water. Transient absorption spectra of (b) Ala-DTC QDs, (c) AmBz-DTC QDs, and (d) MPA QDs at selected time delays, normalized to the maximum intensity of the bleach signal 1 ps after excitation. Horizontal dotted lines represent ΔA equal to zero.

to the nanocrystal surface, rather than simply providing colloidal stability, would therefore be of interest.

In this work, we present the first transient absorption study of colloidal nanocrystals functionalized with dithiocarbamate ligands in water. We used dithiocarbamates derived from β-alanine (Ala-DTC) and 4-aminobenzoic acid (AmBz-DTC) to investigate the impact of alkyl and aryl DTC ligands on the picosecond charge carrier dynamics of CdSe QDs, and found that band edge electron relaxation occurs up to 2 orders of magnitude faster than in a typical hydrophilic thiol-coated sample. We further examined these materials in the presence of a commonly used hole scavenger, sodium sulfite, to assess whether DTCs could promote hole scavenging from QDs, regarded as a rate-limiting step in nanocrystal-based photocatalysis.[3,4] Distinct changes in the bleach recovery kinetics of QDs bearing the aryl-dithiocarbamate ligand Ambz-DTC were observed in the presence of sulfite, consistent with hole scavenging from QDs and a concomitant stabilization of electrons in the conduction band edge state. These results raise the possibility of employing multifunctional ligands in photocatalytic systems that impart colloidal stability and facilitate charge transfer. Where previous reports of related materials have been confined to organic solvents, this work represents a progression toward utilization in aqueous conditions relevant to photocatalysis.

EXPERIMENTAL SECTION

Materials. Cadmium oxide (CdO, PURATRONIC, 99.998%), oleic acid (OA, technical grade, 90%), and trioctylphosphine (TOP, technical grade, 90%) were purchased from Alfa Aesar. 1-Octadecene (ODE, technical grade, 90%), selenium powder (~100 mesh, ≥99.5%), β-alanine (99%), 4-aminobenzoic acid (≥99%), 3-mercaptopropionic acid (MPA, ≥ 99%), and carbon disulfide (CS_2, ≥ 99.9%) were purchased from Sigma-Aldrich. Sodium sulfite (anhydrous powder), hydrochloric acid, methanol, ethanol, hexane, and chloroform were purchased from Fisher. Tetramethylammonium hydroxide pentahydrate (TMAH, 99%) was purchased from Acros Organics. All reagents were used as received. Milli-Q water was produced by using an Elga PURELAB Flex purification system.

Synthesis of Quantum Dots. CdSe QDs were synthesized according to the method of Yu and Peng.[23] Here, 57.6 mg of CdO, 0.427 mL of OA, and 22 mL of ODE were combined and vacuum degassed for 30 min at 80 °C, heated to 300 °C under N_2, and then cooled to 250 °C. To form a stock solution, 64 mg of Se powder, 400 μL of TOP, and 20 mL of ODE were heated under N_2 until all selenium had been dissolved. Next, 6 mL of Se stock solution and 6 mL of ODE were vacuum degassed for 30 min at room temperature, and then injected into the hot Cd precursor solution. After several minutes, the reaction was removed from heat and allowed to cool to room temperature.

To purify the crude QD product solution, portions were mixed with an equal volume of hexane and then flocculated by addition of ethanol and centrifuged. The colorless supernatant was discarded, and the orange CdSe pellet was redispersed in hexane. This cycle was repeated three times before collecting the purified QDs as a concentrated stock solution (10^{-4} M) in chloroform.

Ligand Exchange. To prepare dithiocarbamate ligand solutions, 360 mg of TMAH was dissolved in 1.5 mL of

DOI: 10.1021/acs.jpcc.7b02949
J. Phys. Chem. C 2017, 121, 15160−15168

MeOH, followed by 1 mmol of either β-alanine or 4-aminobenzoic acid. Then 80 μL of CS_2 was added dropwise to the amine solution with rapid stirring. Solutions turned yellow, indicating formation of dithiocarbamate. MPA ligand solutions were prepared by adding 1 mmol of the thiol to a solution of 180 mg of TMAH in 1.5 mL of MeOH. Ligand exchanges were performed by dropwise addition of several hundred microliters of CdSe QD stock in chloroform to the desired ligand solution with rapid stirring at ∼0 °C. After equilibration for 3−4 h, the QD solution was diluted with Milli-Q water and shaken with several milliliters of chloroform. The aqueous phase was transferred to a Sartorius Vivaspin centrifuge tube and concentrated to several hundred microliters to remove excess ligand and amine precursor impurities from dithiocarbamate formation, and then diluted to 2 mL volume with Milli-Q water. Stock solutions of QDs in water were adjusted to pH 9 using TMAH and HCl, as necessary, measured using a HI 83141 pH probe (Hanna).

As reported elsewhere,[14,24] we also observed additional red shifting of the excitonic peak of DTC QDs after ligand exchange. This process was complete after the third day in our experience, so we allowed samples to equilibrate for ∼72 h before performing transient measurements.

Optical Measurements. Extinction spectra were collected on a Shimadzu UV-2600 spectrophotometer in 10 mm path length quartz cuvettes. Photoluminescence was measured with a PerkinElmer LS 55 fluorescence spectrometer with 450 nm excitation.

Transient Absorption Spectroscopy. Femtosecond laser pulses were produced by a PHAROS laser head (Light Conversion, Ltd.) using Yb:KGW as the active medium, operated at a repetition rate of 10 kHz. An ORPHEUS optical parametric amplifier (Light Conversion, Ltd.) in tandem with a LYRA harmonic generator (Light Conversion, Ltd.) produced the desired wavelength for sample excitation. Pump beam intensity was adjusted with a neutral density filter to achieve pulse energies of ∼10 nJ/pulse. A portion of the PHAROS output was also used to pump a sapphire crystal to generate a white light continuum for the probe beam, which provided for spectral observation in the region 475−900 nm. The probe beam was focused on the sample to a spot size of ∼100 μm diameter and was overlapped completely by the pump beam. Spectra were acquired with a HELIOS transient absorption spectrometer (Ultrafast Systems, LLC) with a response time of ∼400 fs (∼1.5× the laser pulse length). Data sets were collected by randomly stepping the optical delay line and averaging for 1 s at each delay time. Samples were diluted to an absorbance of 0.6 and measured in a 2 mm path length quartz cuvette fitted with a rubber septum and purged with Ar. Transient spectra were chirp-corrected using the commercial Surface Xplorer (Ultrafast Systems, LLC) software package.

■ RESULTS AND DISCUSSION

Extinction spectra of the CdSe QDs used in this work are presented in Figure 1a. The excitonic peak at 520 nm for the as-synthesized QDs in chloroform corresponds to an average particle radius of ∼1.3 nm.[25] Strong spatial confinement of charge carriers in CdSe QDs is regarded to occur in particles of radii less than ∼1.9 nm.[26,27] In this regime, the kinetic energy of the hole exceeds the Coulomb potential of the electron−hole pair. Using QDs with dimensions well within this range therefore maximizes the degree of hole delocalization upon ligand exchange with DTCs.[15]

The spectra of QDs functionalized with Ala-DTC or AmBz-DTC in Figure 1a exhibit a significant red shift (>150 meV, 35−45 nm) of the excitonic peak; in contrast, MPA induces a more modest shift of ∼30 meV (∼8 nm). The ligand-induced shift observed in the DTC QDs would correspond to a physical increase in the actual radius of the nanocrystals of ∼0.7 nm,[25] which is relatively large compared to the shifts reported for PTC adsorption on CdSe QDs in organic solvents. Recent calculations have shown that the magnitude of the red shift of the excitonic peak in cadmium chalcogenide QDs as a result of DTC adsorption increases nonlinearly with increasing surface coverage due to electronic coupling between adjacent ligands.[28] The CdSe QDs studied herein were transferred to aqueous solution by a ligand exchange procedure that exposes the particles to a 1000-fold molar excess of dithiocarbamate (or thiol) ligands, so the surface coverage of ligands is expected to be densely functionalized with a high degree of adjacency. The magnitude of the red shift observed here for the DTC QDs is consistent with the predictions of Harris et al. for nearly complete surface coverages,[28] although some native ligands likely persist. Ala-DTC QDs exhibit a slightly larger red-shift of the excitonic peak compared to AmBz-DTC QDs, which we attribute to a higher surface density of the less bulky Ala-DTC ligands which permits increased interligand coupling.

We also measured the photoluminescence of the QDs before and after ligand exchange (Figure S1). As-synthesized QDs in chloroform exhibited band edge emission, however this was quenched after ligand exchange in each QD material. In MPA QDs, the band edge emission was reduced to ∼4% of its pre-exchange intensity, while emission at longer wavelengths related to newly formed trap states appeared to increase slightly, in line with previous observations of MPA-coated CdSe QDs.[29] The photoluminescence of QDs was completely quenched after functionalization with DTC ligands, as reported by other authors.[24,30] Emission quenching is consistent with hole transfer from the nanocrystal core to surface ligands, which has been shown to occur for other hole-accepting ligands adsorbed to CdSe QDs.[31,32] In the case of dithiocarbamates, emission quenching is thought to be related to ligands bound in a monodentate geometry whose lone pairs can efficiently trap holes.[24] The high surface coverage of DTC ligands in the materials studied here likely contributes to the complete quenching of photoluminescence observed.

Transient absorption spectra of CdSe QDs functionalized with Ala-DTC, AmBz-DTC, and MPA are presented in Figure 1b−d, respectively. Given the spectral shifts that occur upon DTC functionalization, we chose to excite all samples at an energy removed from the region where these changes occur. Samples were therefore pumped with 450 nm laser pulses, exciting the 1P(h)−1P(e) transition.[33,34] Sub-picosecond electron cooling from the hot 1P(e) state to the 1S(e) band edge state subsequently occurs, with parallel processes occurring for holes in the valence band.[24,35] Recent work has shown that adsorbed phenyldithiocarbamate does not affect the electron cooling rate in CdSe QDs, although it does impact hole cooling.[24] The prominent negative signals in the spectra correspond to bleaching of the QD ground state by population of the 1S(e) band edge state, and are conventionally referred to as "B1", with the decay of this signal tracking the rate at which electrons depopulate the conduction band.[34,36]

The picosecond charge carrier dynamics of MPA-functionalized QDs have been reported previously by numerous authors.[29,35,37] 3-Mercaptopropionic acid (MPA) is perhaps

DOI: 10.1021/acs.jpcc.7b02949
J. Phys. Chem. C 2017, 121, 15160−15168

the most widely used hydrophilic thiol for stabilizing colloidal cadmium chalcogenide nanocrystals in water, as well as for immobilizing QDs on oxide surfaces, so we have included MPA QDs in our study as a benchmark against which DTC-functionalized QDs from the same synthetic batch can be directly compared. In Figure 1d, the ground state bleach signal decays on the nanosecond time scale, indicating a relatively gradual relaxation of electrons from the conduction band. Adsorption of MPA has been shown to create surface traps for both electrons and holes in CdSe QDs,[29,37,38] and recombination of 1S(e) electrons with holes trapped at the surface becomes the dominant relaxation pathway in MPA-functionalized QDs leading to the recovery of the ground state bleach.[35] In contrast, functionalization of CdSe QDs with DTC ligands results in the dramatic acceleration of the ground state bleach recovery apparent in Figure 1b and c. Such rapid decay of the bleach signal in DTC QDs implies that an efficient relaxation pathway for electrons occupying the 1S(e) state is introduced, such as electron trapping or facilitated electron−hole recombination, associated with the states formed at the QD-ligand interface. Comparing the evolution of the transient spectra in Figure 1, it is clear that dithiocarbamate ligands affect the charge carrier dynamics of CdSe QDs to a much greater extent than MPA.

Positive signals also appear in the transient spectra of all QD samples, consisting of a relatively well-defined peak on the low-energy edge of the bleach and a broader feature that extends into the near-IR; the former is conventionally referred to as "A1" and is associated with biexciton interactions in strongly confined CdSe QDs,[34] while the latter photoinduced absorption is labeled "PA" and attributed to lattice- and surface-trapped holes in CdSe QDs.[35,39] We note that these signals overlap in the spectra but can be distinguished according to their shapes. The A1 feature is present in the spectra of MPA QDs, but is not observed in the spectra of DTC QDs after the initial excitation (~1 ps) (Figure S2), which could be due to the reduced wave function overlap afforded by hole delocalization into the ligand shell. The broader PA signal relating to trapped holes appears in the spectra of all QD samples. In the case of DTC QDs, the total recovery of the ground state bleach within several hundred picoseconds means that the PA signal is fully resolved on the nanosecond time scale.

Hole trapping in CdSe QDs, monitored by the rise time of the PA signal, typically occurs within hundreds of femtoseconds.[24,33,35] Taking the magnitude of this signal at a given time to reflect the population of trapped holes, we compared the kinetics of the PA signal in the different QD materials. Due to the low intensity of the feature, we averaged values across 10 nm regions of the spectrum at each time delay to improve the signal-to-noise ratio of the data. Figure 2 shows the kinetics of the PA signal during the first 50 ps of the transient absorption measurements. In DTC-QDs, the signal related to trapped holes reaches its maximum within <1 ps followed by a rapid decay in the first 10 ps after excitation. Due to the time resolution of our instrument, we cannot investigate subpicosecond time delays; however, it is likely that the PA signal reaches even higher values in the first several hundred femtoseconds. This picosecond decay process is most pronounced for AmBz-DTC QDs, and is not observed in MPA QDs, which instead have a relatively stable PA signal.

Given that the intensity of the ground state bleach (B1) is related to the population of 1S(e) electrons and the PA signal

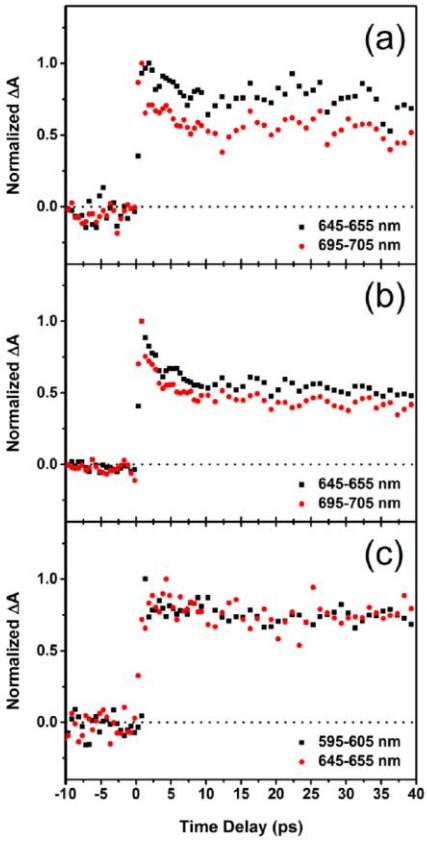

Figure 2. Kinetics of the photoinduced absorption (PA) signal in (a) Ala-DTC, (b) AmBz-DTC, and (c) MPA QDs at early time delays. Values were averaged across the spectral ranges indicated and normalized to the initial signal maximum. Horizontal dotted lines represent ΔA equal to zero.

corresponds to trapped holes, the ratio of their magnitudes at a given time delay represents a measure of the relative population of these states.[24] In Table 1, we evaluated PA_0 and $B1_0$ as the maximum magnitude of the signals within 5 ps of initial excitation. While the proportion of initially trapped holes appears significantly higher in DTC QDs than in MPA QDs, the fast decay component in the PA signal of DTC QDs implies that holes in a subset of traps in DTC QDs can either readily detrap or recombine with electrons via a pathway introduced upon DTC functionalization. After several hundred picoseconds, the PA signal is relatively stable in both DTC and MPA QD materials, indicating that some holes remain trapped over longer time scales.[40]

In MPA QDs, the kinetics of the PA signal closely track those of the ground state bleach signal for the duration of the transient measurement (Figure S3), in line with the hypothesis that recombination of 1S(e) electrons with trapped holes is the dominant relaxation process.[35] For DTC QDs, however, this correspondence is observed only in the first 10 ps after excitation, during the period of fast signal decay. Beyond this point, the magnitude of the ground state bleach continues to decrease to zero, unlike the PA signal. As such, the picosecond

DOI: 10.1021/acs.jpcc.7b02949
J. Phys. Chem. C 2017, 121, 15160−15168

Table 1. Quantification of Initial PA Signal Intensities[a]

	Ala-DTC		AmBz-DTC		MPA	
λ (nm)	650 ± 5	700 ± 5	650 ± 5	700 ± 5	600 ± 5	650 ± 5
$PA_0:B1_0$	0.082	0.101	0.094	0.096	0.050	0.035

[a]Ratios of the magnitudes of the photoinduced absorption (PA) versus the ground state bleach (B1) signals immediately after excitation ($PA_0:B1_0$). PA signal was averaged within the indicated wavelength range.

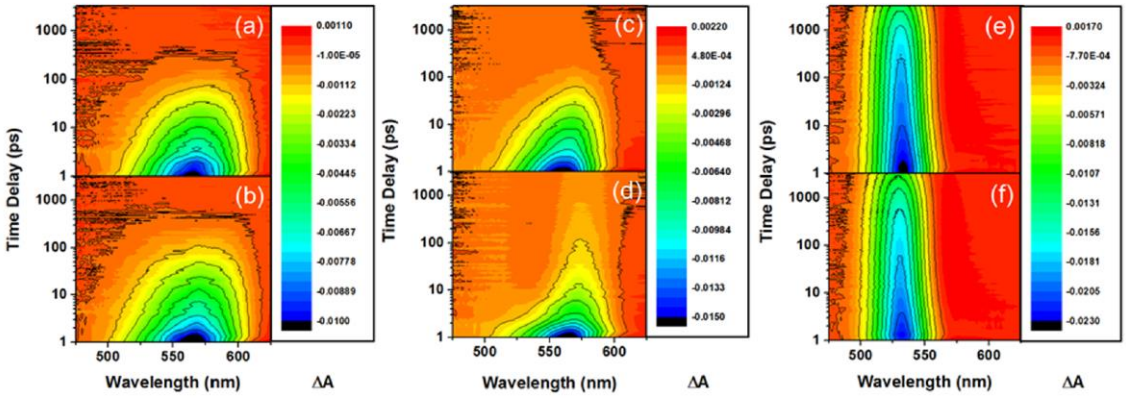

Figure 3. Contour plots detailing the bleach region in the transient absorption spectra of (a) Ala-DTC QDs, (c) AmBz-DTC QDs, and (e) MPA QDs. Spectra recorded in the presence of 0.1 M Na_2SO_3 are shown for each material in (b), (d), and (f), respectively.

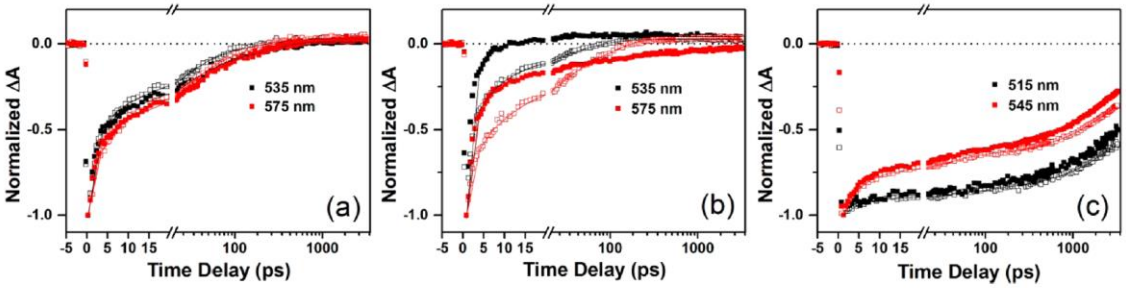

Figure 4. Kinetic plots showing the evolution of the ground state bleach in the absence (open squares) and in the presence (closed squares) of 0.1 M Na_2SO_3, monitored at the wavelengths indicated, for (a) Ala-DTC, (b) AmBz-DTC, and (c) MPA QDs. Note the logarithmic scale after 20 ps time delay. Horizontal dotted lines represent ΔA equal to zero. Solid lines illustrate the triexponential fits used to extract time constants, detailed in Table 2. Additional fitting parameters are detailed in the Supporting Information.

decay process appears to involve only a fraction of the total population of trapped holes, whereas all 1S(e) electrons are affected by DTC functionalization.

Considering the valence band of DTC QDs to be extended into the ligand shell,[14−16] we hypothesized that this delocalization might facilitate hole scavenging by a redox species in solution and slow depopulation of the 1S(e) state. To test this hypothesis, we collected spectra for all QD samples in the presence of 0.1 M sodium sulfite, a common hole scavenger used in semiconductor nanocrystal-based photocatalysis. Figure 3 presents transient absorption spectra of QD samples in the absence (top row) and presence (bottom row) of sulfite. As is evident from Figure 3c and d, sulfite only induced significant changes to the spectrum of AmBz-DTC QDs. Interestingly, rather than affecting the overall spectrum, the addition of sulfite resulted in asymmetric changes to the spectrum at different wavelengths, suggesting that the interaction of sulfite with the QD−ligand complex does not affect the material uniformly but occurs via discrete states.

Due to the quantization of energy levels in QDs, individual spectral features can be assigned to specific transitions between states in the valence and conduction bands.[33,34] In CdSe QDs of the dimensions studied here, the band edge $1S_{3/2}(h)-1S(e)$ transition and the higher energy $2S_{3/2}(h)-1S(e)$ transition are separated by 100−150 meV, and partly overlap to form the characteristic low energy peak in extinction spectra and the B1 bleach feature in transient spectra.[41] We therefore evaluated the kinetics of MPA QDs at 515 and 545 nm, and of DTC QDs at 535 and 575 nm, consistent with the theoretical energy spacing of the two lowest energy transitions, taking into account the greater separation on the wavelength scale in the red-shifted DTC QD spectra.[35,42]

Figure 4 plots the kinetics of the ground state bleach recovery for QDs in the absence and presence of a hole scavenger at wavelengths corresponding to the $1S_{3/2}(h)-1S(e)$

DOI: 10.1021/acs.jpcc.7b02949
J. Phys. Chem. C 2017, 121, 15160−15168

and $2S_{3/2}(h)-1S(e)$ transitions. These kinetics were fit to triexponentials to extract time constants to describe the decay processes, which are detailed in Table 2. Differences exist in the relative rates of $1S_{3/2}(h)-1S(e)$ and $2S_{3/2}(h)-1S(e)$ bleach recovery among the samples even in the absence of sulfite. In AlaDTC QDs, these two transitions recover at nearly identical rates, while in AmBzDTC QDs the $2S_{3/2}(h)-1S(e)$ transition recovers roughly twice as fast as the lower energy transition. The availability of vibrational modes in AmBzDTC associated with the aromatic ring, which are not available in AlaDTC, might contribute to faster relaxation of the $2S_{3/2}(h)-1S(e)$ transition.[43] It is also possible that some variation exists in the binding geometries adopted by the smaller AlaDTC and the larger, more rigid AmBzDTC in the crowded ligand shells, which has been shown to affect relaxation rates.[24,44,45] By comparison, MPA QD bleach recovery is at least 10 times slower than that in the DTC-functionalized materials, with the $1S_{3/2}(h)-1S(e)$ transition recovering marginally faster than $2S_{3/2}(h)-1S(e)$, reflecting different underlying QD−ligand interactions.

Figure 4b shows that sulfite accelerates the recovery of the bleached $2S_{3/2}(h)-1S(e)$ transition at 535 nm in AmBz-DTC QDs, by an order of magnitude overall as quantified by the τ_2 and τ_3 time constants. Indeed, it can be seen in the plot that the signal drops to zero after just ~10 ps in the presence of sulfite, compared to ~100 ps in the absence of the hole scavenger. Concurrently, after a similarly fast decay at early delay times, the recovery of the bleached band edge transition at 575 nm slows markedly, manifesting as a 4-fold increase in τ_3 time constant. This asymmetric effect of sulfite on the transient spectrum of AmBz-DTC QDs is notably absent for Ala-DTC and MPA QDs, where only modest changes in time constants are observed, on the order of the standard errors of the fits. Most significantly, the bleaching of the band edge transition at 575 nm now persists into the nanosecond time scale in the presence of sulfite, indicating a substantial increase in the lifetime of 1S(e) conduction band electrons in AmBz-DTC QDs. These kinetics are presented on a linear scale in Figure S5 to emphasize the extended 1S(e) lifetime.

Given that excitation of the $1S_{3/2}(h)-1S(e)$ and $2S_{3/2}(h)-1S(e)$ transitions populates the same conduction band state, any discrepancy in the recovery kinetics of the bleach signal at the wavelengths associated with these transitions implies a difference in the dynamics of their respective hole states. Such state-specificity involving the $2S_{3/2}(h)$ state in CdSe QDs has been observed following adsorption of phenyldithiocarbate[46] as well as hole-accepting catechols[31] and thiols,[32] and ascribed to hot hole transfer. Unfortunately, the lack of a clear spectroscopic signature for valence band holes in CdSe QDs means that we cannot directly probe these states; however, the fact that different recovery kinetics arise in AmBz-DTC QDs only in the presence of a hole scavenger, and that in this case it is the lifetime of the transient signal associated with conduction band electrons that is extended, offers strong indirect evidence that the conjugated, hole-delocalizing ligands can promote charge transfer between the nanocrystals and redox species in solution.

Ala-DTC QDs provide a useful point of comparison from which to explore possible mechanisms to explain the response of AmBz-DTC QDs to sulfite (Figure 5). Ala-DTC and AmBz-DTC both adsorb to CdSe QDs via the same functional group, resulting in similar red shifts of their excitonic peaks in extinction spectra and faster bleach recovery kinetics in general.

Table 2. Bleach Recovery Time Constants[a]

	Ala-DTC QDs				AmBz-DTC QDs				MPA QDs			
	535 nm		575 nm		535 nm		575 nm		515 nm		545 nm	
	without SO_3^-	with SO_3^-	without SO_3^-	with SO_3^-	without SO_3^-	with SO_3^-	without SO_3^-	with SO_3^-	without SO_3^-	with SO_3^-	without SO_3^-	with SO_3^-
τ_1 (ps)	1.9 ± 0.1	1.5 ± 0.1	2.4 ± 0.1	1.7 ± 0.1	1.0 ± 0.1	0.9 ± 0.1	1.4 ± 0.1	1.5 ± 0.1	3.3 ± 0.5	4.3 ± 1.2	3.5 ± 0.2	3.3 ± 0.2
τ_2 (ps)	22.4 ± 1.3	23.4 ± 1.4	25.7 ± 1.6	25.3 ± 1.2	7.7 ± 0.5	3.3 ± 4.2	12.9 ± 1.0	12.2 ± 0.9	65.5 ± 13.0	75.6 ± 25.1	31.1 ± 2.2	28.7 ± 1.7
τ_3 (ps)	180 ± 20	211 ± 18	184 ± 18	216 ± 14	45.6 ± 3.2	8.7 ± 4.5	78.3 ± 4.7	310 ± 30	3300 ± 400	3300 ± 600	2630 ± 130	2270 ± 80

[a]Time constants derived from triexponential fitting of the ground state bleach recovery kinetics of the QDs, in the absence and presence of 0.1 M Na_2SO_3.

DOI: 10.1021/acs.jpcc.7b02949
J. Phys. Chem. C 2017, 121, 15160−15168

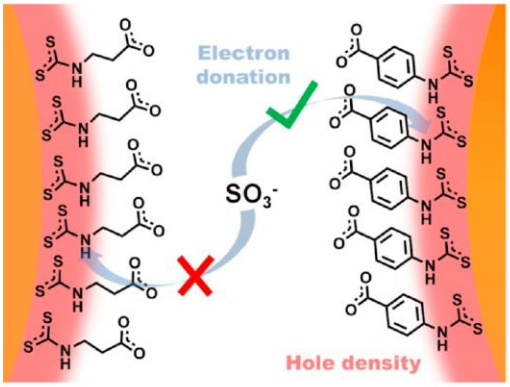

Figure 5. Schematic representation of QD-ligand-solution interfaces in Ala-DTC and AmBz-DTC QDs. Holes delocalized onto dithiocarbamate anchoring groups are isolated at the interface by the alkyl backbone of Ala-DTC, but are accessible to sulfite due to the aromatic bridge of AmBz-DTC.

Calculations by Azpiroz and De Angelis have shown that the orbitals into which hole density primarily delocalizes are on the dithiocarbamate group in such systems, not the aryl group, so it follows that qualitatively similar behavior should be observed for both ligands.[45] The aromatic ring in AmBz-DTC can however conjugate to the dithiocarbamate group; in contrast, an alkyl chain isolates the dithiocarbamate group in Ala-DTC at the QD interface, with MPA having an analogous structure. Jin and co-workers previously reported that a bifunctional conjugated dithiocarbamate linker facilitated electron transfer from a photoexcited porphyrin to CdSe QDs.[17] Work from the same group has also demonstrated hole transfer from a CdS QD to a molecular acceptor via a conjugated dithiocarbamate binding group.[18] Similarly, it is thought the conjugation of the AmBzDTC ligand facilitates electron transfer from sulfite to the dithiocarbamate group where holes are delocalized.

Based on the spectroscopic features discussed above, several processes appear to govern the charge carrier dynamics in DTC QDs in aqueous conditions, summarized in Figure 6. Upon

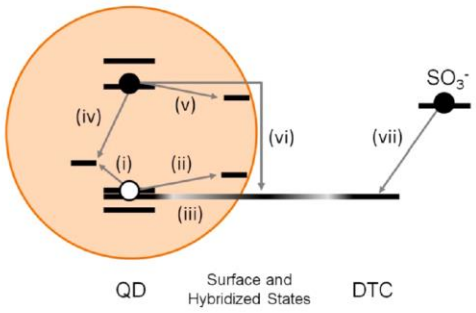

Figure 6. Summary of the proposed processes responsible for the observed charge carrier dynamics in DTC QDs. (i) Hole trapping to core states; (ii) hole trapping to surface states; (iii) hole delocalization into hybridized QD-DTC states; (iv) hole trap-mediated recombination, governs relaxation in MPA QDs; (v) electron trapping; (vi) electron−hole recombination via hybridized QD-DTC states; (vii) electron transfer (hole scavenging) by sulfite in solution.

excitation, an electron−hole pair is created in the CdSe QD core, with electrons populating 1S(e) conduction band states of predominantly QD character in the core.[45] This process results in the appearance of the ground state bleach signal, which recovers on the order of tens of picoseconds as electrons begin to depopulate the conduction band. Within 1 ps of excitation, some valence band holes are trapped at lattice or surface sites, giving rise to the PA signal, while others delocalize in hybridized QD-ligand states. Delocalization of holes beyond the volume of the QD core would induce electron migration to the surface of the QD as a result of Coulomb drag,[47] bringing electrons into closer proximity with surface trapped holes. Electrons could recombine with these trapped holes, leading to the observed picosecond decay in the PA signal of DTC QDs, or be trapped themselves in surface states arising from QD−DTC interactions.[24] Both of these processes would depopulate the 1S(e) state and contribute to recovery of the ground state bleach. Finally, in the presence of sulfite, the rate of depopulation of the conduction band can be slowed by a factor of 4, effectively increasing the lifetime of excited electrons in QDs functionalized with the conjugated dithiocarbamate ligand, AmBz-DTC.[48]

■ CONCLUSIONS

We have described for the first time the picosecond charge carrier dynamics of colloidal CdSe QDs stabilized in water by hydrophilic dithiocarbamate ligands. Using transient absorption spectroscopy, we observed the recovery kinetics of the QD ground state bleach to be vastly accelerated compared to those of thiol-functionalized QDs. Further, we demonstrate that in the presence of a hole scavenger in solution, the lifetime of electrons in the band edge excited state is extended, suggesting that holes have been transferred without hindrance by the layer of stabilizing ligands. These findings have relevance in several fields that rely on charge transfer to and from semiconductor nanocrystals, such as quantum dot-sensitized solar cells and nanocrystal-based photocatalytic systems.

■ ASSOCIATED CONTENT

Supporting Information

The Supporting Information is available free of charge on the ACS Publications website at DOI: 10.1021/acs.jpcc.7b02949.

Photoluminescence of QDs before and after ligand exchange, detail of photoinduced absorption spectral regions, comparison of B1 and PA kinetics, PA kinetics in the presence of sulfite, and bleach kinetics of AmBz-DTC QDs plotted on a linear scale (PDF)

■ AUTHOR INFORMATION

Corresponding Author

*E-mail: fjaeckel@liverpool.ac.uk.

ORCID

Jonathan R. Lee: 0000-0002-5447-0732
Wei Li: 0000-0003-4036-467X
Alexander J. Cowan: 0000-0001-9032-3548

Present Address

[||]W.L.: Chemical Engineering & Applied Chemistry, European Bioenergy Research Institute and Aston Materials Centre, Aston University, Aston Triangle, Birmingham B4 7ET, U.K.

DOI: 10.1021/acs.jpcc.7b02949
J. Phys. Chem. C 2017, 121, 15160−15168

Author Contributions

The manuscript was written through contributions of all authors. All authors have given approval to the final version of the manuscript.

Notes

The authors declare no competing financial interest.

■ ACKNOWLEDGMENTS

Financial support by The University of Liverpool (F.J.) is gratefully acknowledged. J.R.L. thanks the School of Physical Sciences for support through a GTA studentship. The authors further acknowledge support from the EPSRC Laser Loan Pool (EP/G03088X/1). The underlying EPSRC-funded data in this paper is available from http://dx.doi.org/10.17638/datacat.liverpool.ac.uk/368.

■ REFERENCES

(1) Kamat, P. V.; Christians, J. A.; Radich, J. G. Quantum Dot Solar Cells: Hole Transfer as a Limiting Factor in Boosting the Photoconversion Efficiency. *Langmuir* **2014**, *30*, 5716−5725.
(2) Abdellah, M.; Marschan, R.; Zidek, K.; Messing, M. E.; Abdelwahab, A.; Chabera, P.; Zheng, K.; Pullerits, T. Hole Trapping: The Critical Factor for Quantum Dot Sensitized Solar Cell Performance. *J. Phys. Chem. C* **2014**, *118*, 25802−25808.
(3) Berr, M. J.; Wagner, P.; Fischbach, S.; Vaneski, A.; Schneider, J.; Susha, A. S.; Rogach, A. L.; Jäckel, F.; Feldmann, J. Hole Scavenger Redox Potentials Determine Quantum Efficiency and Stability of Pt-Decorated CdS Nanorods for Photocatalytic Hydrogen Generation. *Appl. Phys. Lett.* **2012**, *100*, 223903.
(4) Wu, K.; Chen, Z.; Lv, H.; Zhu, H.; Hill, C. L.; Lian, T. Hole Removal Rate Limits Photodriven H_2 Generation Efficiency in CdS-Pt and CdSe/CdS-Pt Semiconductor Nanorod-Metal Tip Heterostructures. *J. Am. Chem. Soc.* **2014**, *136*, 7708−7716.
(5) Simon, T.; Bouchonville, N.; Berr, M. J.; Vaneski, A.; Adrović, A.; Volbers, D.; Wyrwich, R.; Döblinger, M.; Susha, A. S.; Rogach, A. L.; et al. Redox Shuttle Mechanism Enhances Photocatalytic H_2 Generation on Ni-Decorated CdS Nanorods. *Nat. Mater.* **2014**, *13*, 1013−1018.
(6) Li, W.; Lee, J. R.; Jäckel, F. Simultaneous Optimization of Colloidal Stability and Interfacial Charge Transfer Efficiency in Photocatalytic Pt/CdS Nanocrystals. *ACS Appl. Mater. Interfaces* **2016**, *8*, 29434−29441.
(7) Tarafder, K.; Surendranath, Y.; Olshansky, J. H.; Alivisatos, A. P.; Wang, L. W. Hole Transfer Dynamics from a CdSe/CdS Quantum Rod to a Tethered Ferrocene Derivative. *J. Am. Chem. Soc.* **2014**, *136*, 5121−5131.
(8) Olshansky, J. H.; Ding, T. X.; Lee, Y. V.; Leone, S. R.; Alivisatos, A. P. Hole Transfer from Photoexcited Quantum Dots: The Relationship between Driving Force and Rate. *J. Am. Chem. Soc.* **2015**, *137*, 15567−15575.
(9) Ding, T. X.; Olshansky, J. H.; Leone, S. R.; Alivisatos, A. P. On the Efficiency of Hole Transfer from Photoexcited Quantum Dots to Covalently Linked Molecular Species On the Efficiency of Hole Transfer from Photoexcited Quantum Dots to Covalently Linked Molecular Species. *J. Am. Chem. Soc.* **2015**, *137*, 2021−2029.
(10) Liu, I. S.; Lo, H.-H.; Chien, C.-T.; Lin, Y.-Y.; Chen, C.-W.; Chen, Y.-F.; Su, W.-F.; Liou, S.-C. Enhancing Photoluminescence Quenching and Photoelectric Properties of CdSe Quantum Dots with Hole Accepting Ligands. *J. Mater. Chem.* **2008**, *18*, 675−682.
(11) Liang, Y.; Thorne, J. E.; Parkinson, B. A. Controlling the Electronic Coupling between CdSe Quantum Dots and Thiol Capping Ligands via pH and Ligand Selection. *Langmuir* **2012**, *28*, 11072−11077.
(12) Aruda, K. O.; Amin, V. A.; Thompson, C. M.; Lau, B.; Nepomnyashchii, A. B.; Weiss, E. A. Description of the Adsorption and Exciton Delocalizing Properties of p-Substituted Thiophenols on CdSe Quantum Dots. *Langmuir* **2016**, *32*, 3354−3364.
(13) Tan, Y.; Jin, S.; Hamers, R. J. Influence of Hole-Sequestering Ligands on the Photostability of CdSe Quantum Dots. *J. Phys. Chem. C* **2013**, *117*, 313−320.
(14) Frederick, M. T.; Weiss, E. A. Relaxation of Exciton Confinement in CdSe Quantum Dots by Modification with a Conjugated Dithiocarbamate Ligand. *ACS Nano* **2010**, *4*, 3195−3200.
(15) Frederick, M. T.; Amin, V. A.; Cass, L. C.; Weiss, E. A. A Molecule to Detect and Perturb the Confinement of Charge Carriers in Quantum Dots. *Nano Lett.* **2011**, *11*, 5455−5460.
(16) Frederick, M. T.; Amin, V. A.; Swenson, N. K.; Ho, A. Y.; Weiss, E. A. Control of Exciton Confinement in Quantum Dot−Organic Complexes through Energetic Alignment of Interfacial Orbitals. *Nano Lett.* **2013**, *13*, 287−292.
(17) Jin, S.; Tagliazucchi, M.; Son, H.-J.; Harris, R. D.; Aruda, K. O.; Weinberg, D. J.; Nepomnyashchii, A. B.; Farha, O. K.; Hupp, J. T.; Weiss, E. A. Enhancement of the Yield of Photoinduced Charge Separation in Zinc Porphyrin−Quantum Dot Complexes by a Bis(dithiocarbamate) Linkage. *J. Phys. Chem. C* **2015**, *119*, 5195−5202.
(18) Lian, S.; Weinberg, D. J.; Harris, R. D.; Kodaimati, M. S.; Weiss, E. A. Subpicosecond Photoinduced Hole Transfer from a CdS Quantum Dot to a Molecular Acceptor Bound Through an Exciton-Delocalizing Ligand. *ACS Nano* **2016**, *10*, 6372−6382.
(19) Tan, Y.; Jin, S.; Hamers, R. J. Photostability of CdSe Quantum Dots Functionalized with Aromatic Dithiocarbamate Ligands. *ACS Appl. Mater. Interfaces* **2013**, *5*, 12975−12983.
(20) Zotti, G.; Vercelli, B.; Berlin, A.; Virgili, T. Multilayers of CdSe Nanocrystals and Bis(dithiocarbamate) Linkers Displaying Record Photoconduction. *J. Phys. Chem. C* **2012**, *116*, 25689−25693.
(21) Ben-Shahar, Y.; Scotognella, F.; Waiskopf, N.; Kriegel, I.; Dal Conte, S.; Cerullo, G.; Banin, U. Effect of Surface Coating on the Photocatalytic Function of Hybrid CdS-Au Nanorods. *Small* **2015**, *11*, 462−471.
(22) Chang, C. M.; Orchard, K. L.; Martindale, B. C. M.; Reisner, E. Ligand Removal from CdS Quantum Dots for Enhanced Photocatalytic H_2 Generation in pH Neutral Water. *J. Mater. Chem. A* **2016**, *4*, 2856−2862.
(23) Yu, W. W.; Peng, X. Formation of High-Quality CdS and Other II-VI Semiconductor Nanocrystals in Noncoordinating Solvents: Tunable Reactivity of Monomers. *Angew. Chem., Int. Ed.* **2002**, *41*, 2368−2371.
(24) Azzaro, M. S.; Babin, M. C.; Stauffer, S. K.; Henkelman, G.; Roberts, S. T. Can Exciton-Delocalizing Ligands Facilitate Hot Hole Transfer from Semiconductor Nanocrystals? *J. Phys. Chem. C* **2016**, *120*, 28224−28234.
(25) Yu, W. W.; Qu, L.; Guo, W.; Peng, X. Experimental Determination of the Extinction Coefficient of CdTe, CdSe, and CdS Nanocrystals. *Chem. Mater.* **2003**, *15*, 2854−2860.
(26) Takagahara, T. Biexciton States in Semiconductor Quantum Dots and Their Nonlinear Optical Properties. *Phys. Rev. B: Condens. Matter Mater. Phys.* **1989**, *39*, 10206−10231.
(27) Achermann, M.; Hollingsworth, J. A.; Klimov, V. I. Multi-excitons Confined within a Sub-Excitonic Volume: Spectroscopic and Dynamical Signatures of Neutral and Charged Biexcitons in Ultrasmall Semiconductor Nanocrystals. *Phys. Rev. B: Condens. Matter Mater. Phys.* **2003**, *68*, 245302.
(28) Harris, R. D.; Amin, V. A.; Lau, B.; Weiss, E. A. Role of Interligand Coupling in Determining the Interfacial Electronic Structure of Colloidal CdS Quantum Dots. *ACS Nano* **2016**, *10*, 1395−1403.
(29) Baker, D. R.; Kamat, P. V. Tuning the Emission of CdSe Quantum Dots by Controlled Trap Enhancement. *Langmuir* **2010**, *26*, 11272−11276.
(30) Jin, S.; Harris, R. D.; Lau, B.; Aruda, K. O.; Amin, V. A.; Weiss, E. A. Enhanced Rate of Radiative Decay in CdSe Quantum Dots upon Adsorption of an Exciton-Delocalizing Ligand. *Nano Lett.* **2014**, *14*, 5323−5328.
(31) Singhal, P.; Ghosh, H. N. Hot-Hole Extraction from Quantum Dot to Molecular Adsorbate. *Chem. - Eur. J.* **2015**, *21*, 4405−4412.

DOI: 10.1021/acs.jpcc.7b02949
J. Phys. Chem. C 2017, 121, 15160−15168

(32) Singhal, P.; Ghorpade, P. V.; Shankarling, G. S.; Singhal, N.; Jha, S. K.; Tripathi, R. M.; Ghosh, H. N. Exciton Delocalization and Hot Hole Extraction in CdSe QDs and CdSe/ZnS Type 1 Core Shell QDs Sensitized with Newly Synthesized Thiols. *Nanoscale* **2016**, *8*, 1823−1833.
(33) Kambhampati, P. Unraveling the Structure and Dynamics of Excitons in Semiconductor Quantum Dots. *Acc. Chem. Res.* **2011**, *44*, 1−13.
(34) Klimov, V. I. Spectral and Dynamical Properties of Multiexcitons in Semiconductor Nanocrystals. *Annu. Rev. Phys. Chem.* **2007**, *58*, 635−673.
(35) Schnitzenbaumer, K. J.; Labrador, T.; Dukovic, G. Impact of Chalcogenide Ligands on Excited State Dynamics in CdSe Quantum Dots. *J. Phys. Chem. C* **2015**, *119*, 13314−13324.
(36) Huang, J.; Huang, Z.; Yang, Y.; Zhu, H.; Lian, T. Multiple Exciton Dissociation in CdSe Quantum Dots by Ultrafast Electron Transfer to Adsorbed Methylene Blue. *J. Am. Chem. Soc.* **2010**, *132*, 4858−4864.
(37) Zheng, K.; Žídek, K.; Abdellah, M.; Zhang, W.; Chábera, P.; Lenngren, N.; Yartsev, A.; Pullerits, T. Ultrafast Charge Transfer from CdSe Quantum Dots to P-Type NiO: Hole Injection vs Hole Trapping. *J. Phys. Chem. C* **2014**, *118*, 18462−18471.
(38) Lenngren, N.; Abdellah, M.; Zheng, K.; Al-Marri, M. J.; Zigmantas, D.; Žídek, K.; Pullerits, T. Hot Electron and Hole Dynamics in Thiol-Capped CdSe Quantum Dots Revealed by 2D Electronic Spectroscopy. *Phys. Chem. Chem. Phys.* **2016**, *18*, 26199−26204.
(39) Huang, J.; Huang, Z.; Jin, S.; Lian, T. Exciton Dissociation in CdSe Quantum Dots by Hole Transfer to Phenothiazine. *J. Phys. Chem. C* **2008**, *112*, 19734−19738.
(40) Abdellah, M.; Karki, K. J.; Lenngren, N.; Zheng, K.; Pascher, T.; Yartsev, A.; Pullerits, T. Ultra Long-Lived Radiative Trap States in CdSe Quantum Dots. *J. Phys. Chem. C* **2014**, *118*, 21682−21686.
(41) Klimov, V. I.; McBranch, D. W.; Leatherdale, C. A.; Bawendi, M. G. Electron and Hole Relaxation Pathways in Semiconductor Quantum Dots. *Phys. Rev. B: Condens. Matter Mater. Phys.* **1999**, *60*, 13740−13749.
(42) Norris, D. J.; Bawendi, M. G. Measurement and Assignment of the Size-Dependent Optical Spectrum in CdSe Quantum Dots. *Phys. Rev. B: Condens. Matter Mater. Phys.* **1996**, *53*, 16338−16346.
(43) Swenson, N. K.; Ratner, M. A.; Weiss, E. A. Computational Study of the Enhancement of Raman Signals of Ligands Adsorbed to CdSe Clusters through Photoexcitation of the Cluster. *J. Phys. Chem. C* **2016**, *120*, 20954−20960.
(44) Swenson, N. K.; Ratner, M. A.; Weiss, E. A. Computational Study of the Influence of the Binding Geometries of Organic Ligands on the Photoluminescence Quantum Yield of CdSe Clusters. *J. Phys. Chem. C* **2016**, *120*, 6859−6868.
(45) Azpiroz, J. M.; De Angelis, F. Ligand Induced Spectral Changes in CdSe Quantum Dots. *ACS Appl. Mater. Interfaces* **2015**, *7*, 19736−19745.
(46) Xie, Y.; Teunis, M. B.; Pandit, B.; Sardar, R.; Liu, J. Molecule-like CdSe Nanoclusters Passivated with Strongly Interacting Ligands: Energy Level Alignment and Photoinduced Ultrafast Charge Transfer Processes. *J. Phys. Chem. C* **2015**, *119*, 2813−2821.
(47) Mauser, C.; Da Como, E.; Baldauf, J.; Rogach, A. L.; Huang, J.; Talapin, D. V.; Feldmann, J. Spatio-Temporal Dynamics of Coupled Electrons and Holes in Nanosize CdSe-CdS Semiconductor Tetrapods. *Phys. Rev. B: Condens. Matter Mater. Phys.* **2010**, *82*, 81306.
(48) Berr, M. J.; Vaneski, A.; Mauser, C.; Fischbach, S.; Susha, A. S.; Rogach, A. L.; Jäckel, F.; Feldmann, J. Delayed Photoelectron Transfer in Pt-Decorated CdS Nanorods under Hydrogen Generation Conditions. *Small* **2012**, *8*, 291−297.

DOI: 10.1021/acs.jpcc.7b02949
J. Phys. Chem. C 2017, 121, 15160−15168